72-9033

HAHS, Jimmy Dean, 1940-
COMBINED TORSION, SHEAR AND MOMENT ON PRETENSIONED PRESTRESSED CONCRETE SIMPLY SUPPORTED RECTANGULAR AND L-BEAMS.

The University of Oklahoma, D.Engr., 1971
Engineering, civil

University Microfilms, A XEROX Company, Ann Arbor, Michigan

THIS DISSERTATION HAS BEEN MICROFLIMED EXACTLY AS RECEIVED

Downloaded from SHAREOK. Persistent Handle URL: https://hdl.handle.net/11244/3183

THE UNIVERSITY OF OKLAHOMA

GRADUATE COLLEGE

COMBINED TORSION, SHEAR AND MOMENT ON PRETENSIONED PRESTRESSED CONCRETE SIMPLY SUPPORTED RECTANGULAR AND L-BEAMS

A DISSERTATION

SUBMITTED TO THE GRADUATE FACULTY

in partial fulfillment of the requirements for the

degree of

DOCTOR OF ENGINEERING

BY

JIMMY DEAN HAHS

Norman, Oklahoma

1971

COMBINED TORSION, SHEAR AND MOMENT ON PRETENSIONED PRESTRESSED CONCRETE SIMPLY SUPPORTED RECTANGULAR AND L-BEAMS

APPROVED BY

Welton W. Aldrich

Fulton K. Fears

DISSERTATION COMMITTEE

PLEASE NOTE:

Some Pages have indistinct print. Filmed as received.

UNIVERSITY MICROFILMS

ACKNOWLEDGEMENTS

This study was conducted in the School of Civil Engineering at the University of Oklahoma under the supervision of Dr. H. Aldridge Gillespie and was supported by the Civil Engineering Department and a National Science Foundation Grant.

The writer wishes to express his sincere thanks to Dr. Gillespie for his patience and assistance which have made this study possible. Also, sincere thanks are extended to Dr. Weldon W. Aldridge who introduced the topic and assisted in the establishment of the testing facilities.

Many thanks go to the numerous assistants who helped with the casting and testing of the specimens. Specific thanks are extended to Mr. Howard Martin for his assistance.

The many hours spent by my wife, Ruth, performing the numerous tasks of painting the test equipment, keypunching and typing the drafts of this manuscript and the final figures are sincerely appreciated.

Specific thanks are extended to Mrs. Mary Lou Stokes for her many helpful hints on dissertation format and for her fine typing of this manuscript.

ABSTRACT

Twelve simply supported pretensioned prestressed concrete rectangular beams and 18 L-beams were tested to collapse under combined torsion, shear and bending. The specimens were divided into three series. Series A had a rectangular cross-section of 3"x6" and an effective prestress of 0 psi compression in the top fibers and 1.75 ksi compression in the bottom fibers. Series B and C had a 1"x6" flange added to one side of the top of the basic 3"x6" cross-section. Series C had the same initial prestress as Series A while Series B had 300 psi tension in the top fibers and 1.95 ksi compression in the bottom fibers.

The primary variable was the eccentricity of the load which varied from 0" to 31" measured from the centerline of the web. The eccentricity dominated the load-deformation response of the specimens, crack pattern, cracking and ultimate load capacities. Increased eccentricity reduced the cracking and ultimate loads, transformed the crack pattern from flexure-to-shear to torsional and forced the collapse to move toward the supports and caused the ultimate capacity to approach the initial cracking load.

A unitless three-dimensional interaction surface was developed with the aid of regression analysis. Three-dimensional plots of the surface and the residuals indicate a good correlation with the test data of this investigation as well as that of past research.

LIST OF SYMBOLS

b = overall flange width

b' = width of web

d = distance from extreme compression fiber to tension steel

$\delta_{\mathfrak{L}}$ = vertical deflection at mid-span

δ_H = horizontal deflection

δ_V = vertical deflection

e = eccentricity of load

E_c = modulus of elasticity of concrete

E_s = modulus of elasticity of steel

f'_c = cylinder strength of concrete

f_s = stress in longitudinal steel

h = total depth of beam

M_u = ultimate bending moment

M_{uo} = ultimate bending moment without shear or torsion

μ = Poisson's ratio

P = total load

p = amount of reinforcement (percentage of cross-sectional area)

T_u = ultimate torque

T_{uo} = ultimate torque without bending or shear

V_u = ultimate shear force

V_{uo} = ultimate shear without torsion

x = shorter dimension to a rectangular cross-section

y = longer dimension of rectangular cross-section

TABLE OF CONTENTS

Page

ACKNOWLEDGEMENTS iii

ABSTRACT iv

LIST OF SYMBOLS v

LIST OF TABLES viii

LIST OF FIGURES ix

Chapter

I. INTRODUCTION 1

Three Dimensional Interaction Surfaces 3
Objective and Scope of Study 12

II. TEST SPECIMENS AND LABORATORY TECHNIQUE 16

Introduction 16
Test Specimens 16
Casting and Curing 18
Test Procedure 28
Preparation 28
Loading System 29
Instrumentation 33
Testing 33

III. BEHAVIOR OF TEST SPECIMENS 36

Ultimate Strength 43
Influence of Eccentricity 43
Influence of Overhanging Flange 43
Influence of Effective Prestress 47
Crack Pattern 50
Influence of Eccentricity 50
Shear-Centerline Deflection 55
Influence of Eccentricity 56
Influence of Overhanging Flange 58
Influence of Effective Prestress 58
Torque-Twist Curves 61
Influence of Eccentricity 61

TABLE OF CONTENTS (Cont'd.)

Page

Influence of Overhanging Flange. 63
Influence of Effective Prestress 63
Shear-Slope at the Ends. 66
Influence of Eccentricity. 66
Influence of Overhanging Flange. 68
Influence of Effective Prestress 68
Summary. 68

IV. DEVELOPMENT OF AN INTERACTION SURFACE FOR PRESTRESSED RECTANGULAR AND L BEAMS LOADED WITH TORSION, SHEAR AND MOMENT. 72

Three-Dimensional Interaction of Torsion, Shear and Moment 73
Proposed Unitless Interaction Surface. 82
Comparison of Proposed Interaction Surfaces. 86

V. CONCLUSIONS AND RECOMMENDATIONS. 94

BIBLIOGRAPHY. 97

APPENDIX A

Detailed Discussion of Each Specimen 101

APPENDIX B

Load-Deformation Curves. 131

APPENDIX C

Material Properties. 146

APPENDIX D

Load Cell Calibration Curves 149

VITA. 151

LIST OF TABLES

Table		Page
3.1	INITIAL CRACKING AND CRACK PATTERNS	37
3.2	ULTIMATE CAPACITY, ULTIMATE CRACK PATTERN AND LOAD DEFORMATION RESPONSE.	39
4.1	PURE MOMENT, SHEAR AND TORQUE CAPACITIES.	76

LIST OF FIGURES

Figure		Page
1.1	Interaction Surface of Combined Torsion, Shear and Bending for a Symmetrically Reinforced Beam	4
1.2	Unitless Interaction Surface of Combined Torsion, Shear and Bending of Reinforced Concrete Beams.	4
1.3	Failure Criteria	6
1.4	Skewed Bending Failure	8
1.5	Effect of Axial Prestress on the Torsional Capacity of Rectangular Specimens	8
1.6	Torsion-Shear Interaction Diagram.	9
1.7	Unitless Interaction Surface for Combined Torsion, Shear and Bending of Prestressed Concrete Rectangular Beams Containing Secondary Web Reinforcement.	11
1.8	Typical Cross-Sections Tested.	14
1.9	Schematic Loading Diagram.	15
2.1	Test Specimens	17
2.2	Secondary Web Reinforcement for Beam A-7	19
2.3	Dimensions of Test Specimens	20
2.4	Formwork	22
2.5	Prestressing System.	24
2.6	Curing of Specimens.	26
2.7	Specimen Movement During Pretensioning Transfer.	26
2.8a	General Loading System	30
2.8b	Small and Intermediate Eccentricity Loading System	31
2.8c	Large Eccentricity Loading System.	31

LIST OF FIGURES (Cont'd.)

Figure		Page
2.9	Two-Point Loading System	32
2.10	General Test Instrumentation	34
3.1a	Ultimate Capacity Interaction Surface for Series A	44
3.1b	Ultimate Capacity Interaction Surface for Series B	45
3.1c	Ultimate Capacity Interaction Surface for Series C	46
3.2	Influence of the Overhanging Flange on the Ultimate Capacity Interaction Surfaces	48
3.3	Influence of Effective Prestress on the Ultimate Capacity Interaction Surfaces	49
3.4	Typical Crack Pattern for Zero Eccentricity.	52
3.5	Typical Crack Pattern for Large Eccentricity	53
3.6	Typical Crack Pattern for Intermediate Eccentricity. . . .	54
3.7	Influence of Eccentricity on the Shear-Centerline Deflection.	57
3.8	Influence of the Overhanging Flange on the Shear- Center-line Deflection	59
3.9	Influence of Effective Prestress on the Shear-Centerline Deflection.	60
3.10	Influence of Eccentricity on the Torque-Twist Response . .	62
3.11	Influence of Overhanging Flange on the Torque-Twist Response.	64
3.12	Influence of Effective Prestress on the Torque-Twist Response.	65
3.13	Influence of Eccentricity on the Shear-Slope at the Ends Response.	67

LIST OF FIGURES (Cont'd.)

Figure		Page
3.14	Influence of Overhanging Flange on the Shear-Slope at the Ends Response	69
3.15	Influence of Effective Prestress on the Shear-Slope at the Ends Response	70
4.1	Unitless Interaction Surface for Series A by Regression Analysis	79
4.2	Unitless Interaction Surface for Series B by Regression Analysis	80
4.3	Unitless Interaction Surface for Series C by Regression Analysis	81
4.4	Basic Assumptions of the Proposed Unitless Interaction Surface for Torsion, Shear and Moment	84
4.5	Proposed Unitless Interaction Surface for Torsion, Shear and Moment	87
4.6	Proposed Unitless Interaction Surface with Series A, B, and C	88
4.7	Proposed Unitless Interaction Surface with Mukherjee's Test Data	89
4.8	Mukherjee's Proposed Interaction Surface with Series A, B and C	90
4.9	Unitless Interaction of Torsion and Shear	93

COMBINED TORSION, SHEAR AND MOMENT ON PRETENSIONED PRESTRESSED CONCRETE SIMPLY SUPPORTED RECTANGULAR AND L-BEAMS

CHAPTER I

INTRODUCTION

The combined loading of torsion, shear and moment has become a major design consideration in the concrete industry in recent years. Smaller factors of safety have resulted from further research and the application of the computer in the solution of more precise, but heretofore impractically cumbersome, equations of structural and material behavior. Added confidence in skill and knowledge has lead to more complex structures being designed and built. Refinement in the design for shear and moment has also resulted from extensive testing of these types of loadings. Until recent years factors of safety were sufficiently large in most cases to permit the designer to neglect the secondary torsional effects. This omittance is verified by noting that the 1963 ACI Building Code gives the designer no information on torsional design.

Many researchers have recently turned their efforts to understanding the ultimate capacity of members loaded with torsion, shear and moment. The two most comprehensive studies are by Kemp, Sozen and Siess (1961) and ACI SP-18 (1968). These two studies primarily deal with plain and reinforced concrete and will not be discussed in detail here. Zia (1970) presented a summary of recent work on torsion in plain

and reinforced concrete members. However, the reader has only a limited amount of information [Cowan, 1957], [Humphreys, 1957], [Zia, 1960] on pure torsion of eccentrically prestressed concrete members.

Experimental research on prestressed specimens loaded with shear and moment has resulted in fairly well accepted design equations as presented in the 1963 ACI Building Code. As previously noted, no information is given in this code to allow the designer to consider torsional effects.

The present trend in the reinforced concrete industry is to correlate the three primary variables (torsion, shear and moment) by a three dimensional interaction diagram. This technique appears to be not only a justifiable approach but a practical means for the designer to obtain the required data. The two main limitations at present appear to be the lack of sufficient test results to describe the interaction surface adequately and the complexity of the surface. These surfaces range from a quarter of a sphere [Navaratnarajah, 1968] to a surface composed of several intersecting planes [Collins, Walsh, and Hall, 1968], [Mirza and McCutcheon, 1968], to that of double curved surfaces [Behera, 1970].

The primary reason for the wide variance in the types of interaction surfaces for reinforced concrete specimens is the number of variables that are involved. A few of which are concrete strength, cross-sectional shape, type of loading, sequence of loading, type and placement of reinforcement, shear-span to depth ratio, etc. When the additional variable of prestress is added to the surface,it is even more complex and the test data is almost non-existent.

Three Dimensional Interaction Surfaces

The following discussion gives a detail correlation of past research on prestress specimens and a general correlation with that of reinforced concrete specimens.

The present trend in presenting the data for specimens loaded with torsion, shear and moment is shown in Figure 1.1. In order to make the surface more general and eliminate part of the scale effects, a non-dimensional interaction surface as shown in Figure 1.2 is being adopted by some of the most recent researchers [Hsu, 1968] where

T_u = ultimate torque

M_u = ultimate bending moment

V_u = ultimate shear force

T_{uo} = ultimate torque without bending or shear

M_{uo} = ultimate bending moment without shear or torsion

V_{uo} = ultimate shear without torsion

The moment and shear axes, as well as the moment-shear plane have been extensively researched and acceptable design equations are given in the 1963 ACI Building Code for reinforced and prestressed concrete members.

The torsion axis has been partially studied for plain [ACI-SP 18], reinforced [ACI-SP 18] and prestressed members [Cowan, 1955], [Zia, 1960], [Hsu, 1968].

Researchers have attempted to apply the classical torsional analysis as presented by Coulomb (1787), Saint-Venant (1853), Prandtl (1903) (soap-film analogy), and the sand heap analogy with no general

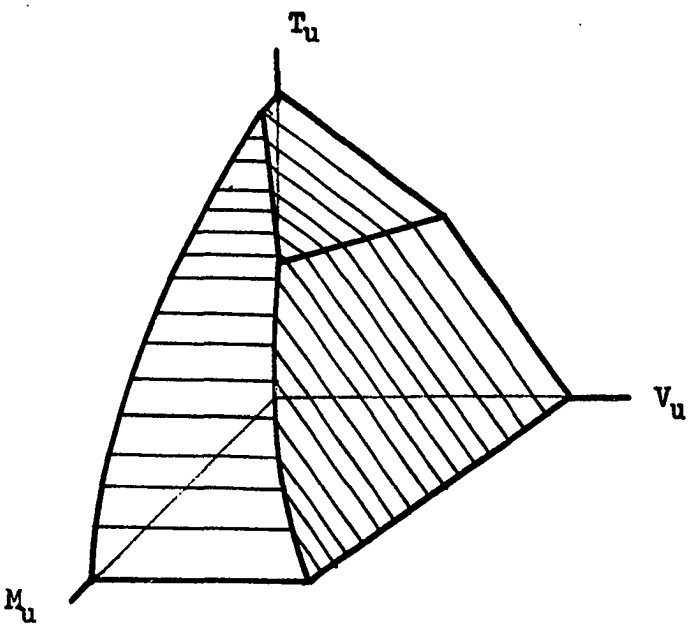
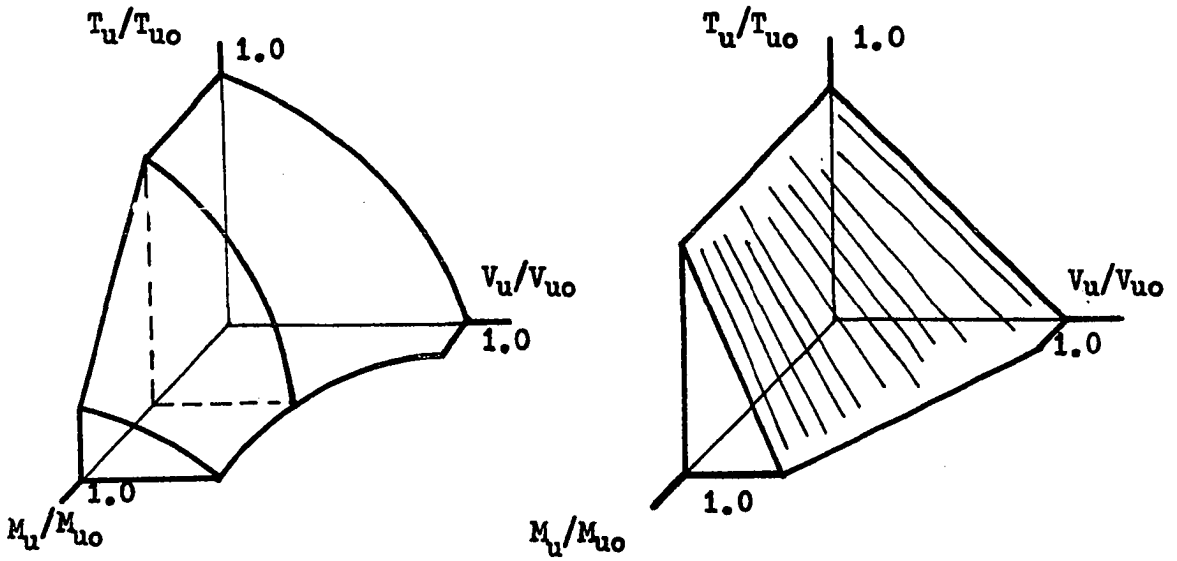


Figure 1.1 Interaction Surface of Combined Torsion, Shear and Bending for a Symmetrically Reinforced Beam (Collins, Walsh and Hall, 1968)



(a) General Forms (Hsu, 1968)

(b) Simplified Form (Mirza and McCutcheon, 1968)

Figure 1.2 Unitless Interaction Surface of Combined Torsion, Shear and Bending of Reinforced Concrete Beams

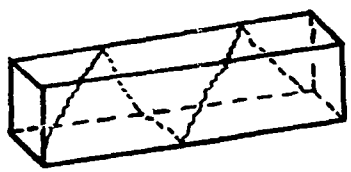
method being found acceptable for all concrete cross-sections and strengths. The prominent objection to each of these methods is that concrete does not satisfy the basic assumptions of the methods i.e., concrete is not homogeneous, isotropic, linear elastic or elastic-perfect-plastic.

The failure criteria commonly used for the analysis of prestressed concrete in torsion are shown in Figure 1.3. It should be noted that Cowan's theory is a dual criterion which combines Rankine's maximum stress theory for cleavage failure and the internal friction theory for shear failure. The modified Cowan theory, as suggested by Zia (1960) may be regarded as a closer approximation to Mohr's generalized internal friction theory. A comparison of these theories can be seen from the interaction curves in Figure 1.3b. Considerable difference among the theories is obvious although each clearly indicates that up to an axial compressive stress of 0.60 f'_c, which is a practical limit and is considerably above the 1963 ACI Building Code of 0.45 f'_c, may result in a substantial increase in the apparent torsional strength of prestressed concrete.

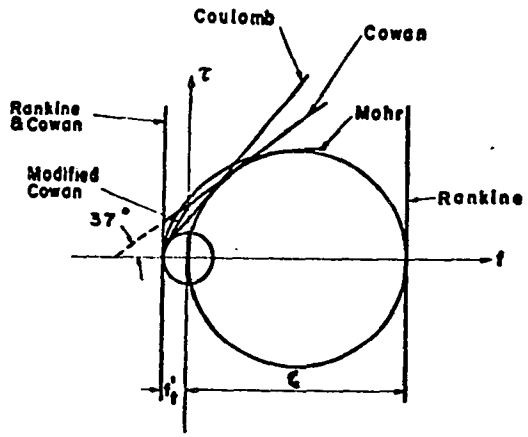
Hsu (1968) developed the following relationships for the torsional capacity of rectangular specimens with a uniform prestress of σ without web reinforcement by modifying a skewed bending failure (Figure 1.4):

$$T_{uo} = T_{uo\ plain} \sqrt{1 + 10\sigma/f'_c} \ .$$

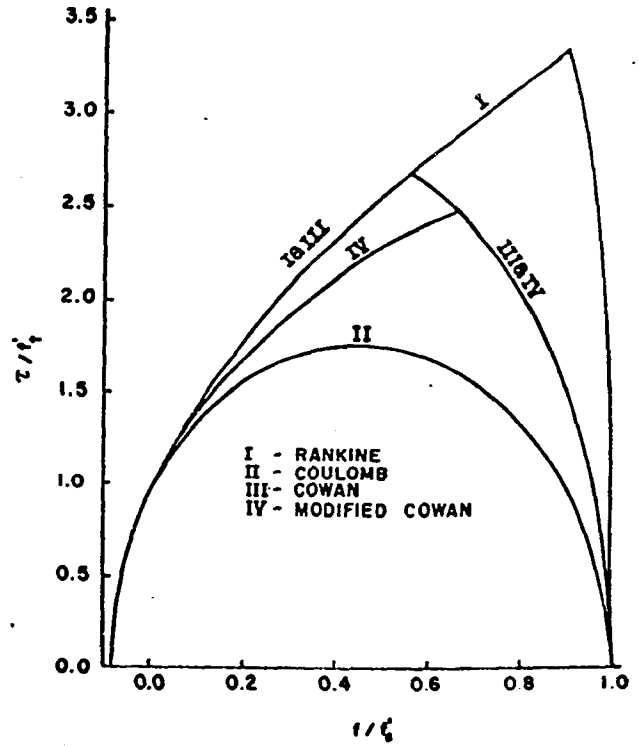
It should be noted that the modification factor derived by the skewed bending mode of failure for prestressed members results in the same



(a) Helical Cracks of Plain Concrete Section Under Pure Torsion



(b) Failure Theories for Concrete Under Combined Stresses



(c) Interaction Curves According to the Various Failure Theories ($f'_t = 0.10f'_c$)

Figure 1.3 Failure Criteria

modification factor as that derived by considering the effect of the prestress on the principal tensile stress. Figure 1.5 shows the effectiveness of axial prestress on the torsional capacity per Hsu (1968). This method of skewed bending failure mode has been reported by many recent researchers [Lessig, 1959], [Yudin, 1962], [Gesund, 1964], [Hsu, 1968], [Collins, 1968] for torsion, shear and moment of reinforced concrete members.

There have been only a relatively few tests made in the torsion-moment plane for prestressed concrete members. Reeves (1962), Rowe (1958) and Gardner (1960) tested eccentrically prestressed T-beams, rectangular beams and I-beams, respectively, in combined bending and torsion. The general results are shown in Figure 1.6 which is a two-dimensional interaction diagram since there was no shear force in the test region. The general testing procedure consisted of developing a constant moment region with a two-point load system and then loaded with increments of torsion until the ultimate load was obtained.

It should be noted that in the torsion-moment plane the addition of moment increased the torsional capacity of the T-beams and the rectangular beams but had no appreciable effect upon the I-beams. In the high moment range a decrease in torsional capacity was observed.

Cowan's (1955) eccentrically prestressed beams showed the same basic trend in the high moment region but he had no specimens in the low moment region for comparison. His concentrically prestressed beams showed only slight increase in torsional capacity due to the application of a small moment.

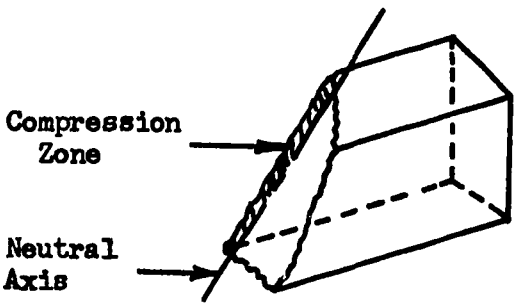


Figure 1.4 Skewed Bending Failure

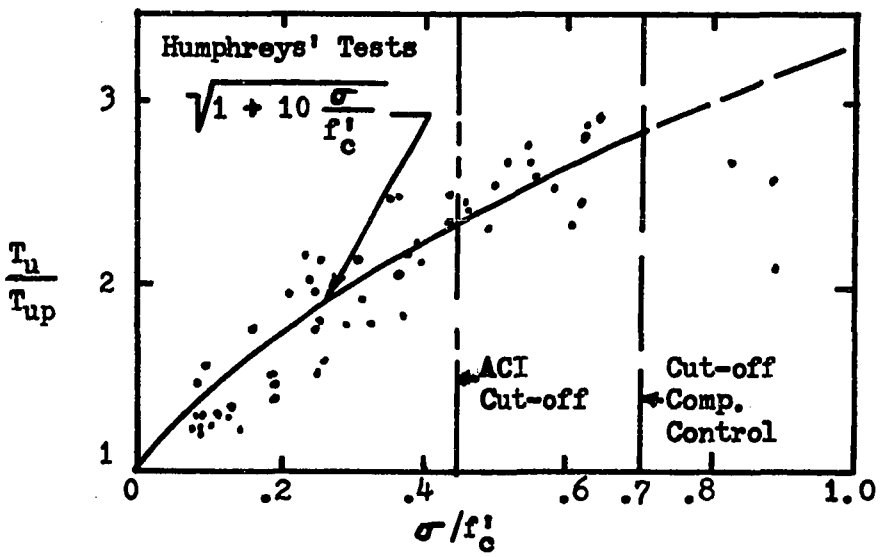


Figure 1.5 Effect of Axial Prestress on the Torsional Capacity of Rectangular Specimens

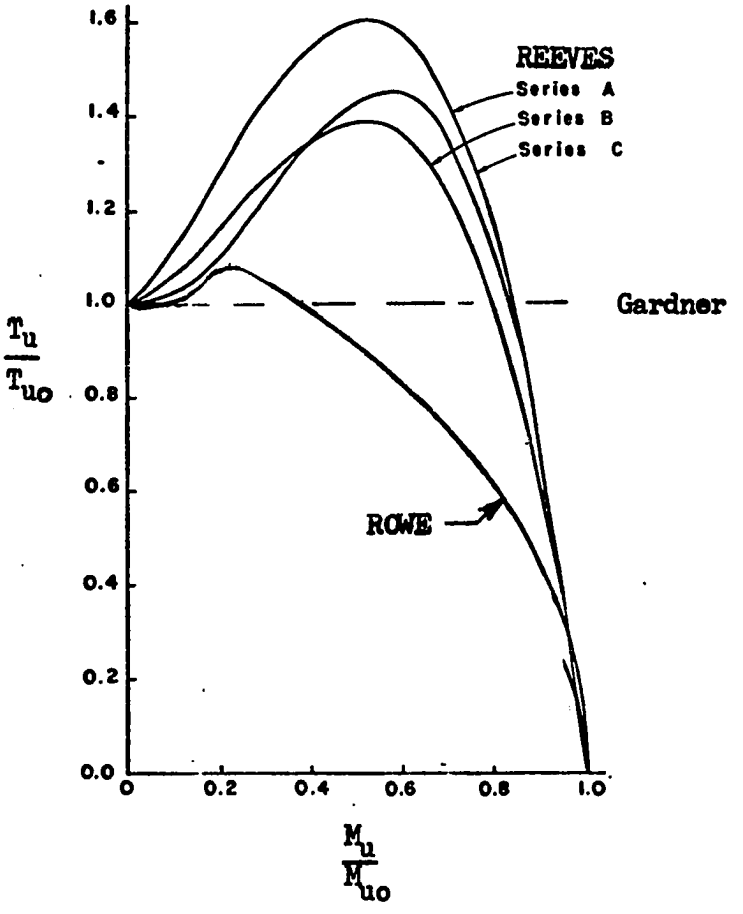


Figure 1.6 Torsion-Shear Interaction Diagram (Reeves, 1962), (Rowe, 1958) and (Gardner, 1960)

Mukherjee and Warwaruk (1971) have presented a three dimensional surface (Figure 1.7) for prestressed rectangular beams containing reinforcement in both the transverse and the longitudinal directions. The following basic assumptions were used to allow this surface to the developed:

1. The trace of the surface on the torsion-shear plane is a straight line as proposed by Nylander (1945).
2. If shear reinforcement is used, there is no interaction between shear and moment, the result of which is a square plot on the moment-shear plane.
3. The trace of the interaction surface on the torsion-moment plane was obtained by statistical regression analysis of their test data.
4. The trace of the interaction surface on the plane $M_u/M_{uo}=1$ is a straight line BC, parallel to LE.
5. The trace of the interaction surface on the plane $V_u/V_{uo}=1$ is a straight line CD, passing through point D on the shear axis.
6. The shape of the line FG on any cross-sectional plane, such as FGHK parallel to the torque-shear plane is a straight line bounded at its extremities by curve AFB and line CD.

The equation for the curved interaction surface AFBCGD deduced by assuming an equation for the straight line, FG, and then evaluating the unknown coefficients from the defined end conditions at F and G is given by

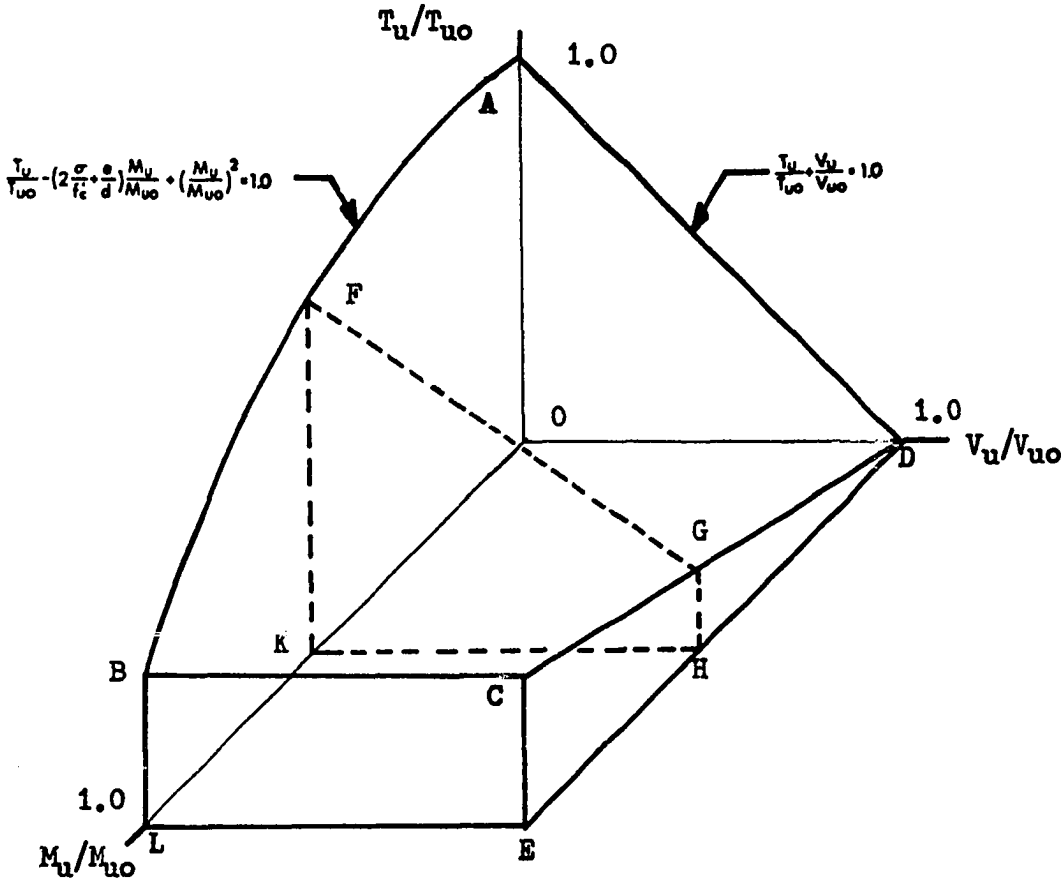


Figure 1.7 Unitless Interaction Surface for Combined Torsion, Shear and Bending of Prestressed Concrete Rectangular Beams Containing Secondary Web Reinforcement (Mukherjee and Warwaruk, 1971)

$$\frac{T_u}{T_{uo}} - \left(2\frac{\sigma}{f'_c} + \frac{e}{d}\right)\frac{M_u}{M_{uo}} + \left(\frac{M_u}{M_{uo}}\right)^2 + \left[1-\left(\frac{M_u}{M_{uo}}\right)^2\right]\frac{V_u}{V_{uo}} = 1.0$$

if

$$\frac{T_u/T_{uo}}{M_u/M_{uo}} \geq \left(2\frac{\sigma}{f'_c} + \frac{e}{d}\right) .$$

The specified limit of this equation was based on the consideration that the points on the curved interaction surface must be situated above plane OBCD. Below this plane, the interaction surface may be the rectangle BCEL, or triangle CED, the equations for which are

$$\frac{M_u}{M_{uo}} = 1.0 \qquad \text{if} \qquad \frac{V_u}{V_{uo}} < 1.0$$

$$\frac{V_u}{V_{uo}} = 1.0 \qquad \text{if} \qquad \frac{M_u}{M_{uo}} < 1.0 \quad .$$

Objective and Scope of Study

Since torsion in combination with bending and shear is becoming more and more of a practical design consideration due to the type of present day construction and analysis, it seems apparent from the meager amount of information presently existing that more research in this field is needed.

Since present day construction procedures of monolithic concrete construction result in T-beams and L-beams, the basic cross-section for the study reported herein was determined to be L-beams with a series of rectangular beams to be used as a basis of comparison as shown in

Figure 1.8. Details of the specimens are discussed in Chapter II and shown in Figure 2.1. Eccentrically prestressed specimens were chosen because of their practical usage in industry especially when bending is one of the primary design factors.

A simply supported span of 6 feet, center of support to center of support, with the load at mid-span was used as the primary test set-up with torsion resulting from the load being placed at an eccentricity of "e" from the centerline of the web. Figure 1.9 shows schematically the loading along with the torsion, shear and moment diagrams.

The primary objective of the study was to explore experimentally the load-deformation response of eccentrically pretensioned prestressed concrete beams loaded in combined torsion, shear and moment with effective prestress, torque-to-shear ratio, torque-to-moment ratio and over-hanging flange being the important variables. Care was also taken to obtain the crack patterns of the specimens.

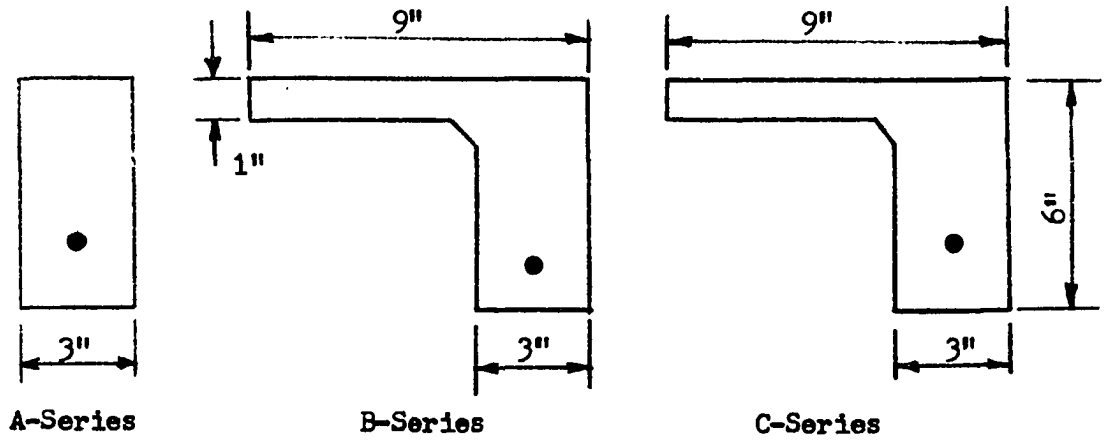


Figure 1.8 Typical Cross-Sections Tested

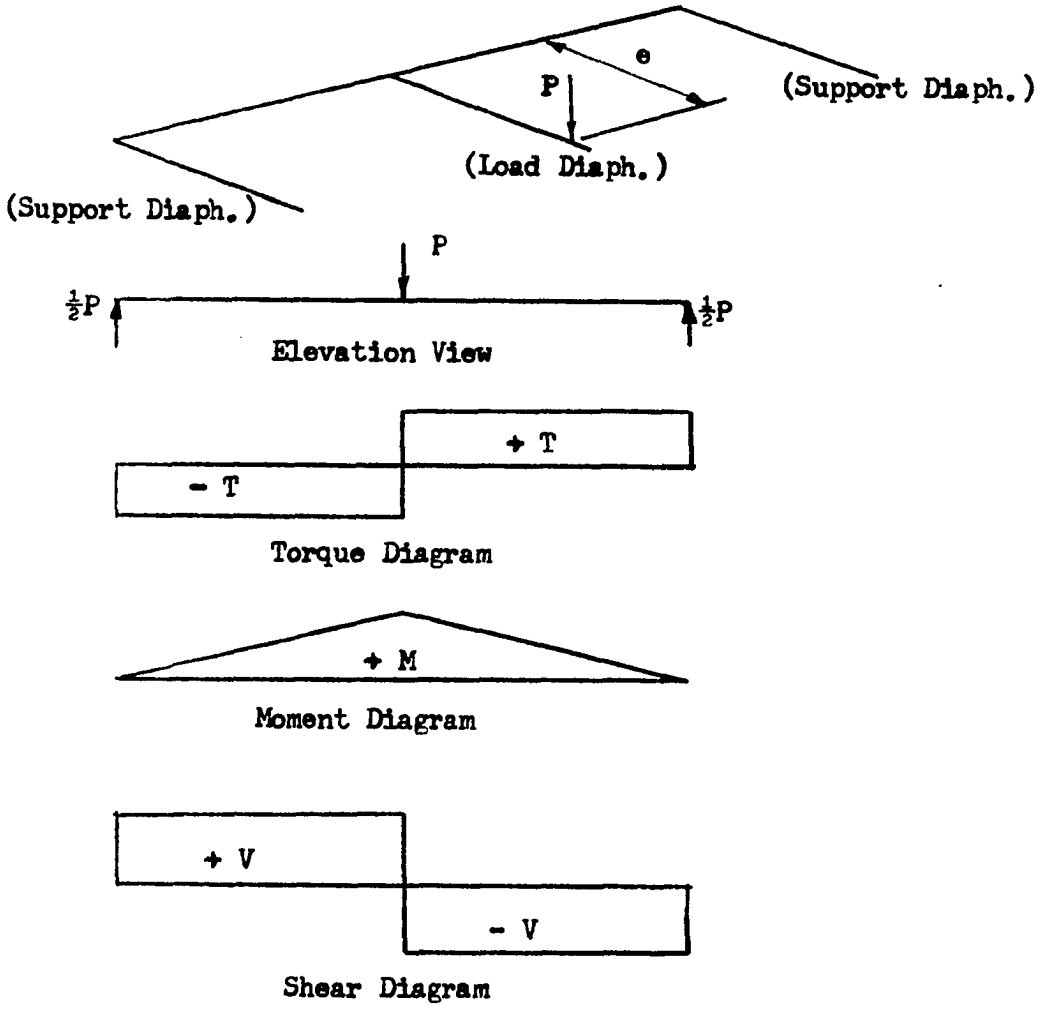


Figure 1.9 Schematic Loading Diagram

CHAPTER II

TEST SPECIMENS AND LABORATORY TECHNIQUE

Introduction

Twelve simply supported pretensioned prestressed concrete rectangular beams and 18 L-beams were tested to collapse under combined torsion, shear and bending. All of the specimens were composed of the basic rectangular section (3"x6") with the primary variable being the addition of a (1"x6") flange to one side of the basic cross section. The other variables were effective prestress, torque-to-shear and torque-to-moment ratios.

Test Specimens

The specimens tested have been previously discussed and are shown in Figure 2.1. Test specimens were divided into three groups according to the addition of a flange and the amount of effective prestress. Series A had no flange and an effective prestress producing 0 ksi tension in the top fibers and 1.75 ksi compression in the bottom fibers. The overhanging flange for series B and C was 1"x6". The effective prestress for series B was 0.3 ksi tension in the top fibers and 1.90 ksi compression in the bottom fibers, while series C had 0 ksi tension in the top fibers and 1.75 ksi compression in the bottom fibers. In series B and C 1/2"x1/2" fillets were provided at the junction of the flange and the web in order to reduce the stress concentration.

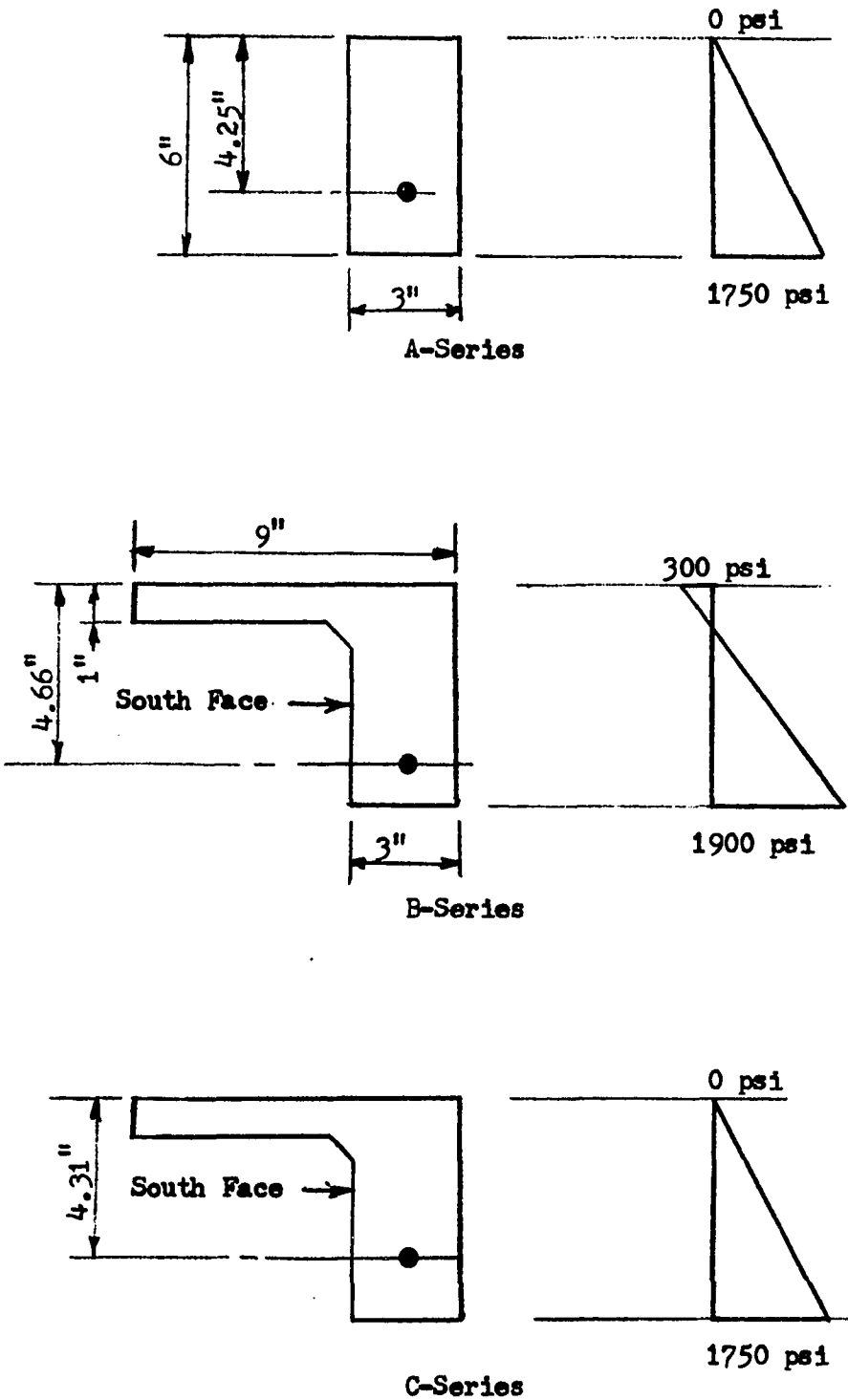


Figure 2.1 Test Specimens

All of the beams contained one 3/8" diameter, 7 wire, 270 kips strand located as shown in Figure 2.1. The load-strain curve for the prestressing steel is given in Appendix C. Only specimens A-7, B-8, and C-7 contained web reinforcement (Figure 2.2). These were tested with a two-point load system to obtain the pure moment capacity of the section and did not contain web reinforcement in the pure moment test region.

The general dimensions of the test specimens along with the reinforcement of the diaphragms are shown in Figure 2.3. The vertical stirrups used in the load and support diaphragms were made of either 3/16" ϕ wire (fy = 40 ksi). The load and support diaphragms were cast monolithically with the beams and were of uniform depth.

Throughout this text, the web on the overhanging flange side (in the direction of the eccentricity) will be referred to as the "south face" and the web opposite to the direction of the eccentricity as the "north face". Also, the eccentricity of the load at mid-span measured from the centerline of the web will be referred to as the "eccentricity".

Casting and Curing

The concrete mix was designed to provide a seven day strength of 5500 psi. A 1:1.5:1.7 (cement:sand:gravel) mix by weight with a water cement ratio of 0.5 was used throughout the investigation. The large sized aggregate was a graded crushed rock which passed a 3/4" screen. The sand was a well graded river sand with a sieve analysis as shown in Appendix C.

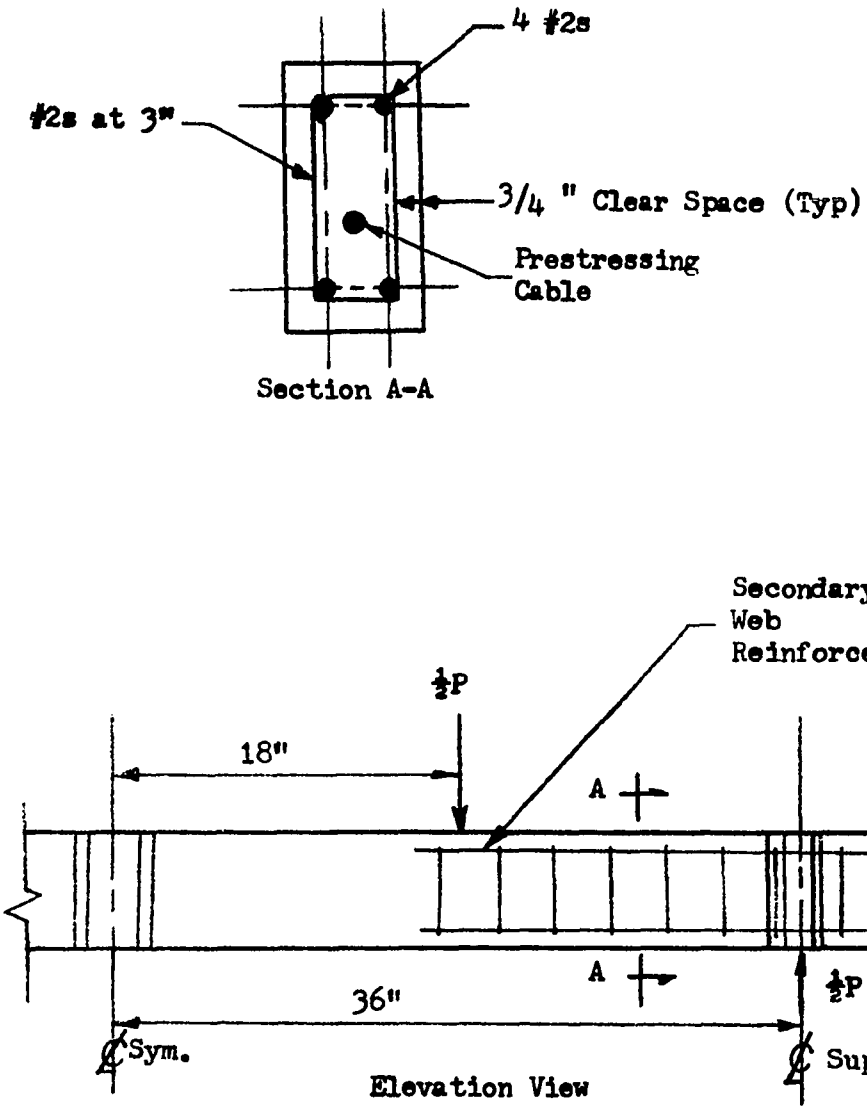
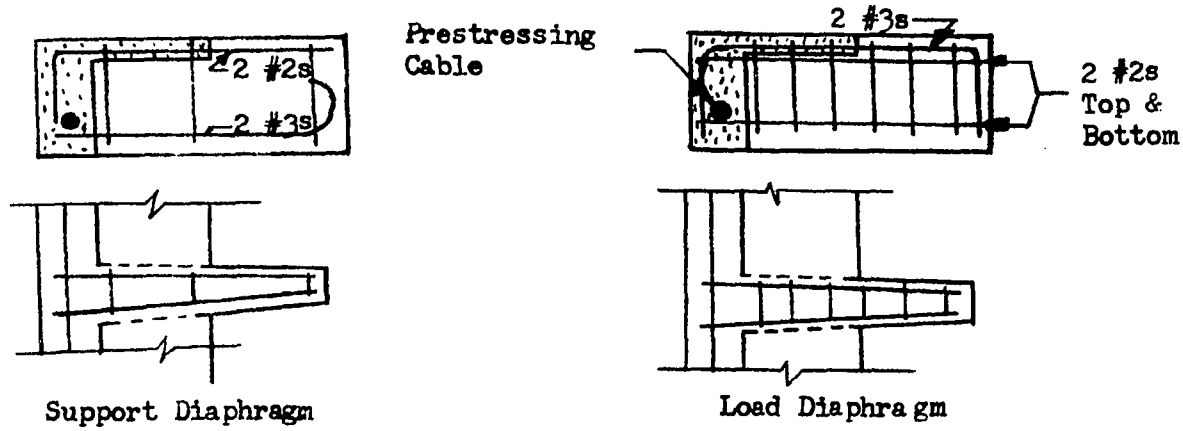
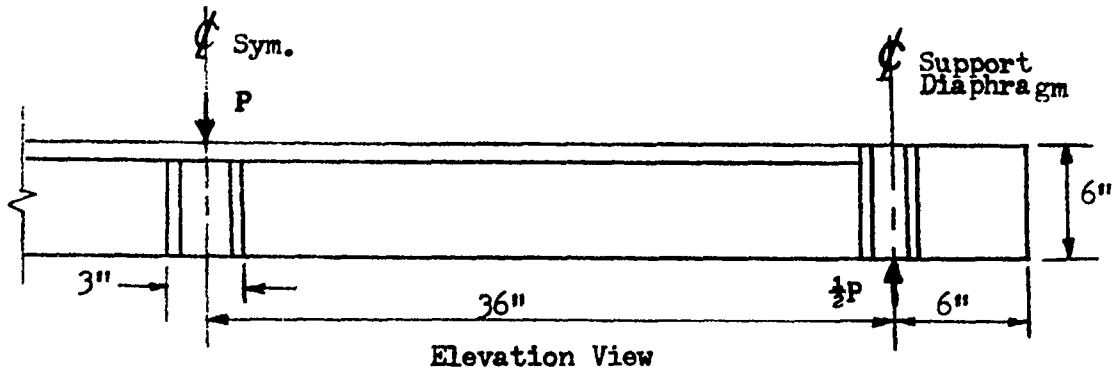


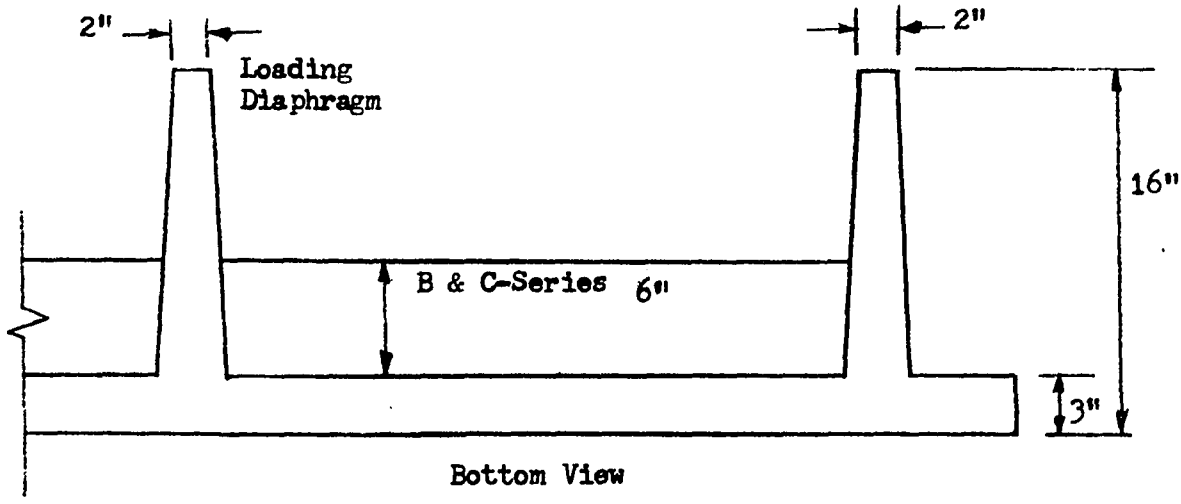
Figure 2.2 Secondary Web Reinforcement for Beam A-7

(B-8 and C-7 similar except with flange)





Elevation View



Bottom View

Figure 2.3 Dimensions of Test Specimens

The formwork for the specimens was made of plywood with an epoxy coating used as waterproofing. The basic form was a plywood plate supported by four 3/4" threaded rods (Figure 2.4) which allowed the forms to be positioned in proper alignment with the prestress cable. Figure 2.4 shows typical formwork for three specimens.

The north face of each specimen was formed by bolting a trimmed 2"x8"x8' board attached to a 3 1/2"x1/4" angle to the plywood. The south face of each specimen was formed by bolting two 5" deep box sections to the plywood with 1" thick strips of wood screwed to the box sections at proper distances to give the overhanging flange. The box sections were tapered to allow them to be pulled from between the loading arm and the support diaphragm, but with the large flanges of series B and C it was found that the forms needed to be more flexible. A 3/4" gap was cut in the box sections which was covered with a light gage aluminum strip during the casting operation.

After the forms were assembled and placed in approximate position, the cable was threaded through the prestressing bed and the forms and tensioned with 3 kips to remove the slack. The forms were then positioned and anchored. The prestress cable was then removed and the joints of the forms were taped to prevent the mortar from leaking. The forms were oiled to prevent the concrete bonding to them. After the reinforcement for the diaphragms was positioned, the prestress cable was threaded through the forms and the diaphragm reinforcement. Care was taken to keep the oil off the cable and a rag soaked with acetone was used to wipe the cable before the concrete was placed.

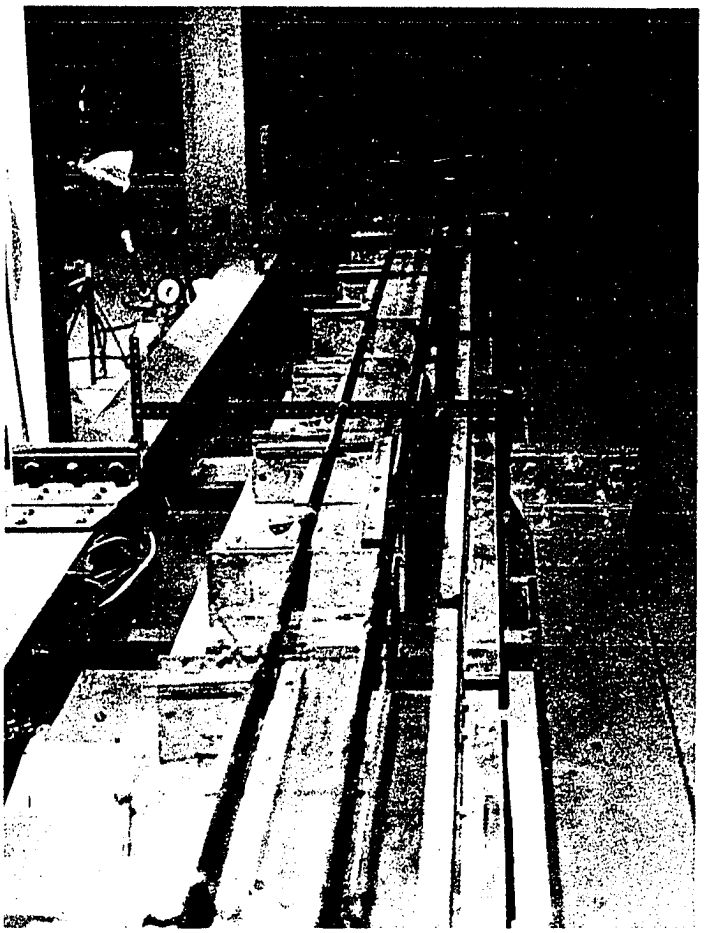


Figure 2.4 Formwork

The general pretensioning process consisted of anchoring the east end of the cable to the prestressing bed allowing a chuck to bear on a plate (Figure 2.5). The west end was threaded through a chuck, a chair, a center-hole hydraulic cylinder, a load cell and a chuck, respectively. The cable was tensioned by expanding the cylinder between the chair and the chuck on the west end with the load being monitored by the load cell. Spacers were added between the second chuck on the west end and the prestressing bed. The pressure was released from the cylinder thereby transferring the load to the second chuck.

The concrete was then placed in the forms with a separate batch being made for each specimen. Control cylinders were cast at the same time as the specimens in accordance with ASTM C 192-54 except that nominal 3"x6" paper molds were used.

The tops of the specimens were finished and allowed to gain enough strength so that the covering material would not mar the surface. Wet burlap sacks were placed over the specimens and the cylinders and intermittently wetted for twenty-four hours (Figure 2.6). After twenty-four hours, the south face of the forms and the paper cylinders were removed and the wet burlap sacks replaced and intermittently wetted for another twenty-four hours. Series B and C were allowed to remain in the forms forty-eight hours before the box sections were removed to allow the overhanging flange to gain more strength. The burlap sacks were then removed to let the specimens air cure for twenty-four hours before the pretension force in the cable was transferred to the specimens.

The transfer of the prestress to the specimens was accomplished by reassembling the chair, hydraulic cylinder and west chuck and jacking

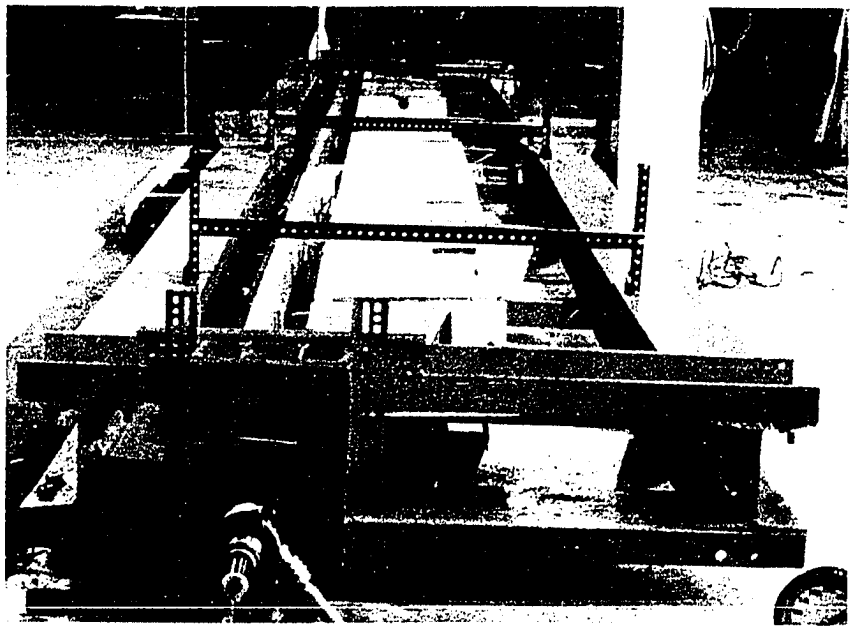
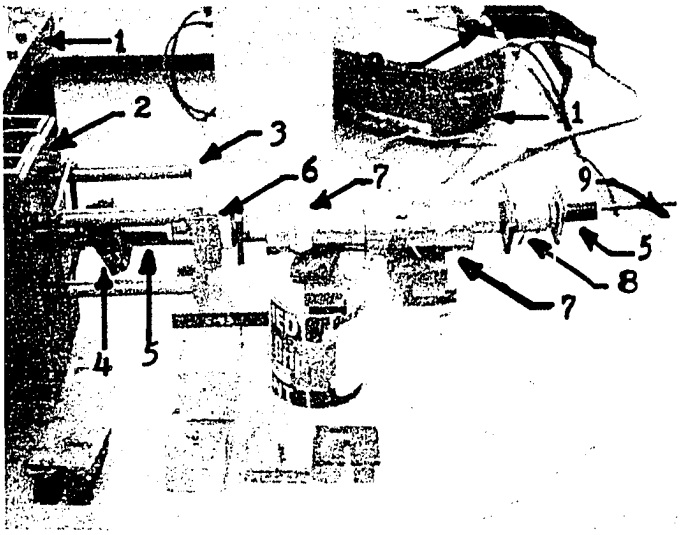
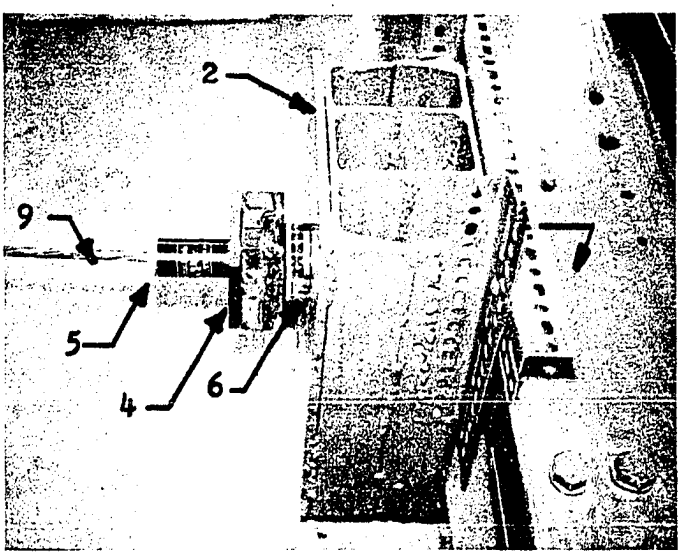


Figure 2.5 Prestressing System



West End



East End

1. Prestressing Frame
2. Distribution Box
3. Chair
4. Slotted Spacer
5. Supreme Chuck
6. Bearing
7. Hydraulic Ram
8. Load Cell
9. Prestressing Cable
10. Hydraulic Pump
11. Strain Indicator

Figure 2.5 continued

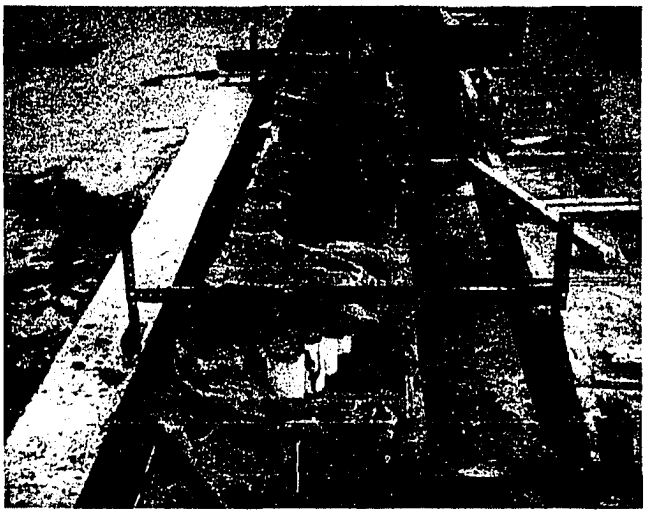


Figure 2.6 Curing of Specimens

Specimen Movement

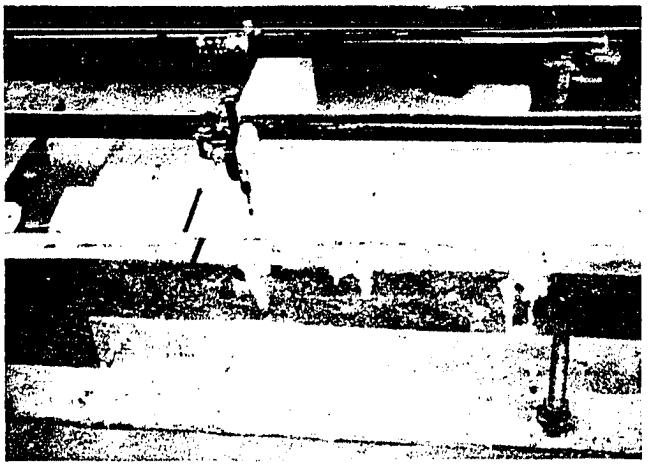


Figure 2.7 Specimen Movement
During Pretensioning Transfer

against the west chuck and the chair just sufficient to allow the spacers to be removed. The pressure was released slowly from the cylinder which then transferred the tension in the cable to the specimens during a time interval of approximately 1 to 2 minutes.

The specimens were allowed to sit for approximately four hours and then the cable between the specimens was cut with a torch. The specimens were then removed and stored under ambient conditions until tested.

The first modification to the tensioning process was the addition of a spacer between the east chuck and the prestressing bed. When the tension in the cable was released from the west end only, the specimens tended to slide on the forms (Figure 2.7) but the friction between the forms and the specimens allowed some tension to remain between the specimens and, in particular, between the east chuck and the east specimen. With the removal of the additional slotted spacers, the tension on the east end of the cable could be removed.

The second modification to the tensioning process was a result of the cable tending to untwist during the tensioning process. Two types of bearings were used to allow the cable to have freedom of twist. The first set consisted of plates with ballbearings placed between them. These were placed on each end of the cable. The second set, which were front pinion bearings for a Buick automobile, was adopted mostly for convenience in handling (Item 6 of Figure 2.5).

The third modification to the pretensioning process was the addition of another hydraulic cylinder to allow complete tensioning without an intermediate adding of spacers and pressure release.

Test Procedure

Preparation

Since the north face of each specimen was formed using a rigid section, it was used as a base line for all north-south measurements during the assembling and testing of the specimens.

Although the north-south dimensions were referenced to the north face of the specimen during testing, the eccentricity of the load was converted to the distance from the centerline of the web rather than to the elastic shear center. Measurements from the centerline rather than from the shear center were used for two reasons. First, in practice the design engineer will usually use the centerline of the web rather than the shear center. Secondly, it has been shown [Ersoy, 1965] for cross sections of the dimensions used in this investigation that the shear center of reinforced concrete sections is very close to the centerline of the web. Ersoy also pointed out that the shear center is not a unique point for a concrete beam during loading after cracking.

The contact points of the deflection gages were modified in one of three general ways depending on the initial texture of the concrete surface. If the surface was fairly smooth, the contact point was sanded. If the surface was rough, it was made smooth by applying a small patch of plaster of Paris at the contact point or a small piece of plexiglass was glued to the concrete at the point. This precaution was used to eliminate dial gage reading errors due to the roughness of the surface.

Loading System

The general loading condition is shown in Figure 2.8a. The load to the specimen was distributed by a small plate which was cushioned by a thin layer of plaster of Paris. The load was applied to the plate through a bearing system which gave a point load condition. The magnitude of applied load was monitored by a load cell and was applied through a lever system supported by a hinge connection as shown in Figure 2.8b. The hydraulic cylinder provided the active force to the lever.

In order to keep the dead load of the system to a minimum and for safety reasons the lever system was counterbalanced with a weight and pulley system as shown in Figure 2.8a.

For large eccentricities, two modifications were made to the load system as shown in Figure 2.8c. First, an extension to the loading diaphragm was adopted. The load on the extension was transferred to the concrete loading arm by bearing and friction.

The second modification was the addition of collars around the support diaphragms. These collars had a round bar placed parallel to and between the support diaphragms and the top plate of the collar to allow freedom of moment but to give the collar the ability to resist torsion.

The loading system for specimens A-7, B-8, and C-7 was revised to produce a pure moment region as shown in Figure 2.9. The load was transferred from the lever system through the load cell to the aluminum I-beam which divided it equally between two points symmetrical with respect to mid-span giving a pure moment test region.

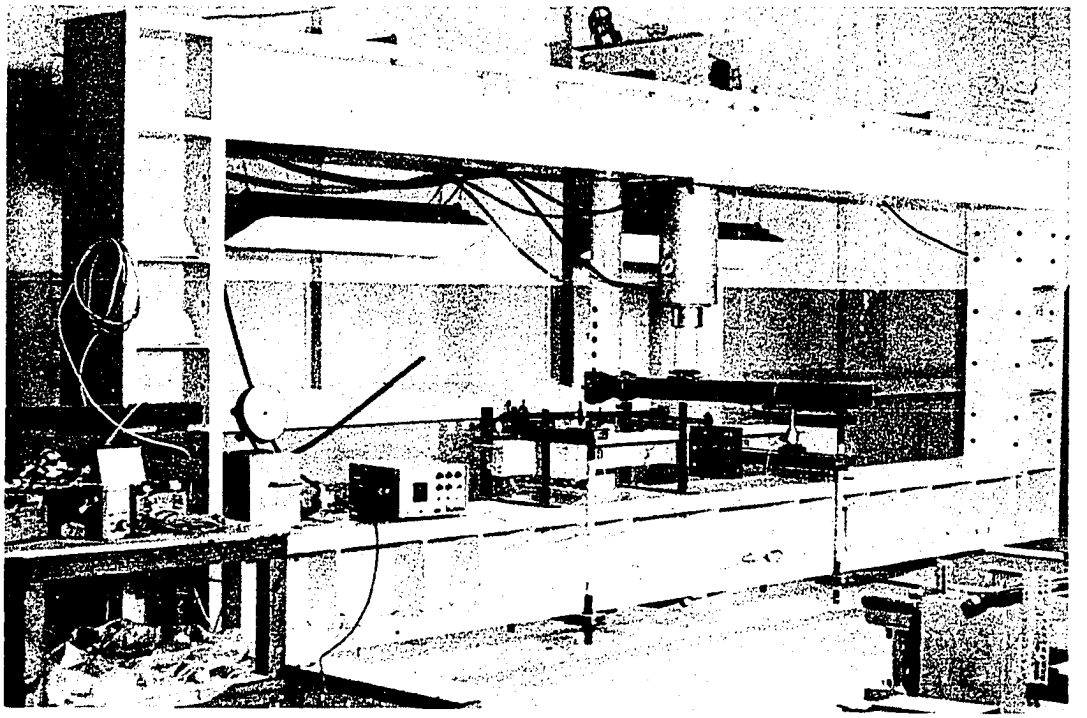
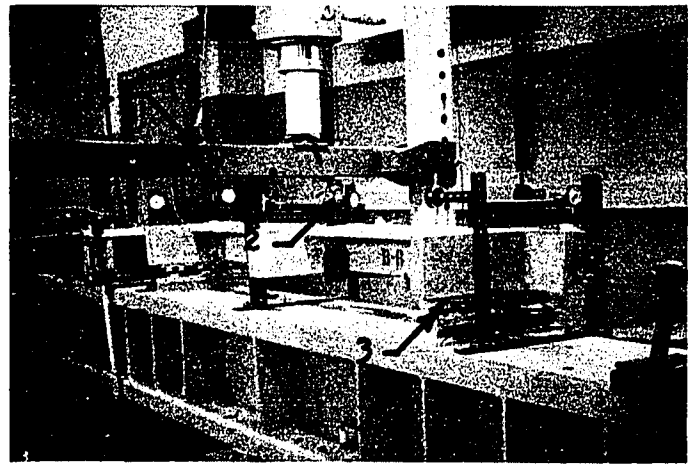
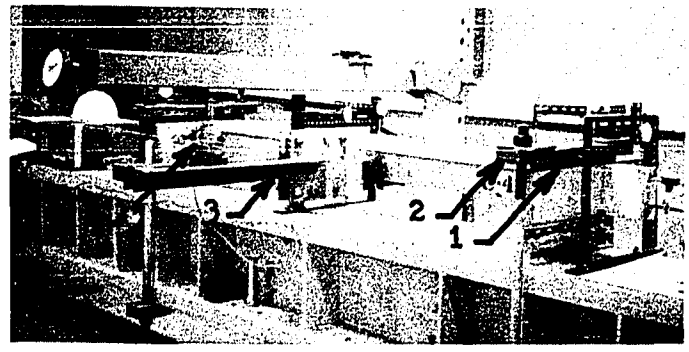


Figure 2.8a General Loading System



1. Lever System 2. Load Cell 3. Roller Support

Figure 2.8b Small and Intermediate Eccentricity Loading System



1. Roller Support
2. Support Diaphragm Collar
3. Loading Arm Extension
4. Load Cell

Figure 2.8c Large Eccentricity Loading System

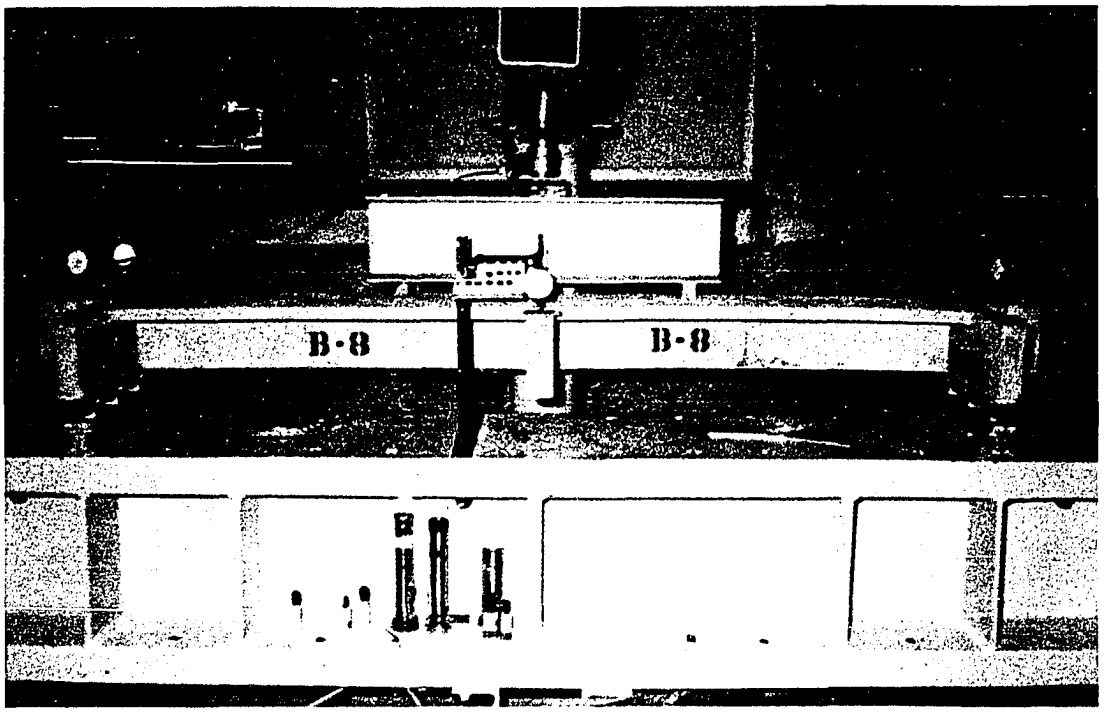


Figure 2.9 Two-Point Loading System

An initial load of approximately 100 pounds was applied to each specimen to hold the load cell and bearing system in position.

Instrumentation

The number of dial gages varied from eleven to fifteen depending on the type of loading. The gages were supported from a small structural frame that was attached to the large test frame (Figure 2.10). Due to the structural rigidity of the large test frame, its deflection was negligible for the small loads used in this study.

Three dial gages were placed on each diaphragm. Two were used to measure vertical deflection and one was used to measure the horizontal deflection of each diaphragm. The vertical gages were also used to measure the twist of the specimens.

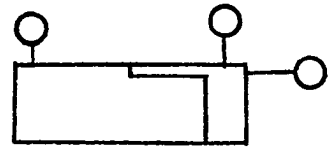
Two gages were attached to the cable of each specimen as shown in Figure 2.10 to check for draw-in of the cable during testing.

Two gages were mounted on the web extension of most of the beams to allow the slope of the ends of the beams to be measured. As a check on the centerline deflection, a gage was mounted at the west quarter-point on most of the beams.

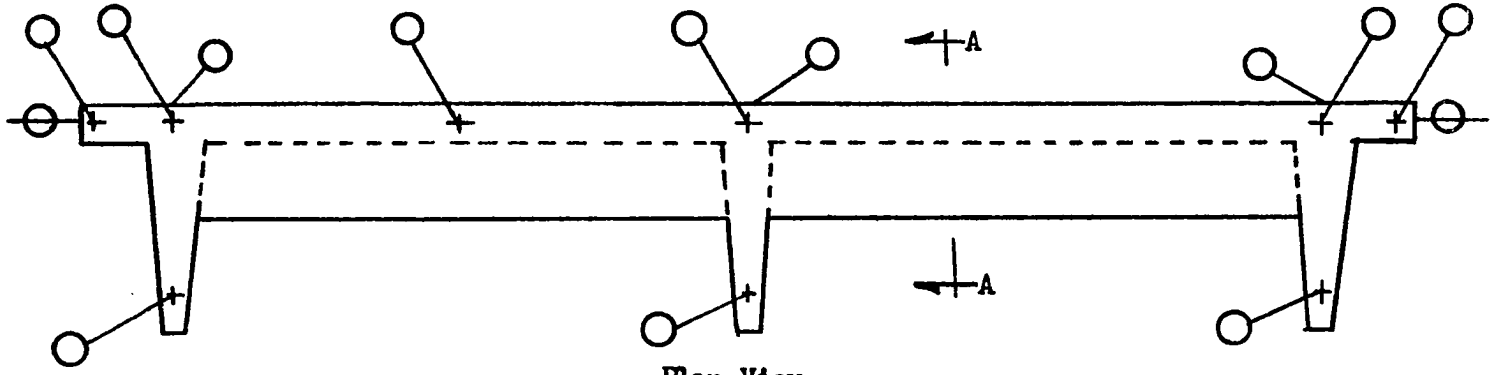
It was noted during testing of some of the specimens that the loading diaphragm developed small tension cracks in the top. Since the dial gage used to measure the twist was mounted on the loading diaphragm, an attachment and gage was added as a check on the twist measurement.

Testing

Initial readings were taken and checked by another reader with the initial load applied as previously explained. The load was applied



Section A - A



Plan View

Figure 2.10 General Test Instrumentation

in increments the magnitude of which varied depending upon the estimated ultimate capacity of the specimen. After each incremental loading was applied and held constant, the dial gages read and recorded, the specimen was then checked for any new cracks and if found they were marked. A magnifying glass was used to help find new cracks and extensions of former ones and mirrors were used to observe the bottom of the beam. The cracks were marked with continuous lines with a hatch mark at the visible end and a number corresponding to the load level. Any cracks that formed during actual collapse were marked with dashed lines.

After all cracks had been marked, the load was adjusted to proper value and the critical dial gages at midspan measuring centerline deflection and angle of twist were checked for creep. If significant changes in the dial reading had taken place, an additional set of data was taken. Otherwise, the load was incremented to the next load level and the procedure repeated.

When the load approached the failure range, the critical gages were monitored carefully to try to obtain the readings at collapse. For safety reasons, the load was allowed to creep off approximately one third of the previous load increment while the cracks were being marked.

The above general loading procedure was followed with but few exceptions which are discussed in Appendix A where a detailed description of each specimen's response is presented.

CHAPTER III

BEHAVIOR OF TEST SPECIMENS

The primary objective of this experimental investigation was to study the behavior of simply supported eccentrically pretensioned prestressed concrete rectangular and L-beams without web reinforcement under the combined loading of torsion, shear and bending. This chapter is devoted to a discussion of the resultant behavior of the test specimens and the effects of flange width, effective prestress, torque-to-shear ratio and torque-to-moment ratio on beam behavior. This discussion is presented as general results with emphasis placed upon ultimate capacity, load-deformation responses and crack patterns. A detailed discussion of the response of each specimen is presented in Appendix A.

The eccentricity, initial cracking shear, torque and moment, type and location of initial cracks are shown in Table 3.1. The ultimate shear, torque, and moment, type and location and symmetry of the ultimate crack pattern and load deformation responses of each specimen are shown in Table 3.2.

The concrete strength was an unintentional variable in this investigation and was accounted for by multiplying torsion and shear by $\sqrt{5500/f'_c}$ and moment by $(5500/f'_c)$. This has been standard practice for many past researchers [Ersoy, 1965], [Farmer and Ferguson, 1967].

TABLE 3.1. INITIAL CRACKING CAPACITY AND CRACK PATTERNS

BEAM	Ecc. (in)	f'_c (psi)	Cracking Capacity			Initial Cracking	
			Shear (kip)	Moment (in-kip)	Torque (in-kip)	Type[a]	Location[b]
A-1	0.0	5036	1.38	49.5	0.06	A	B
A-2-1	6.38	5490	No crack	-	-	-	-
A-2-2	6.38	5490	1.11	40.0	6.72	A	B
A-3	10.0	4833	1.07	21.4	10.16	B	20E
A-4	31.0	5671	0.44	0.0	11.33	B	OE-OW
A-5	1.5	5054	1.28	46.0	1.88	A	B
A-6	21.5	6013	0.59	0.0	11.23	B	OE-OW
A-7-1	0.0	5360	No Crack	-	-	-	-
A-7-2	0.0	5360	1.83	44.0	.06	A	B
A-8	3.5	5371	1.33	43.0	4.48	A	B
A-9	0.0	5481	1.53	55.0	.06	A	B
A-10	26.5	5551	.56	3.4	13.09	B	6E-6W
A-11	16.5	5676	.84	20.0	12.87	B	OE-24W
A-12	1.5	6247	1.53	55.0	2.25	A	B
B-1	0.0	4995	2.10	75.5	.14	A	B
B-2	6.38	4608	1.60	57.5	9.80	A	B
B-3	31.0	4347	2.56	1.1	14.55	B	OW-4E
B-4	26.5	6147	0.46	1.4	10.38	B	OE-6W
B-5	3.5	5787	1.84	66.2	6.29	A	B
B-6	1.5	4300	1.84	66.2	2.78	A	B
B-7	10.0	5369	1.25	35.0	11.84	A	OE-28.5W
B-8	0.0	5536	2.42	58.0	.14	A	B
B-9	21.5	4502	0.57	0.0	10.52	B	OW
C-1	3.5	5575	1.54	55.5	5.26	A	B
C-2	6.38	6075	1.54	55.5	9.47	A	B

TABLE 3.1 (Cont'd.)

BEAM	Ecc. (in)	f'_c (psi)	Cracking Capacity			Initial Cracking	
			Shear (kip)	Moment (in-kip)	Torque (in-kip)	Type[a]	Location[b]
C-3-1	0.0	5135	1.54	55.5	.14	A	B
C-3-2	0.0	5135	-	-	-	-	-
C-4	31.0	7596	0.57	3.4	14.96	B	OE-12W
C-5-2	10.0	6687	1.54	55.5	14.77	A	B
C-6	1.5	5438	1.54	55.5	2.34	A	B
C-7	0.0	5145	1.84	44.2	.14	A	B
C-8	21.5	5109	0.80	8.0	15.55	B	18E-OW
C-9	6.38	5072	1.54	55.5	9.47	A	B

[a](A) implies that the initial crack was a vertical tension crack while (B) implies the initial crack was torsional.

[b]The location of the initial crack in the east half of the beam is given as " " inches from the centerline of the support diaphragm while the initial crack in the west half of the beam is referenced to the centerline of the west support diaphragm. (B) implies that initial cracking occurred near-mid-span and usually more than one crack was observed.

TABLE 3.2. ULTIMATE CAPACITY, ULTIMATE CRACK PATTERN AND LOAD DEFORMATION RESPONSE

BEAM	Ecc. (in)	Ultimate Capacity[a]			Ultimate Cracks		Load Deformation Response[d]	
		Shear (kip)	Moment (in-kip)	Torque (in-kip)	Type[b]	Location[c]	Shear-℄ Def.	Torque-Twist
A-1	0.0	1.73	49.71	.06	B	27.5 E None W	1	-
A-2-2	6.38	1.24	37.57	7.50	B	27.5 E 30 W	3	3
A-3	10.0	1.14	29.76	10.82	D	24.5 E None W	2	2
A-4	31.0	.43	2.85	11.15	D	8.5 E 4.5 W	2	2
A-5	1.5	2.48	73.37	3.69	B	28.5 E 0 W	1	1
A-6	21.5	.57	2.74	10.73	D	4.5 E 4.5 W	2	2
A-7-2	0.0	0.0	84.79	.06	A	Two Pt. Load	1	-
A-8	3.5	1.97	60.33	6.75	C	29.0 E 31.5 W	1	3
A-9	0.0	2.17	53.22	.06	B	None E 29.5 W	1	-
A-10	26.5	.57	9.29	13.52	D	15.0 E 18.0 W	2	2
A-11	16.5	.86	24.40	13.21	D	29.5 E 28.5 W	2	2
A-12	1.5	2.06	50.99	3.06	B	24.0 E 24.0 W	1	3

TABLE 3.2. ULTIMATE CAPACITY, ULTIMATE CRACK PATTERN AND LOAD DEFORMATION RESPONSE (Cont'd.)

BEAM	Ecc. (in)	Ultimate Capacity[a]			Ultimate Cracks		Load Deformation Response[d]	
		Shear (kip)	Moment (in-kip)	Torque (in-kip)	Type[b]	Location[c]	Shear-℄ Def.	Torque-Twist
B-1	0.0	2.86	89.93	.15	B	None E 30 W	1	-
B-2	6.38	2.11	67.12	12.99	C	24.5 E 28 W	3	3
B-3	31.0	.62	8.19	16.20	D	16.5 E 7 W	2	1
B-4	26.5	.59	5.64	13.00	D	6 E 13.5 W	2	3
B-5	3.5	2.28	65.66	7.83	C	31.5 E 27.5 W	1	3
B-6	1.5	2.91	94.49	4.83	C	None E 28.5 W	1	1
B-7	10.0	1.37	40.43	13.02	C	None E 28.5 W	3	3
B-8	0.0	0.0	102.03	.14	A	Two Pt. Load	1	-
B-9	21.5	.77	5.97	14.86	D	6 E 8 W	3	3
C-1	3.5	2.26	64.39	7.76	C	29 E 29 W	1	1
C-2	6.38	1.64	44.21	10.13	C	28 E 28.5 W	2	2
C-3-2	0.0	2.62	72.35	.14	B	None E 27 W	1	-

TABLE 3.2. ULTIMATE CAPACITY, ULTIMATE CRACK PATTERN AND LOAD DEFORMATION RESPONSE (Cont'd.)

BEAM	Ecc. (in)	Ultimate Capacity[a]			Ultimate Cracks		Load Deformation Response[d]	
		Shear (kip)	Moment (in-kip)	Torque (in-kip)	Type[b]	Location[c]	Shear-℄ Def.	Torque-Twist
C-4	31.0	.54	6.00	14.22	D	9 E 18 W	2	2
C-5-2	10.0	1.43	32.78	13.72	C	24 E 28.5 W	2	2
C-6	1.5	2.47	64.80	3.72	B	None E 26 W	1	1
C-7	0.0	0.0	97.05	.14	A	Two Pt. Load	1	-
C-8	21.5	.83	4.9	16.10	D	28 E 6 W	2	2
C-9	6.38	1.94	54.27	12.00	C	31 E 31 W	3	3

[a] Shear, moment and torque values converted to f'_c = 5500 psi by multiplying by $\sqrt{5500/f'_c}$, $5500/f'_c$ and $\sqrt{5500/f'_c}$, respectfully.

[b] (A) implies a vertical flexural type crack, (B) implies a flexural-to-diagonal tension crack, (C) implies flexural-to-diagonal tension with torsional effects noticeable and (D) implies torsional with secondary shear cracks.

[c] The location of the ultimate crack in the east half of the beam is given as " " inches from the centerline of the support diaphragm while the ultimate crack in the west half of the beam is referenced to the centerline of the west support diaphragm.

[d] (1) implies initially linear load deformation response up to first cracking with long nonlinear portion after first cracking, (2) implies initially linear response up to first cracking with reduction in capacity at first cracking and (3) implies a transition between the two responses.

Shear-centerline deflection, shear-slope of ends and torque-twist curves are given in Appendix B. In these figures no adjustment was made for any variance of concrete strength, but the dead load due to the web, flange, loading diaphragm and the loading system was included in the recorded values. The shear and torque was calculated at the support in order to give a consistent calculation.

The twist of the specimen at each diaphragm was calculated by dividing the difference between the deflections of the two vertical dial gages by the horizontal distance between them. The net twist of the loading diaphragm was calculated by algebraically subtracting the average of the end twists. The unit twists were obtained by dividing the net twists by the distance between mid-span and the end of the span.

The relative centerline deflection was calculated by algebraically subtracting the average of the end deflections from that measured by the dial gage placed at mid-span.

Most of the specimens were equipped with a dial gage at the quarter point to allow the vertical deflection at the quarter point to be measured. These quarter point deflections were used as a check on the centerline deflections.

The slope at each end of most of the specimens was calculated by dividing the difference between the deflection of the support and the deflection of the web extensions by the distance between the gages.

These slopes were measured to give an indication of the symmetry of the collapse of the specimen and a check on the centerline deflection.

Ultimate Strength

Influence of Eccentricity

The eccentricity (the perpendicular distance from the centerline of the web to the point of application of the load) had a definite effect upon the ultimate capacity of the specimens primarily because the magnitude of the eccentricity had an effect upon the failure mode. With small eccentricities, the failure mode was similar to that of a flexure-to-shear type failure. The specimens tested with small eccentricities had rather large load capacities compared to those of the large eccentricities which caused torsional type failures.

Since the shear was directly related to the load (the live load was equal to twice the live shear) and the moment was directly related to the shear (the specimens were simply supported) for the particular test set-up that was used in this study, the shear and moment capacities appeared to decrease as the eccentricity was increased as shown by the interaction surfaces and the projections on the torque-moment and the torque-shear planes of Figures 3.1 a, b and c.

The torsional capacity of the specimens, however, appeared to increase as the eccentricity was increased because the torque was related to the product of shear and eccentricity.

Influence of the Overhanging Flange

Two flange widths were used as explained in Chapter II. These overhanging flange widths were zero inches for series A and 6 inches

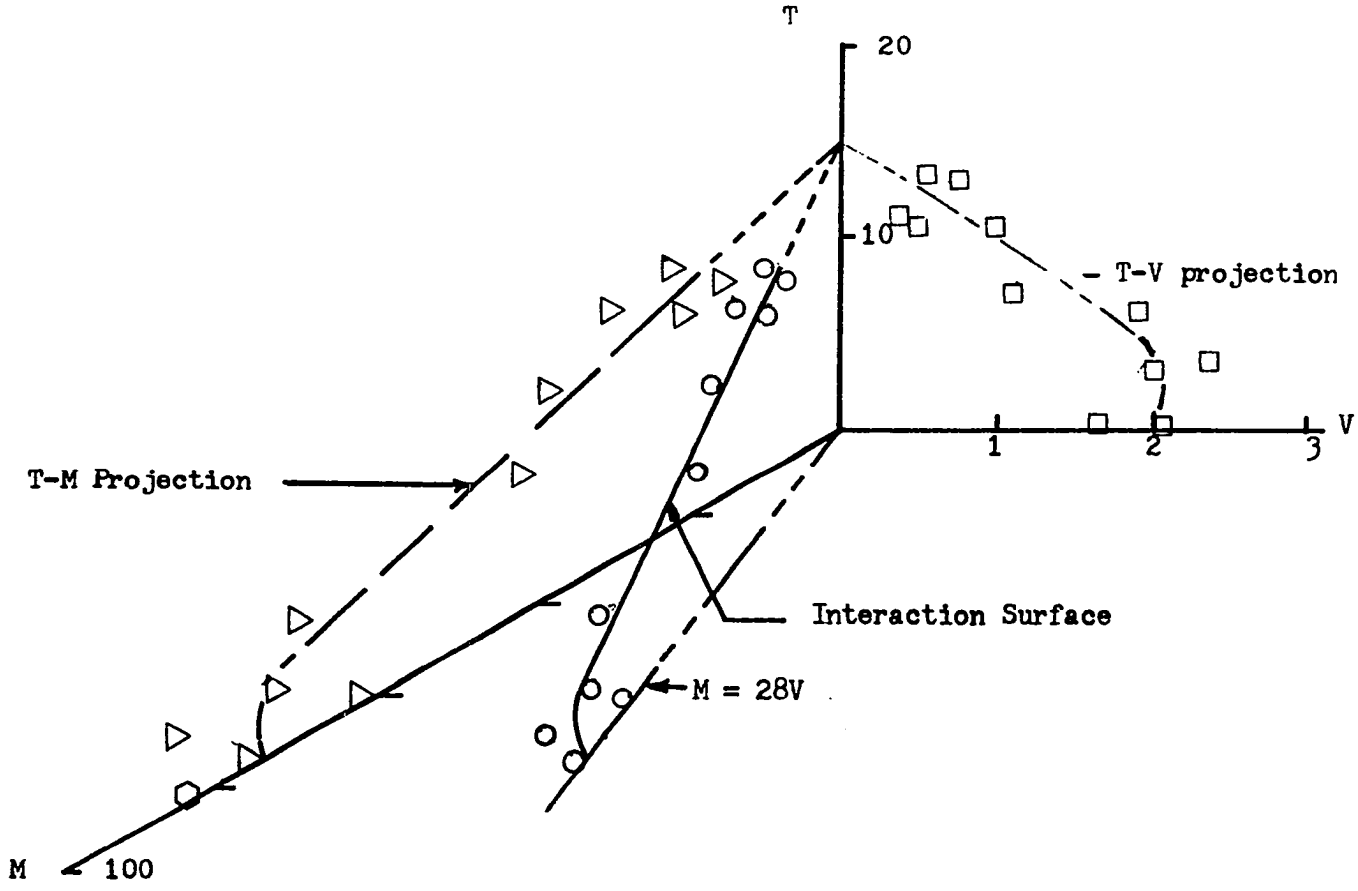


Figure 3.1a Ultimate Capacity Interaction Surface for Series A

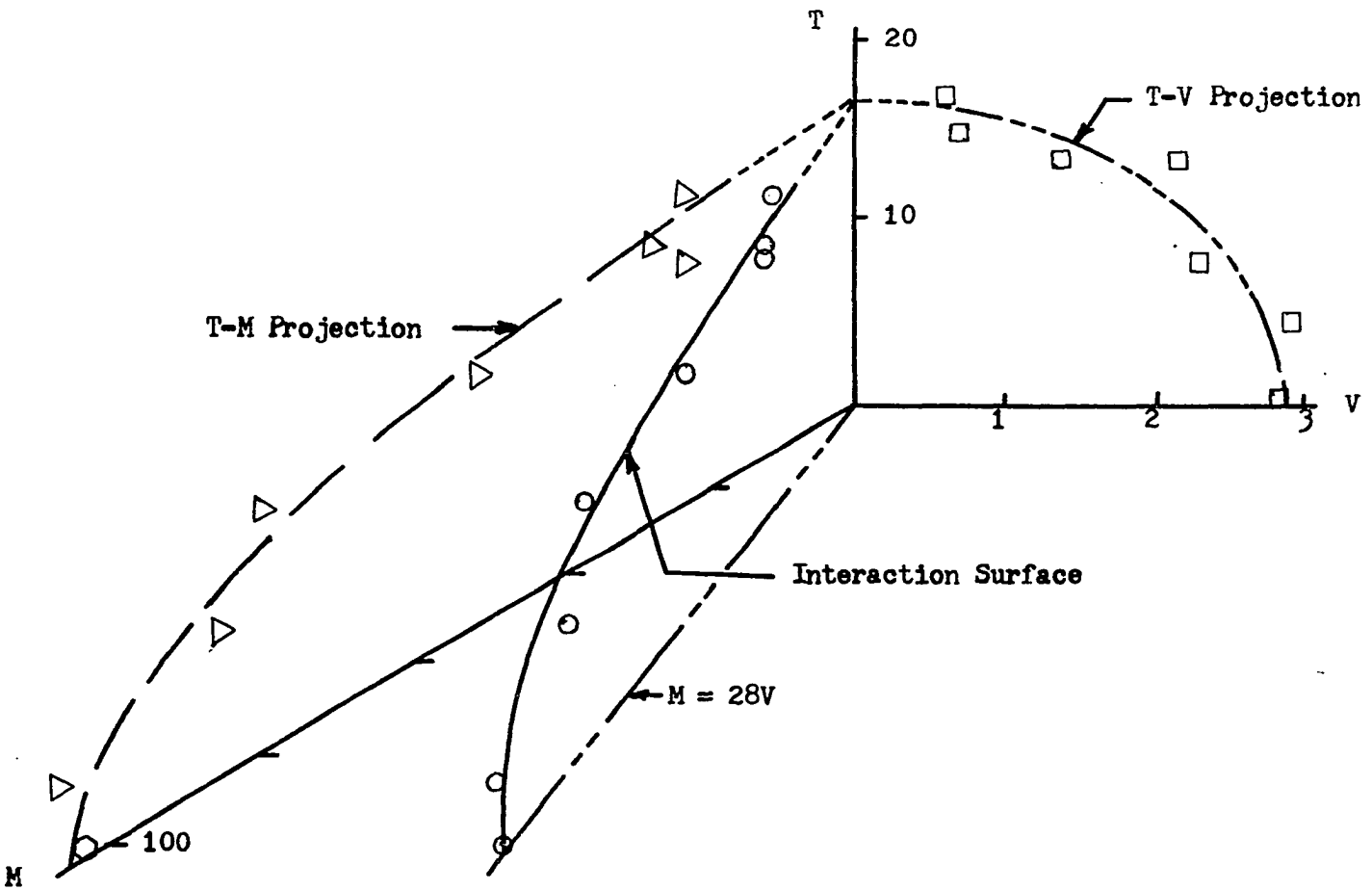


Figure 3.1b Ultimate Capacity Interaction Surface for Series B

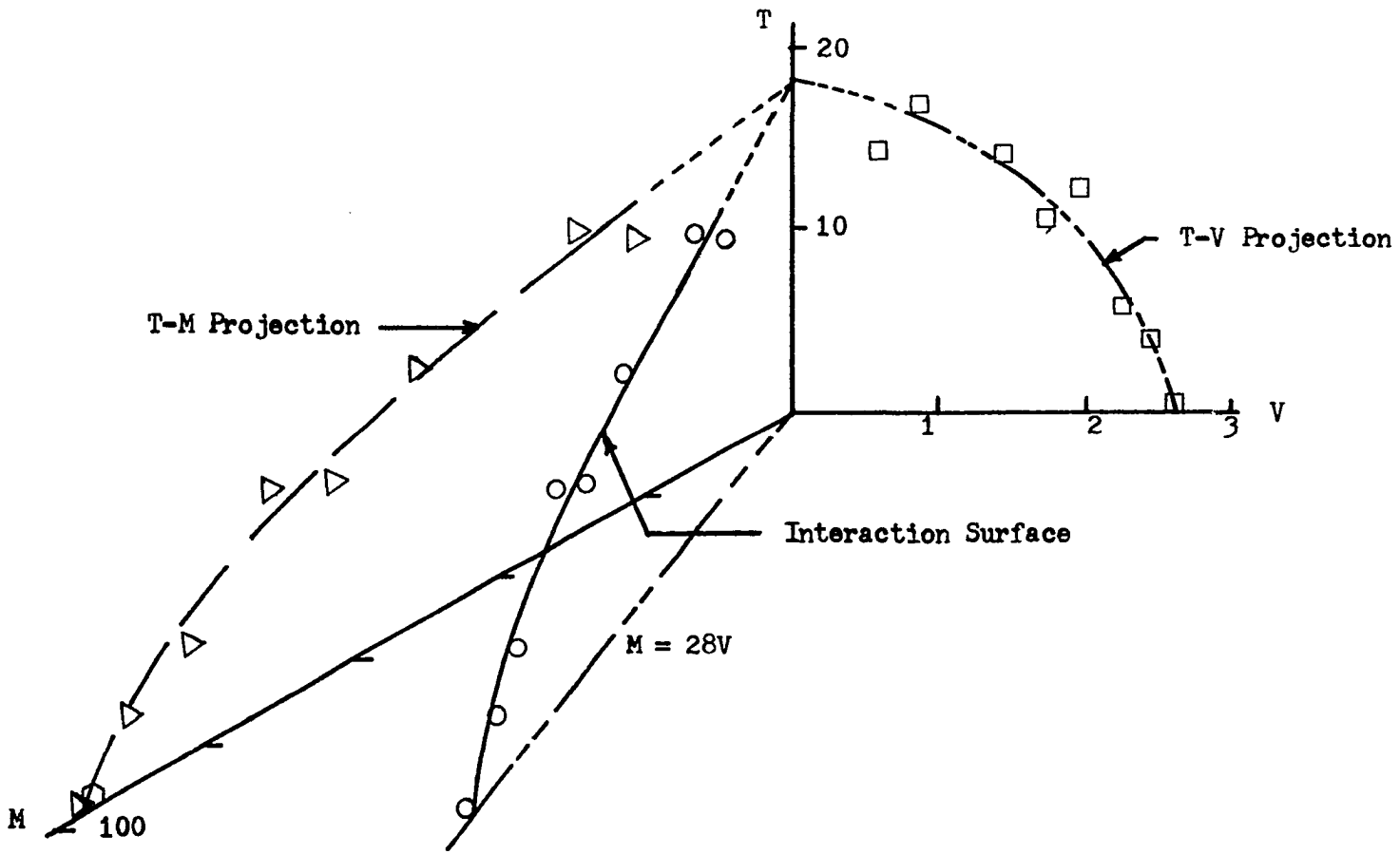


Figure 3.1c Ultimate Capacity Interaction Surface for Series C

for series B and C. Since the effective prestress of series C was comparable to that of series A, the influence of the overhanging flange was made by comparing these two series.

The interaction surfaces of series A and series B are shown in Figure 3.2. The most apparent effect of the overhanging flange can be observed by noting that the surface for series A lies totally inside that of series C indicating that the capacity of series C was larger than that of series A for all eccentricities tested.

Influence of Effective Prestress

Since the only variable between series B and C was the effective prestress, the influence of the effective prestress can be observed by comparing the interaction surfaces of series B and series C. The cable for series B was located lower than that of series C (Figure 2.1) giving more initial compression in the bottom fibers of series B. Figure 3.3 shows the two interaction surfaces from which it can be observed that each can be represented by a separate smooth curve.

The second basic observation is that the two surfaces intersect. This intersection implies that at approximately 20 inches of eccentricity the two series had the same ultimate capacities. This can be explained partly by noting that series C had a greater initial compression stress at the center of the vertical face than did series B. This gave series C more resistance to principal tensile stress due to torsion which was the primary failure mode for large eccentricities. The larger compression stress in the bottom fibers of series B as compared to series C gave series B more ultimate flexural capacity than series C.

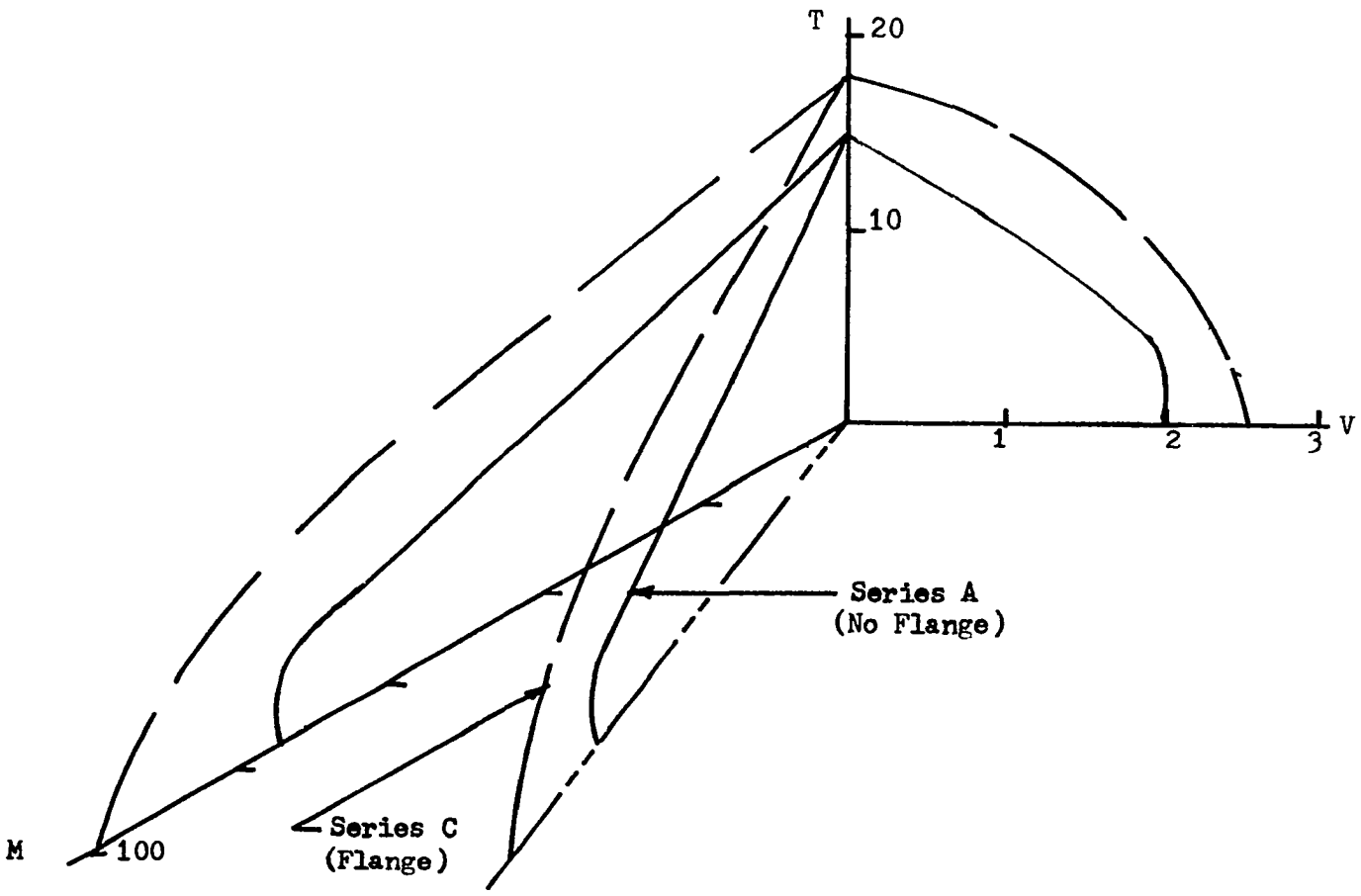


Figure 3.2 Influence of the Overhanging Flange on the Ultimate Capacity Interaction Surfaces

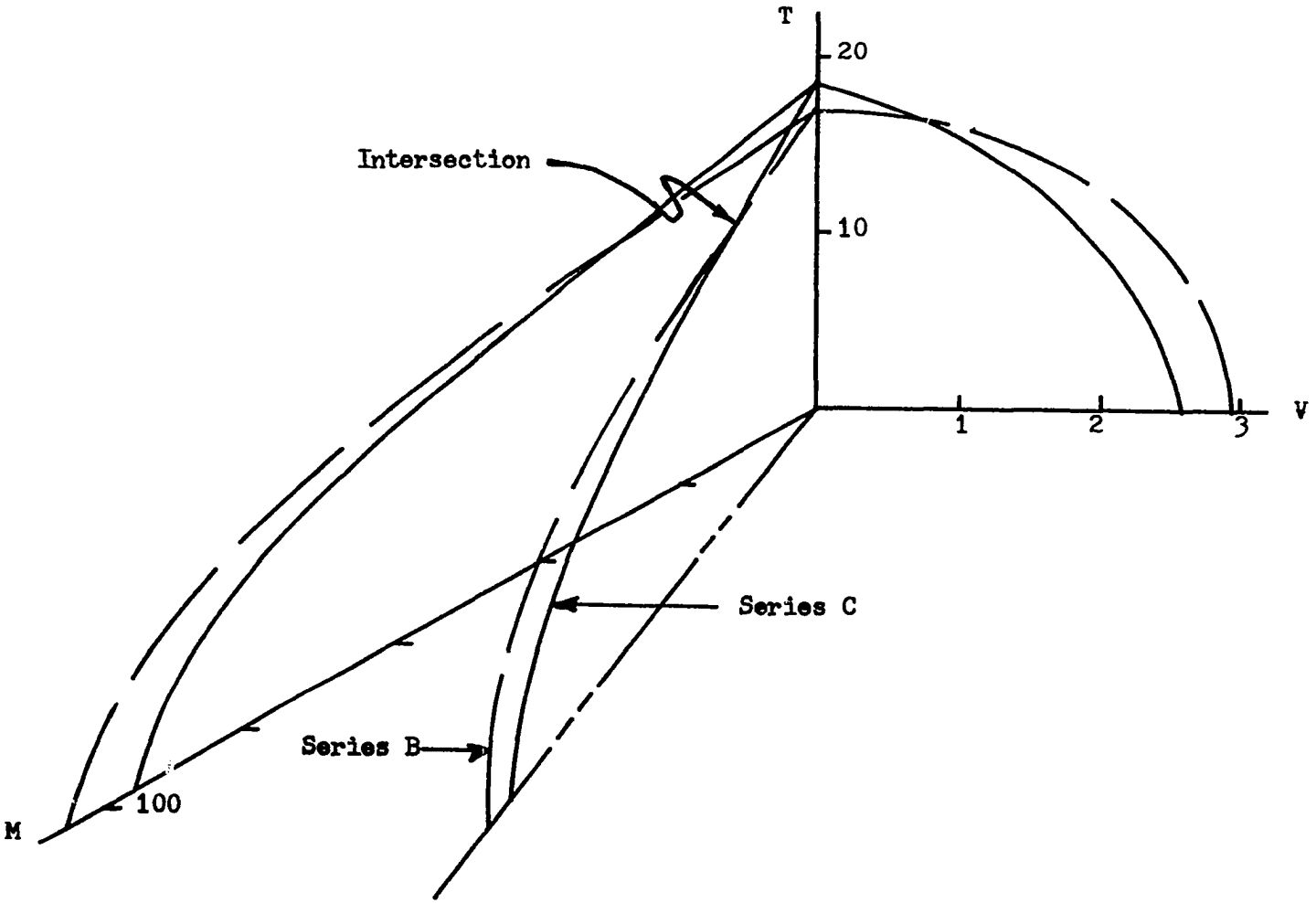


Figure 3.3 Influence of Effective Prestress on the Ultimate Capacity Interaction Surfaces

Since series C was more efficient in torsion than series B and series B was more efficient in flexure than series C, the two interaction surfaces should intersect as indicated.

Crack Pattern

A detailed description of initial cracking and ultimate cracking for each specimen is presented in Appendix A. The purpose of this section is to present a composite picture of the crack patterns of the different series and how some of the most important parameters affected the crack patterns.

It should be kept in mind that the torsional stresses and the shear stresses were of an additive nature on the south face while they tended to cancel each other on the north face.

It should also be remembered that the specimens of this study did not contain web reinforcement which would indicate that certain types of cracks would cause immediate collapse upon their formation, namely torsional and diagonal tension cracks.

Influence of Eccentricity

The effect of the eccentricity was observed by the different failure modes that were obtained with all three series showing the same general trend. The failure modes and the crack patterns varied between two distinct types.

Figures 3.4, 3.5 and 3.6 show the three typical crack patterns of specimens tested with small, large and intermediate eccentricity, respectfully. On each page, starting from the bottom, the first picture is the general view of the tested specimen; the second, the south view; the third, the top view; the fourth, the north view; the fifth, the bottom view, respectfully. The pictures are positioned in such a way in each view that the east end of the specimen is on the right-hand side of the page to allow the cracks to be traced from one view to the next. The white marks on the support table were placed at an equal spacing of 6" to allow relative distances to be visible.

When the eccentricity was small, the failure mode was a flexure-to-shear type collapse as shown in Figure 3.4. This mode in general had first cracks of vertical tension type in the bottom of the web with an initial linear load-deformation response. When the load was increased, the flexural cracks extended and new ones developed until a diagonal tension crack developed and propagated through the compression zone.

Large eccentricities resulted in the other distinct type of failure mode which usually consisted of only a very few cracks near the support diaphragms as shown in Figure 3.5. These were the typical spiral cracks up the south face and over the top of the web. In most of the specimens secondary shear caused the cracks at the top of the north face to turn back toward the support rather than continue on their spiral path. Since no web reinforcement was used in the specimens of this study, this type of collapse occurred at the initial cracking load which was also the ultimate capacity.

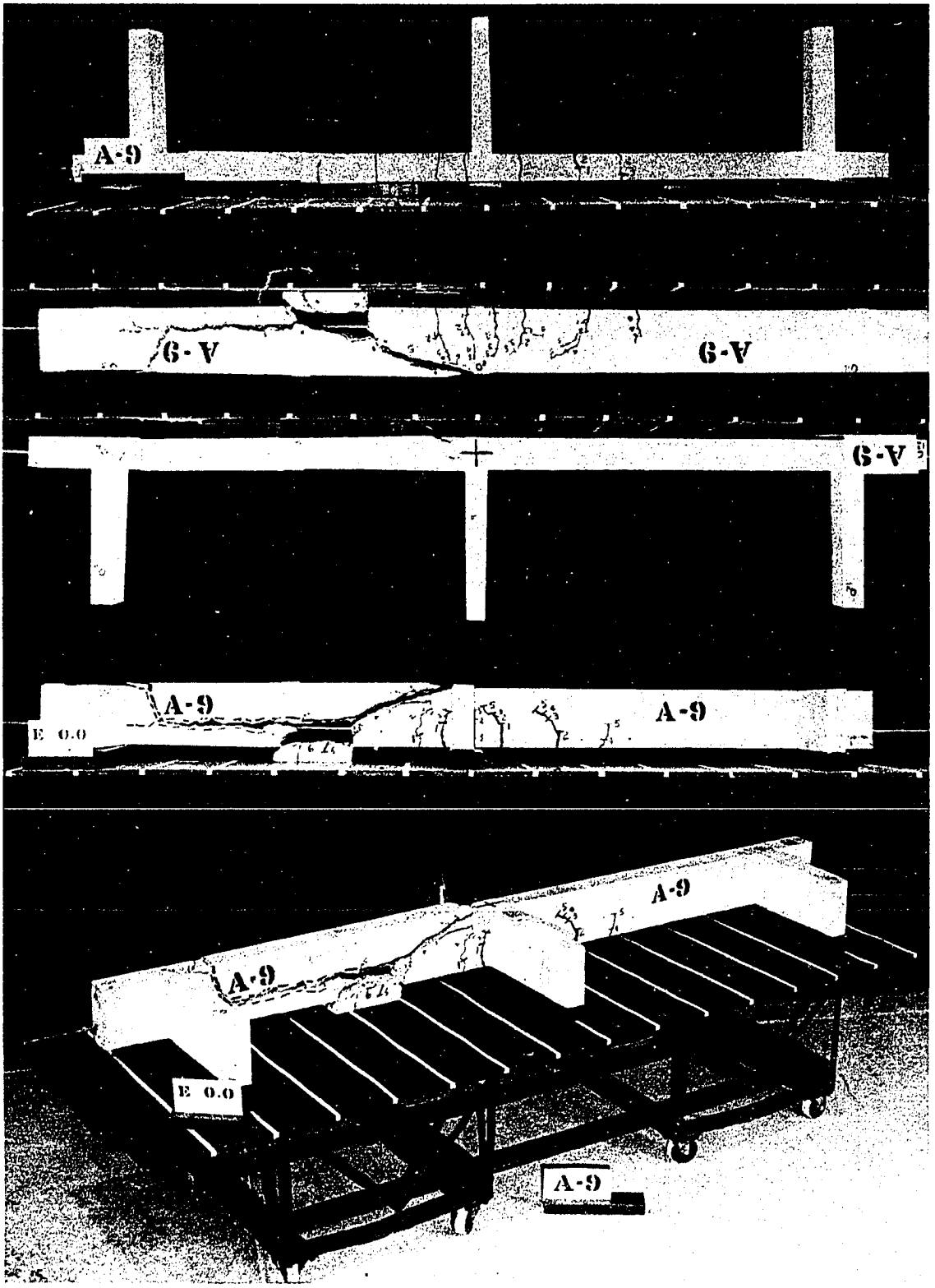


Figure 3.4 Typical Crack Pattern for Zero Eccentricity (A-9)

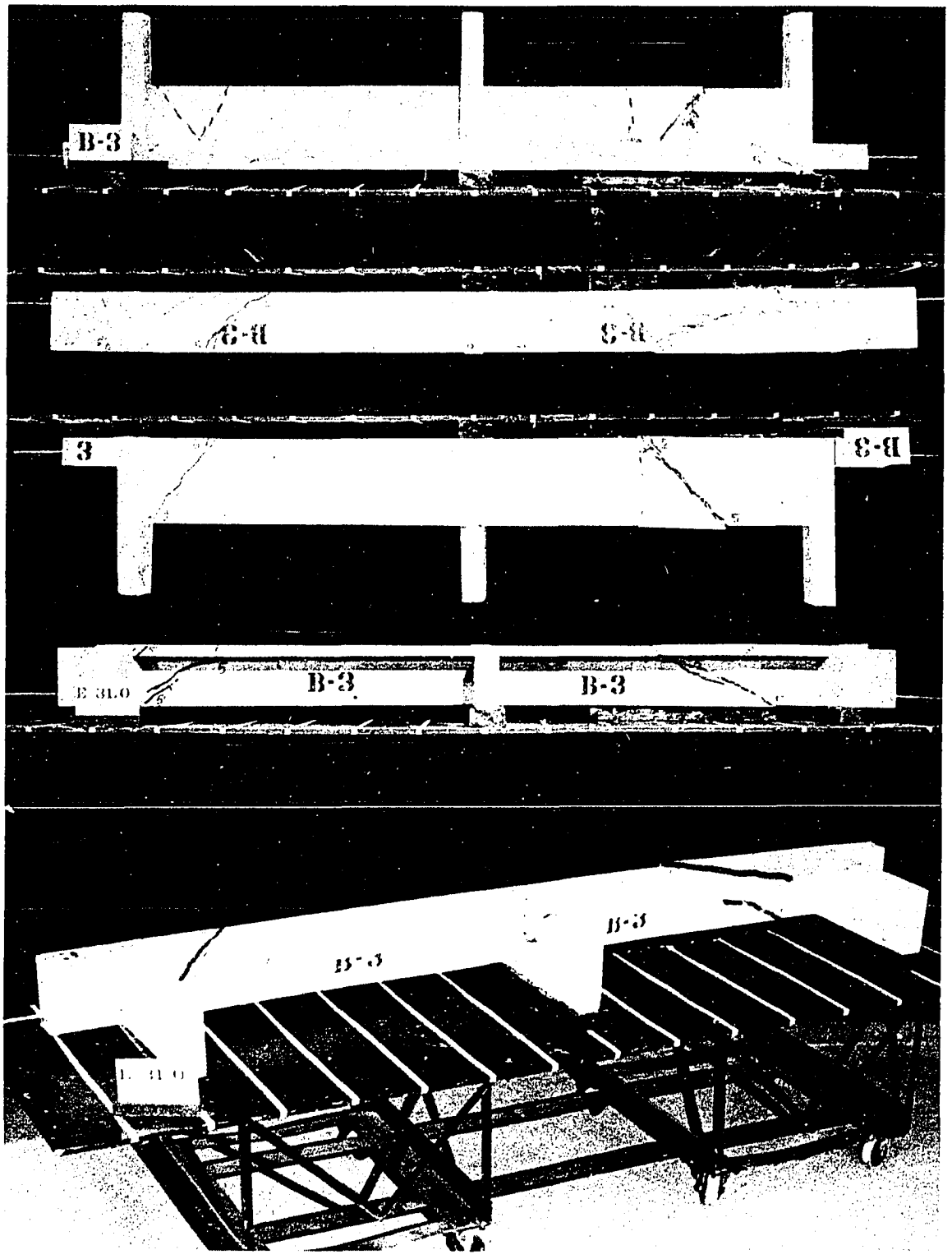
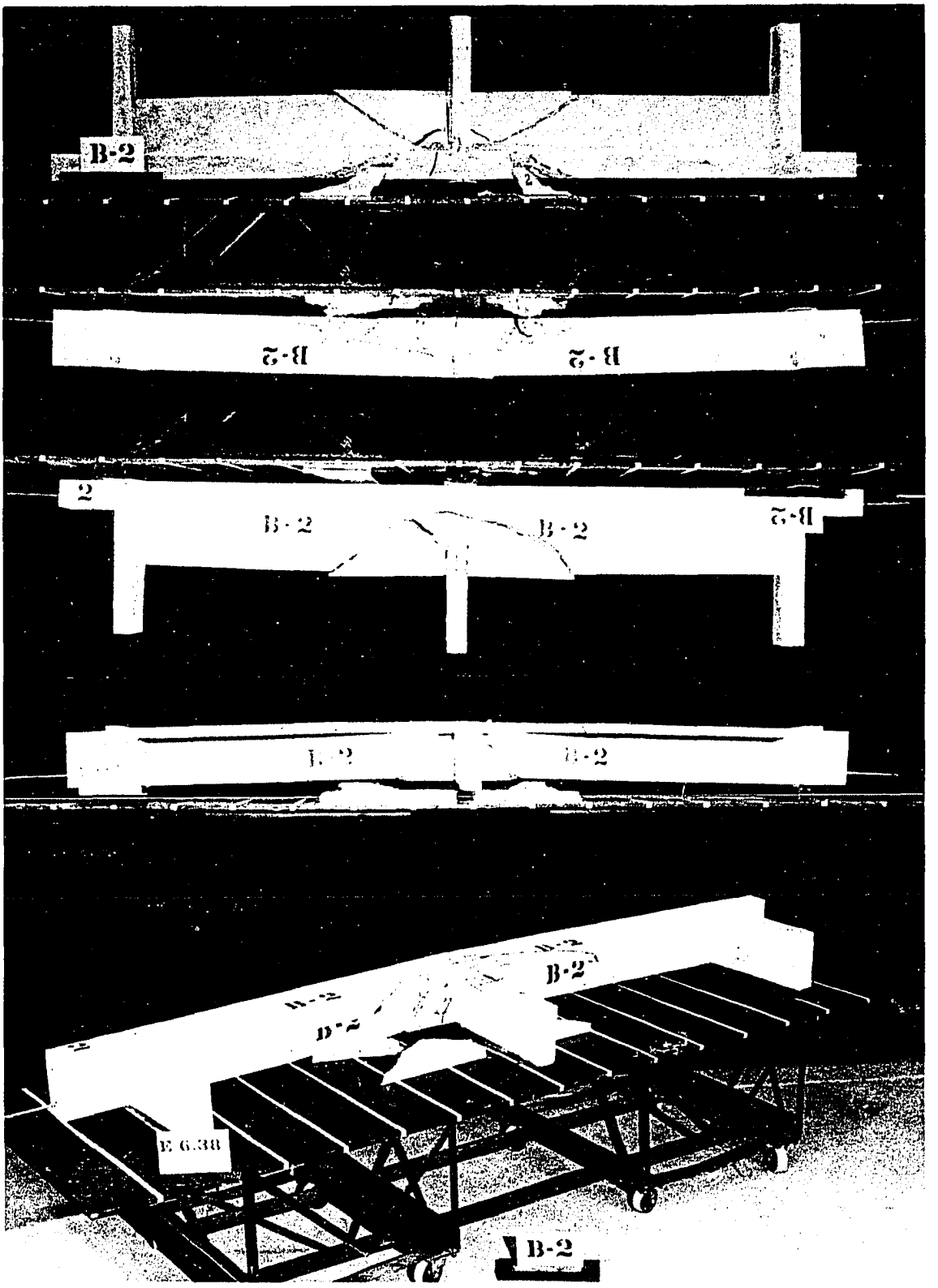


Figure 3.5 Typical Crack Pattern for Large Eccentricity (B-3)


B-2
B-2
B-2

The crack patterns of the specimens tested with intermediate eccentricities were made up of a combination of the two distinctive crack patterns with the dominating one depending upon the magnitude of the eccentricity (See Figure 3.6). Most of the intermediate crack patterns appeared to be flexure-to-shear type failures when only the south face was observed. The effect of the eccentricity could be seen by noting, first, that the vertical cracks in the north face did not propagate as far as their companions in the south face, and second, that many of the failure cracks did not reach the top of the specimen in the north face as they did in the south face.

Horizontal bending was noted in specimens of series B and C loaded with small and intermediate eccentricities by the formation of tension cracks in the south edge of the overhanging flange near midspan (see Figure 3.6). These cracks occurred in the upper range of the loading history and propagated perpendicularly to the longitudinal axis of the specimen. Since series A did not have the overhanging flange, the horizontal bending was not directly observable by noting the crack pattern.

Shear-Centerline Deflection

The shear-centerline deflection curve for each of the beams is given in Appendix B. A detailed discussion of the shear-centerline deflection for each individual specimen can be found in Appendix A. The

purpose of this section is to discuss the shear-centerline deflection as it was influenced by the most important parameters of this study.

Influence of Eccentricity

The eccentricity of the load was the primary cause of the deviations of the general shapes of the shear-centerline deflection curves. The curves fall in a transition zone between that of zero eccentricity and that of large eccentricity. Figure 3.7 shows the two extreme curves for each series. The short linear curves are those for the specimens tested with an eccentricity of 31.0 inches and are linear up to the ultimate load of the specimens.

The curves with the long non-linear portions are those for the specimens tested with zero eccentricity and show an initial linear portion up to the initial cracking shear at which point they tend to show the nonlinearity of the cracked section's response. The ultimate deflection of the specimens loaded with zero eccentricity had a magnitude of from 8 to 10 times that of the elastic deflection.

The shear-centerline deflection curves for intermediate eccentricities fall inside the two extremes with the general shape depending upon the magnitude of the eccentricities.

The magnitude of the eccentricity had no effect upon the initial rigidity of the specimens as shown by the initial slopes of each series of the shear-centerline deflection curves being the same for zero and large eccentricities (Figure 3.7).

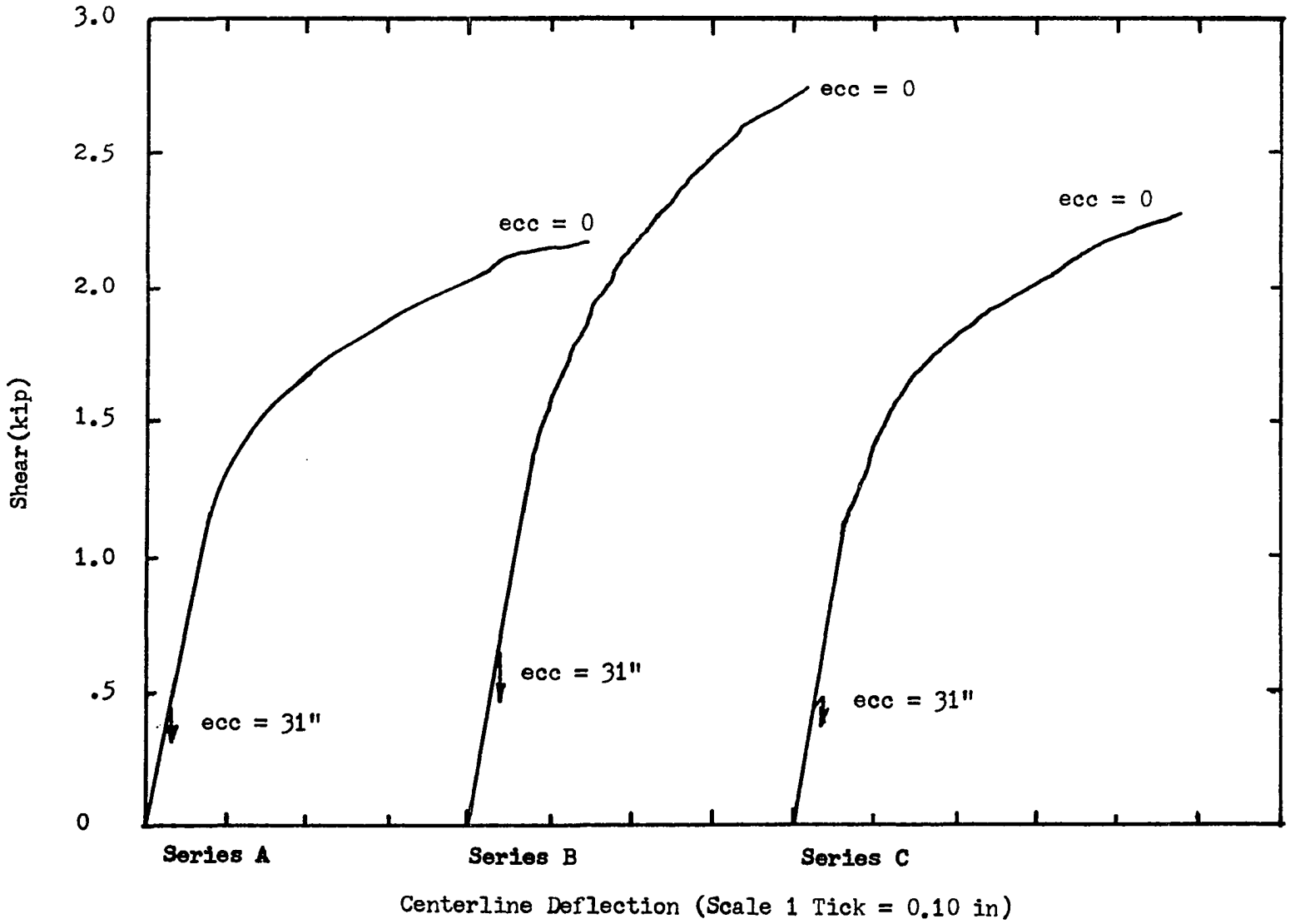


Figure 3.7 Influence of Eccentricity on the Shear-Centerline Deflection

Influence of the Overhanging Flange

The influence of the flange upon the shear-centerline deflection is shown in Figure 3.8 which is a composite plot of the two extreme eccentricities (0 inches and 31.0 inches) for series A and C. Series A and C are compared since the effective prestress of these two series was the same. The initial slope of the series C is larger than that of series A due to the increased moment of inertia of series C resulting from the addition of the flange.

The magnitude of the cracking and ultimate shear was also larger for series C for small and large eccentricities as shown by the heights of the curves in Figure 3.8.

Influence of Effective Prestress

The influence of the effective prestress can be seen in Figure 3.9 by comparing series B to that of series C for common eccentricities.

At low eccentricities, the shear-centerline deflection curves for series B indicate a larger ultimate shear capacity than that of series C. The trend is just the reverse for larger eccentricities with the transition zone at an eccentricity of approximately 10 inches.

The slope of the initial linear portions of series C is slightly larger than that of series B. This additional slope can be explained by noting that the specimens of series B had small tension cracks in the top due to the initial prestress. These initial cracks decreased the initial moment of inertia of the specimens of series B.

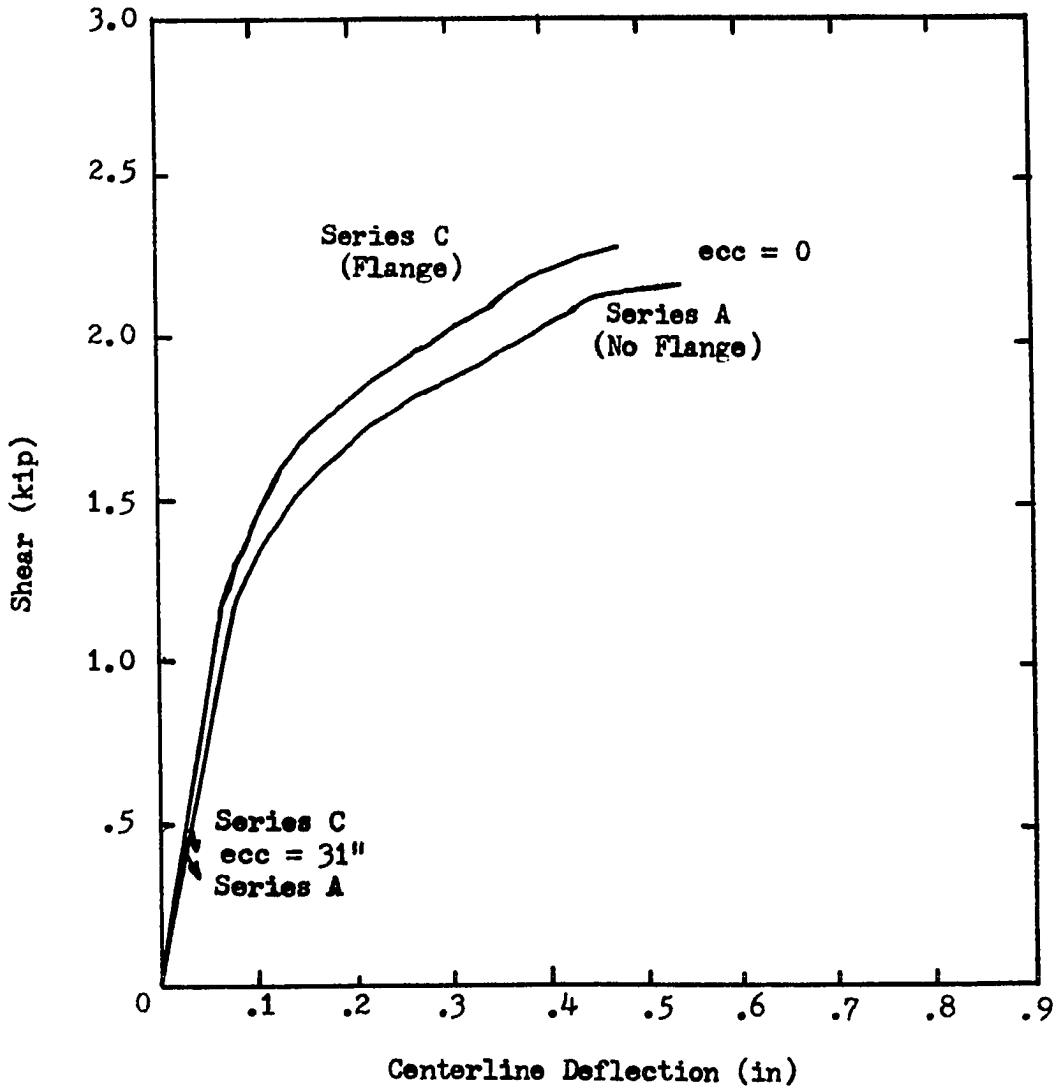


Figure 3.8 Influence of Overhanging Flange on the Shear-Centerline Deflection

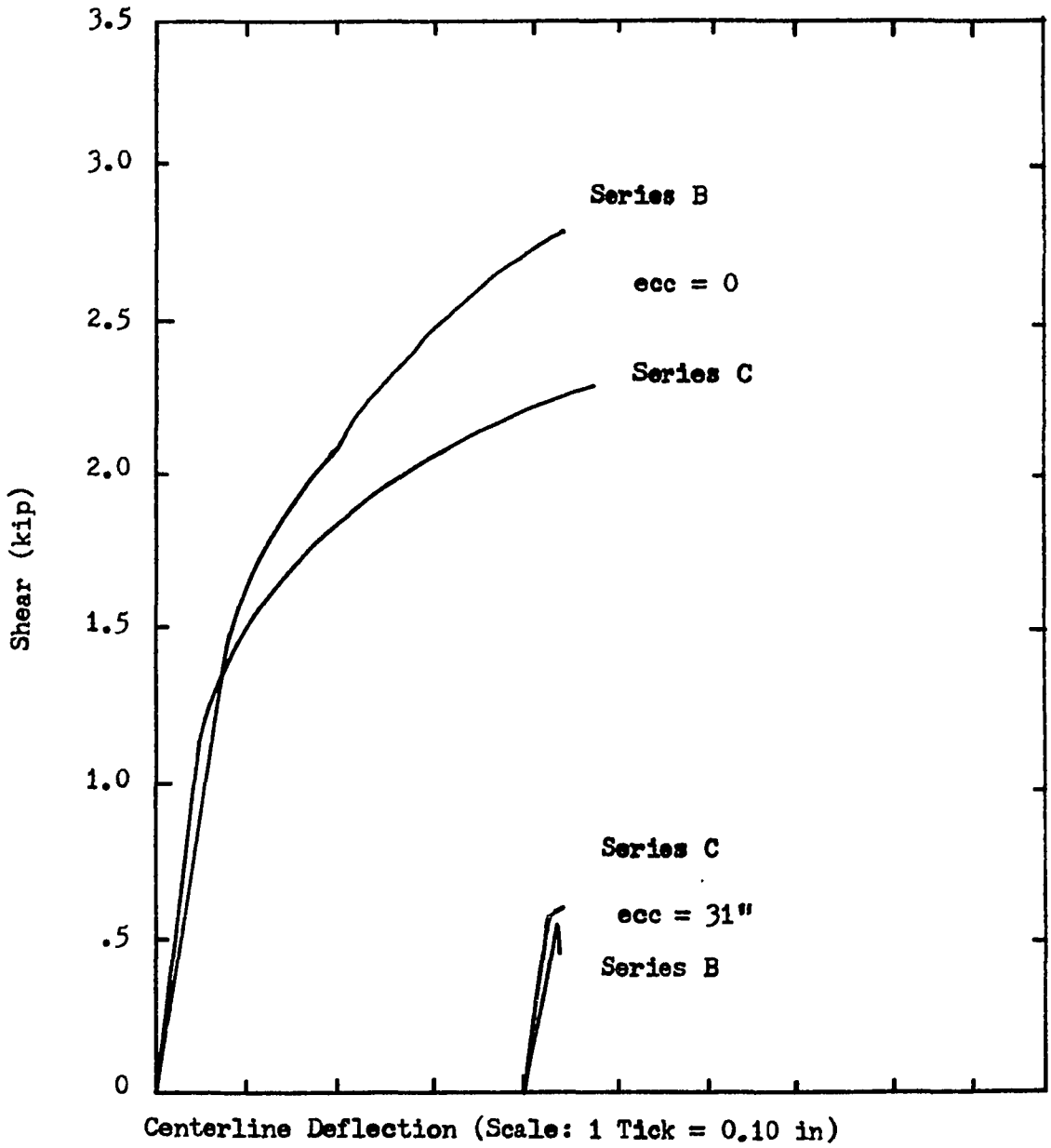


Figure 3.9 Influence of Effective Prestress on the Shear-Centerline Deflection

Torque-Twist Curves

The torque-twist curve for each of the beams is given in Appendix B. A detailed discussion of the torque-twist curve for each individual specimen can be found in Appendix A. The purpose of this section is to discuss the torque-twist curve as it was influenced by the most important parameters of the study.

Influence of Eccentricity

The eccentricity of the load was the primary cause of the deviations of the general shapes of the torque-twist curves. The curves fall in a transition zone between that of a small eccentricity and that of a large eccentricity. Figure 3.10 shows the two extreme curves for each series.

Large eccentricity resulted in large torque but the initial cracking load was also the ultimate capacity of the specimen as can be noted by the shape of the taller almost linear curves for all three series of Figure 3.10. These curves exhibit only a slight amount of non-linear response before a drastic decrease in the capacity of the specimens occurred.

The shorter curves for all three series for an eccentricity of 1.5 inches had a long non-linear response before the ultimate capacity of the specimen was obtained. This long non-linear portion of the curve can be explained by noting that small eccentrically loaded specimens failed in a flexure-to-shear type of collapse. With this type of collapse, the specimen had several vertical cracks in the web which reduced the torsional rigidity of the specimen resulting in large twists for small torques.

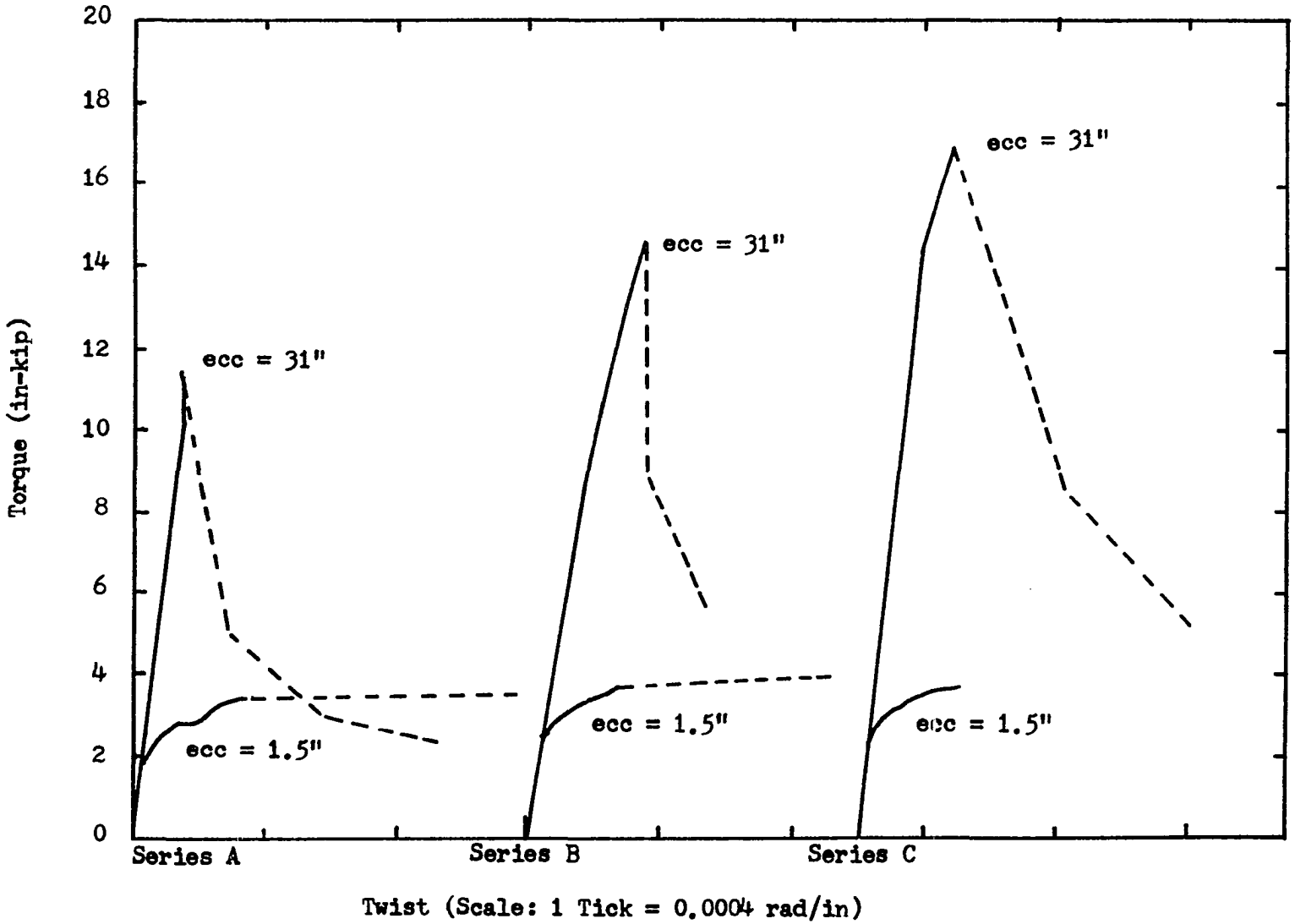


Figure 3.10 Influence of Eccentricity on the Torque-Twist Response

The initial curves for all of the specimens of a particular series had the same slope indicating that the amount of the eccentricity had no effect upon the initial torsional rigidity of the specimen.

Influence of the Overhanging Flange

The influence of the overhanging flange upon the torque-twist curve is shown in Figure 3.11 which is a composite plot of the small and large eccentricities for series A and C. The primary variable between these two series was the overhanging flange since the initial prestress was the same for the two series.

The initial slope of the torque-twist curves for series C are greater than that of series A indicating that series C had a greater initial torsional rigidity than that of series A. Figure 3.11 indicates the initial cracking, as well as, the ultimate capacity of series C was greater than that of series A as was explained previously in this chapter.

Influence of Effective Prestress

The effect of the prestress can be seen in Figure 3.12 which is a composite plot of the torque-twist curves of large and small eccentricities for series B and C. The slope of the initial linear portions of the curves for series C is slightly greater than that for series B indicating that series C had a slightly greater torsional rigidity than the series B.

Figure 3.12 also indicates that the cracking torque and the ultimate torque for series C were greater than that of series B for large eccentricities.

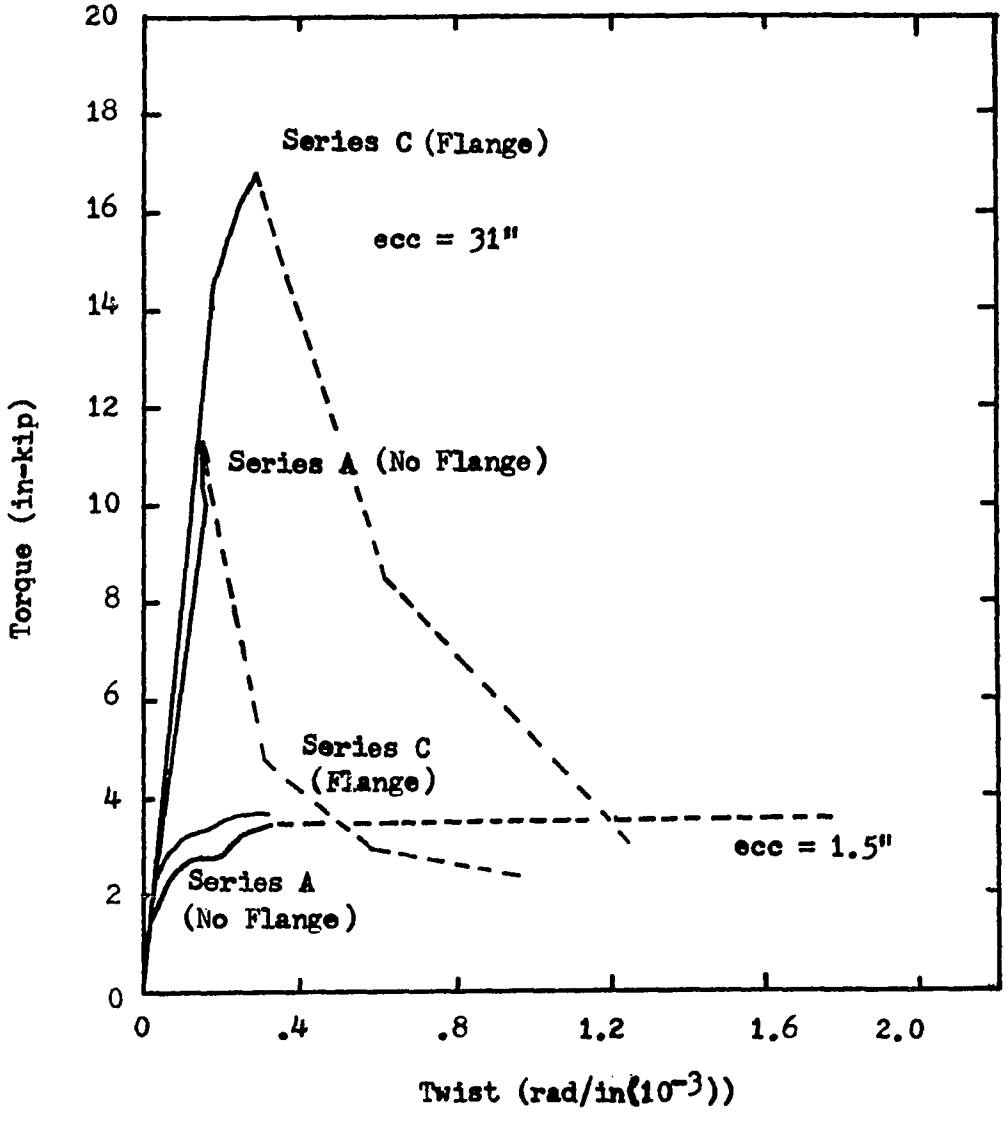


Figure 3.11 Influence of Overhanging Flange on the Torque-Twist Response

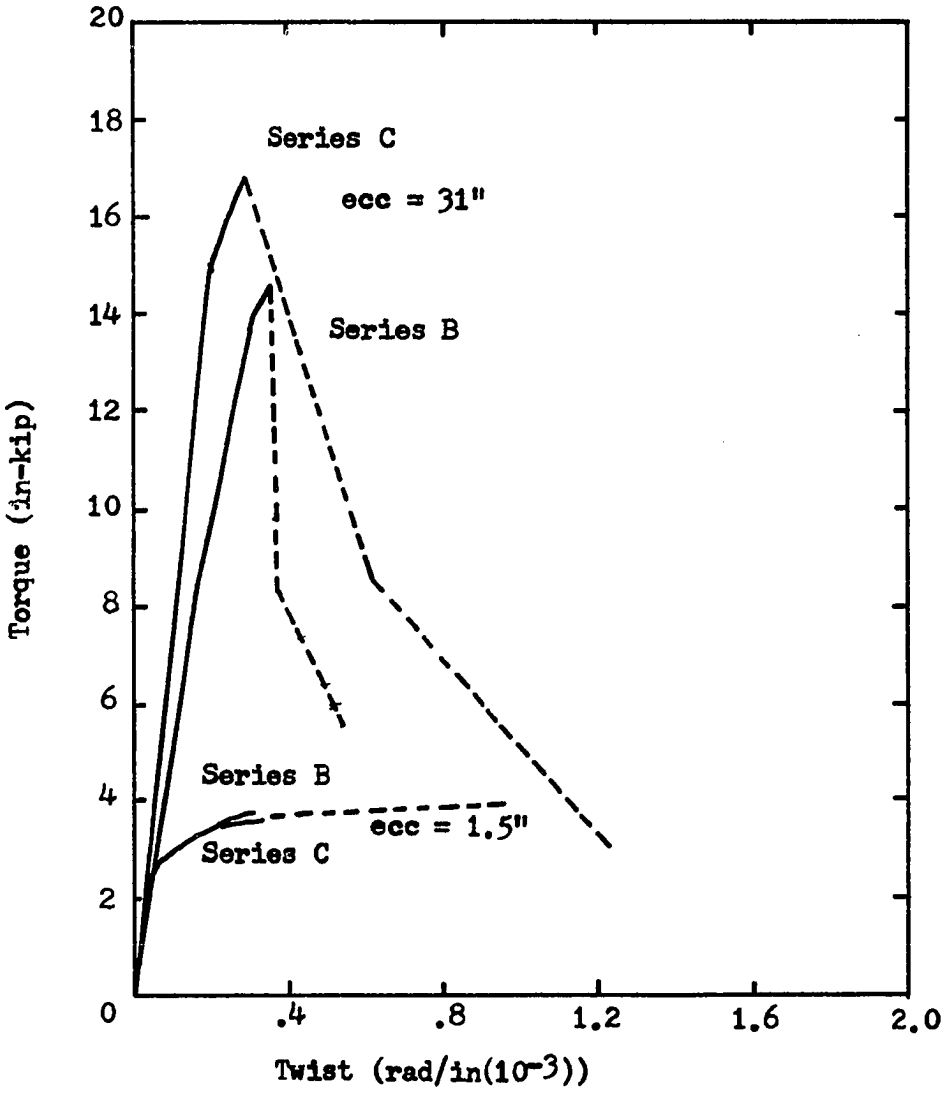


Figure 3.12 Influence of Effective Prestress on the Torque-Twist Response

Shear-Slope at the Ends

The primary reasons for measuring the slope at the ends was to have some means of checking the symmetry of the response of the specimens and as a check on the center-line deflection. A detailed description of the shear-slope at the ends curves for each specimen is presented in Appendix A and the curves are contained in Appendix B.

The general characteristics of the curves for the three series are presented in this section as well as how the most important variables affected the general shapes of the curves.

Influence of Eccentricity

Since the slope at the ends was directly related to the flexural response of the specimen, the eccentricity had a definite effect upon the general slope of the curve as is shown in Figure 3.13.

The initial portions of the curves are linear and the initial slopes of the curves appear to be independent of the eccentricity. With large eccentricities the specimens cracked and failed while still in the linear range of the curve. The small eccentrically loaded specimens, on the other hand, exhibited a non-linear response before failure as shown in Figure 3.13. Specimens tested with intermediate eccentricity showed a response between the two extremes.

When the specimens responded very symmetrically, the shear-slope at the end curve of the west end was almost identical to that of the east end, for example see C-6 of Appendix B. When the specimen's collapse was unsymmetrical, the two curves show the discrepancy, for example see C-3 of Appendix B.

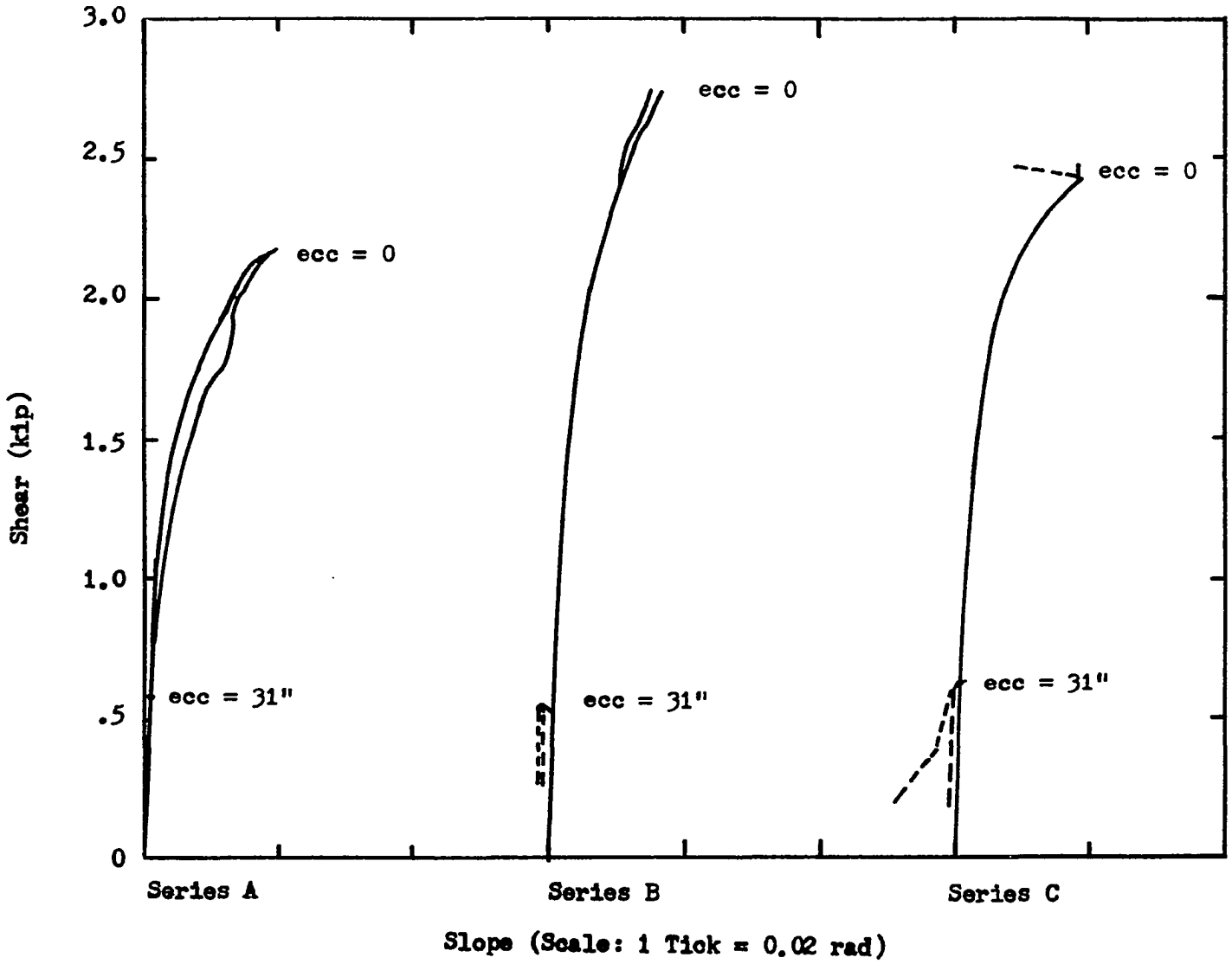


Figure 3.13 Influence of Eccentricity on the Shear-Slope at the Ends Response

Influence of the Overhanging Flange

The influence of the overhanging flange can be seen in Figure 3.14 which is a composite plot for the extreme eccentricities for series A and series C. The two series have the same general shaped curves.

The curves for series C have a greater initial slope than those of series A indicating that the flange increased the rigidity of series C compared to that of series A. Also, the ultimate capacities of the specimens of series C was greater than that of series A.

Influence of Effective Prestress

Figure 3.15 is a composite plot of the shear-slope at the ends curves for series B and C. The curves of series C have a greater initial slope than those of series B indicating that series C had a larger initial moment of inertia. Figure 3.15 shows the capacity of series B at small eccentricities was greater than that of series C but that for large eccentricities series C had greater capacity than that of series B.

Summary

The general behavior of the test specimens can be summarized as follows:

1. Increased eccentricity i.e, torsion caused the initial cracking and the ultimate load to decrease for all three series.
2. The load-deformation response was linear up to first cracking for all of the specimens. Increase in eccentricity caused the load-deformation curves to show less non-linear response with the total curve being linear for large eccentricities.

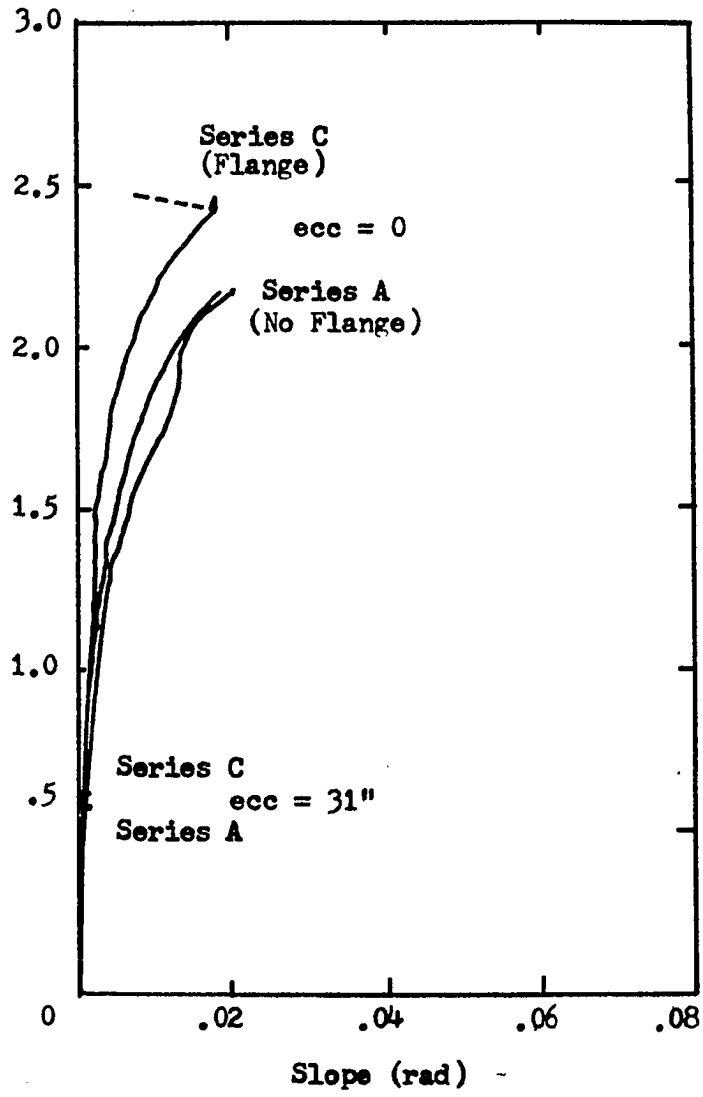


Figure 3.14 Influence of Overhanging Flange on the Shear-Slope at the Ends Response

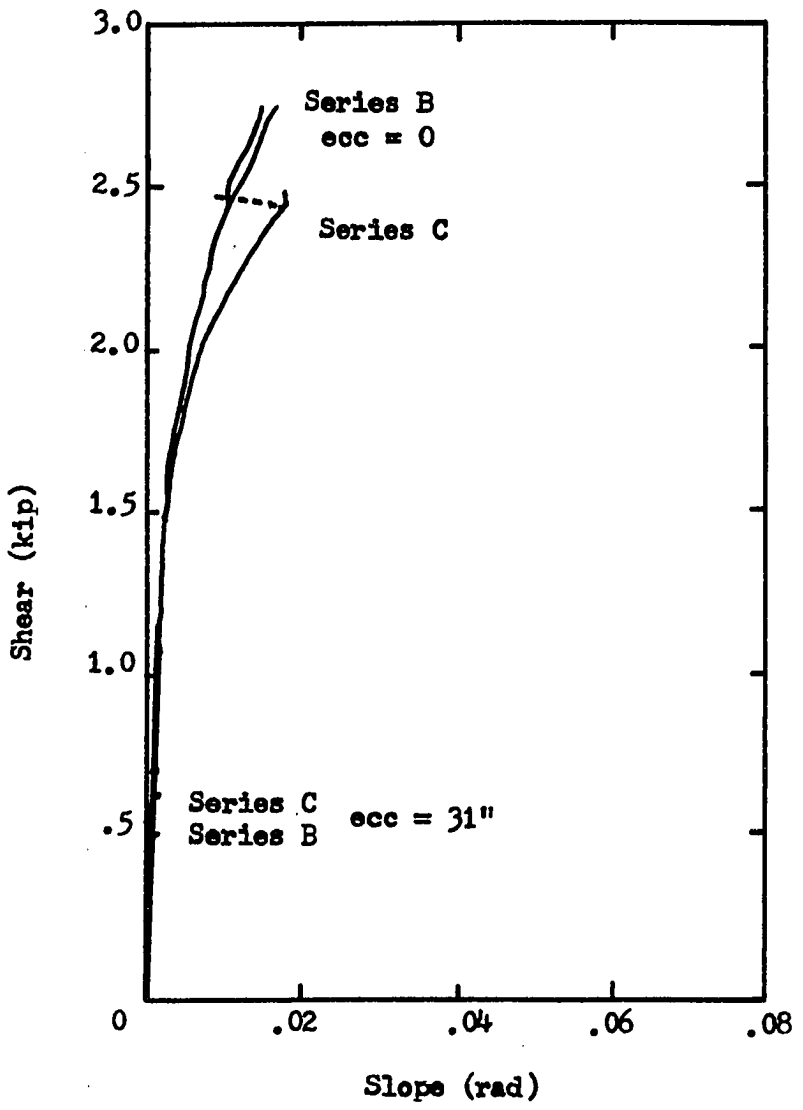


Figure 3.15 Influence of Effective Prestress on the Shear-Slope at the Ends Response

3. The eccentricity had no effect upon the initial torsional or flexural rigidity of the specimens.
4. With an increase in eccentricity, the crack pattern was changed from a flexure-to-shear type to a torsional type. An increase in eccentricity moved the point of collapse the supports where the moment approached zero.
5. The shear-centerline deflection curves for the specimens with and without the flange had similar shapes except the flanged specimens had steeper slopes and showed more capacity. These two exceptions indicate that the torsional and moment rigidities, cracking loads and ultimate capacities were increased with the addition of the flange.
6. An increase in the effective prestress increased the cracking and ultimate loads for small eccentricities but the reverse was true for the large eccentricities.
7. The failure mode was symmetrical with respect to mid-span for most of the specimens especially up to the final loading stages.

CHAPTER IV

DEVELOPMENT OF AN INTERACTION SURFACE FOR PRESTRESSED RECTANGULAR AND L-BEAMS LOADED WITH TORSION, SHEAR AND MOMENT

The interaction surface for torsion, shear and moment on a prestressed concrete beam is a multi-dimensional surface depending on the number of variables considered, i.e., cross-sectional shape, concrete strength, torsion-to-shear ratio, torsion-to-moment ratio, shear-to-moment ratio, loading history, size effect, effective prestress, steel percentage, web reinforcement, type of structure, etc.

Chapter III presented in Figures 3.1 a, b and c three-dimensional plots of the test results of series A, B and C, respectively. Three-dimensional plots were appropriate since the variables were limited in this investigation to torsion, shear and moment within a series, and cross-sectional shape and effective prestress between the series. The shear-to-moment ratio was not a controlled variable in that collapse was not forced to be at a particular location, but the ratio was essentially constant for this investigation due to the specimens failing in one of two zones. At zero, small and intermediate eccentricities the specimens failed in a zone approximately 28 inches from the centerline of the support while specimens loaded with large eccentricities failed near the supports. The loading conditions caused a constant shear over the span (as shown in Figure 1.9) except for a small linear variation due to the uniform weight of the specimen. The

combination of a constant distance to the failure zone and a uniform shear diagram resulted in a constant shear-to-moment ratio, i.e., the intersection of a plane passing through the torsional axis and the interaction diagram. Although the data points for large eccentricities did not have the same shear-to-moment ratio, they fell approximately on this intersection for the following reasons. First, the zones of collapse were at or close to the supports which produced zero or small moments at the critical zones and secondly, the shears causing collapse for large eccentricities were small which also produced small moments (Figure 1.9). Each of these conditions forced the data points for large eccentricities to fall close to the torsional axis.

The only points that did not fall approximately on the described intersections were the pure moment specimens A-7, B-8 and C-7 which fell on the moment axis.

Three-Dimensional Interaction of Torsion, Shear and Moment

The mathematical model used for the regression analysis development of the three-dimensional interaction surfaces is given by

$$Y = \beta_1 + \beta_2 X_1 + \ldots + \beta_q X_q + e$$

where

Y = the dependent vector (Torsion)

X_i = the ith independent vector

e = the error term

β_i = the ith linear coefficient.

The independent variables (X_i) were assumed to be as follows

$$X_1 = \text{moment}$$

$$X_2 = \text{shear}$$

$$X_3 = X_1(X_2)$$

$$X_4 = X_1^2$$

$$X_5 = X_2^2$$

$$X_6 = X_1(X_5)$$

$$X_7 = X_4(X_2)$$

$$X_8 = X_1^3$$

$$X_9 = X_2^3$$

The original model included terms of higher order but was reduced for practical reasons due to the fluctuations in the surfaces when they were extrapolated outside the test data sets.

The model was transformed into unitless terms to allow unitless three-dimensional interaction surfaces to be developed and to produce data that could be more conveniently processed by computer methods.

The following data transformation to a unitless set has been suggested by past researchers in the reinforced concrete industry [ACI SP-18, 1968]:

$$Y = T_u/T_{uo}$$

$$X_1 = M_u/M_{uo}$$

$$X_2 = V_u/V_{uo}$$

where

T_{uo} = ultimate torque capacity without shear or moment

M_{uo} = ultimate moment capacity without shear or torque

V_{uo} = ultimate shear capacity without torsion.

Table 4.1 shows the values for M_{uo}, T_{uo} and V_{uo} used in the following analysis for series A, B and C. The experimental value of T_{uo} for this investigation was not obtained since it would have taken major revisions of the testing arrangement thus adding another variable of test set-up to the investigation. The value of T_{uo} for each series was obtained by extrapolating the curves of Figures 3.1a, b and c, respectively. This method appears to be justifiable due to the extreme eccentricities (over 30") used in testing respective specimens (see Table 3.1). This method has also been used by past reinforced concrete researchers [Ersoy, 1965], [Farmer, 1967].

The value of M_{uo} was determined from results of specimens A-7, B-8 and C-7, respectively. These specimens were tested such that torsion and shear did not exist in the failure zone (Figure 2.9).

The value of V_{uo} has been obtained by different means by past researchers. It should be noted that shear in the absence of moment is extremely difficult to obtain in a test facility except at an inflection point. Pure shear conditions could not physically occur under the loading conditions of this investigation, except at the support with zero length. With these two conditions in mind and remembering that the specimens failed with large values of shear did so at approximately 28" from the support, the value of V_{uo} was determined by the specimens loaded with zero eccentricity.

The actual computations for the regression analysis were performed on an IBM 360-50 computer using "BMD02R STEPWISE REGRESSION", a sub-program of the Biomedical Computer Programs package [Dixon, 1970] from the University of California.

TABLE 4.1. PURE MOMENT, SHEAR AND TORQUE CAPACITIES

Series	M_{uo} (in-kip)	V_{uo} (kip)	T_{uo} (kip)
A	84.8	2.0	13.5
B	102.0	2.85	14.5
C	97.1	2.60	15.5

> "This program computes a sequence of multiple linear regression equations in a stepwise manner. At each step one variable is added to the regression equation. The variable added is the one which makes the greatest reduction in the error sum of squares. Equivalently it is the variable which has highest partial correlation with the dependent variable partialed on the variables which have already been added; and equivalently it is the variable which, if it were added, would have the highest F value."

The output of the computer program consisted of the following statistical quantities: multiple correlation coefficient, standard error of estimate, analysis-of-variance table, regression coefficients, standard errors, the covariance matrix, the correlation matrix, and plots of the residuals.

Several computer trials were made with variations in the input data. The first consisted of three data sets which were series A (12 points), series B (9 points) and series C (9 points). The results of this attempt were plotted by a program written by the writer that presents a three dimensional visualization of the surface. In addition to contours on the surface, the test data and the calculated values are plotted giving an indication of the residual in the dependent variable. These plots showed that the surfaces should not be extrapolated to obtain intersections with the planes of the axes, especially the torsion-shear planes. The intersection in the torsion-shear plane did not correspond to either the straight line approach or the circular approach suggested by past researchers [Cowan, 1953], [Mukherjee, 1971]. It should be remembered at this point that the test data fell approximately on the intersection of a vertical plane containing the vertical torsional axis and the interaction surface of torsion, shear and moment.

In order to force the data surface to have a practical intersection with the torsion-shear plane, two basic approaches were studied. The first approach assumed the intersection of the interaction surface and the torsion-shear plane to be a quarter circle $T_u/T_{uo}=[1-(V_u/V_{uo})^2]^{\frac{1}{2}}$. This circular interaction has been suggested by many past researchers [ACI SP-18]. The projection of the writer's test data onto the torsion-shear plane at $M_u/M_{uo} = 0$ also indicates a smooth decreasing curve. Three sets of equally spaced data were taken from this assumed quarter circle containing twenty, ten and five points, respectively. Each of these series were used as additional data points with series A, B and C and new stepwise regression surfaces were computed.

The second approach was the same as the one previously described except the intersection in the torsion-shear plane was assumed to be a straight line $T_u/T_{uo} = 1-V_u/V_{uo}$. Nylander (1945) suggested a linear relationship in the torsion-shear plane at $M_u/M_{uo} = 0$ and Mukherjee also adopted the straight line approach as discussed in Chapter I.

The results of these trials were studied both from the statistical and practical view point. Figures 4.1, 4.2 and 4.3 show plots of the interaction surfaces for the regression analysis coefficients using ten points from the assumed quarter circle in the torsion-shear plane at $M_u/M_{uo} = 0$ and the test data of series A, B and C, respectively. The residuals in the dependent, torsional, variable are shown in these figures also. Since many of the plots of the regression analysis surfaces obtained by using the data and the selected points from the assumed

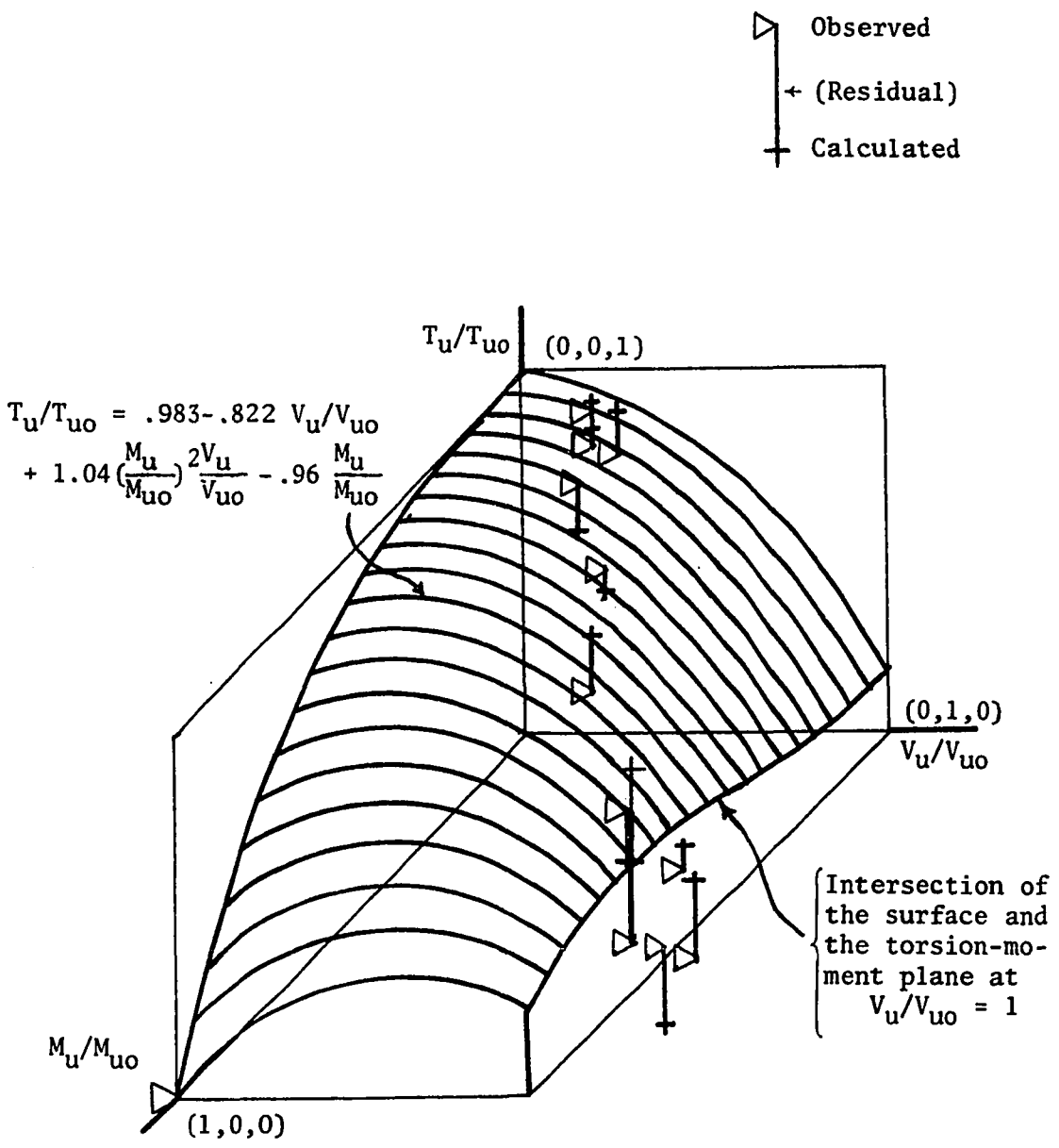


Figure 4.1 Unitless Interaction Surface for Series A by Regression Analysis.

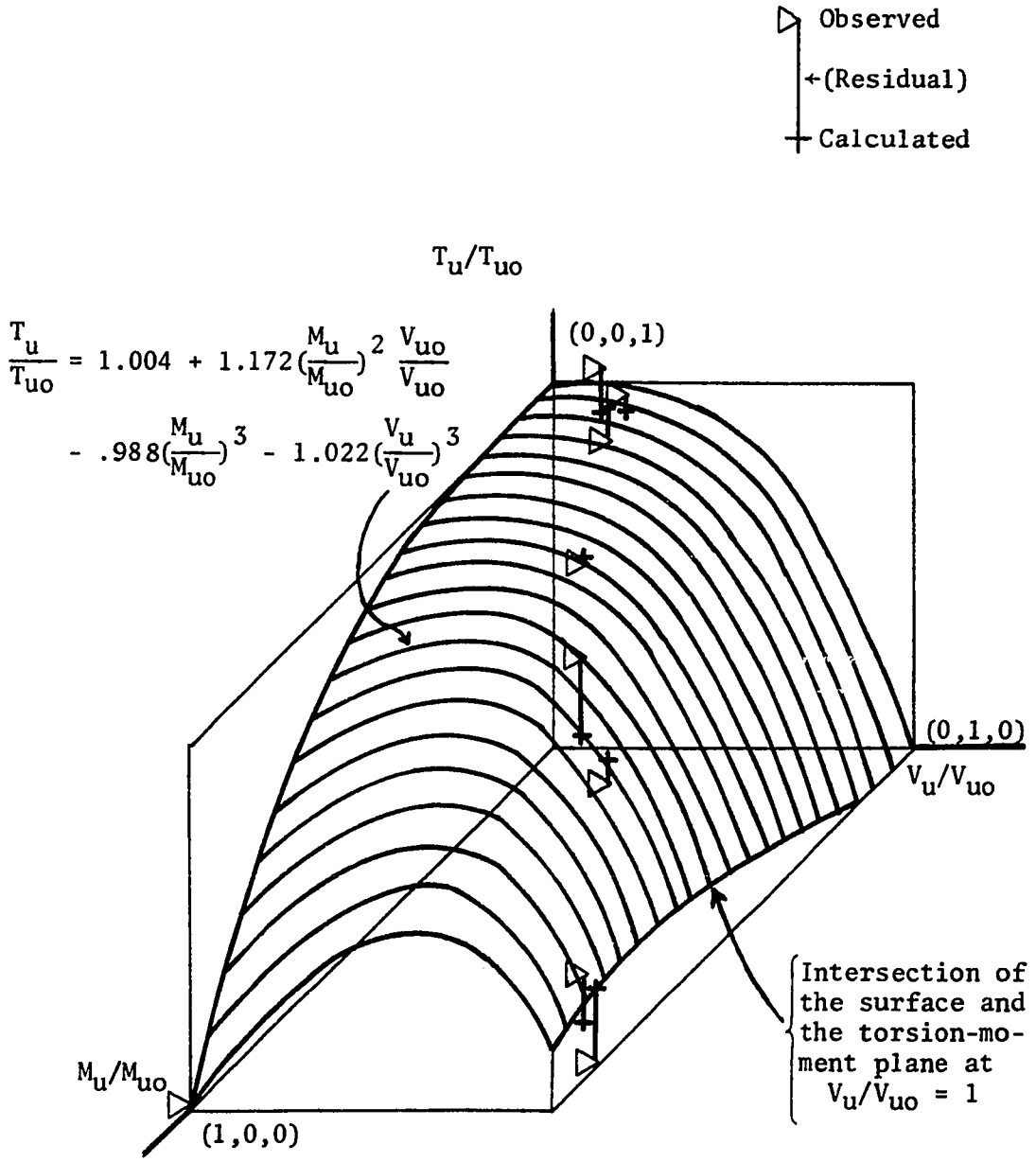


Figure 4.2 Unitless Interaction Surface for Series B by Regression Analysis

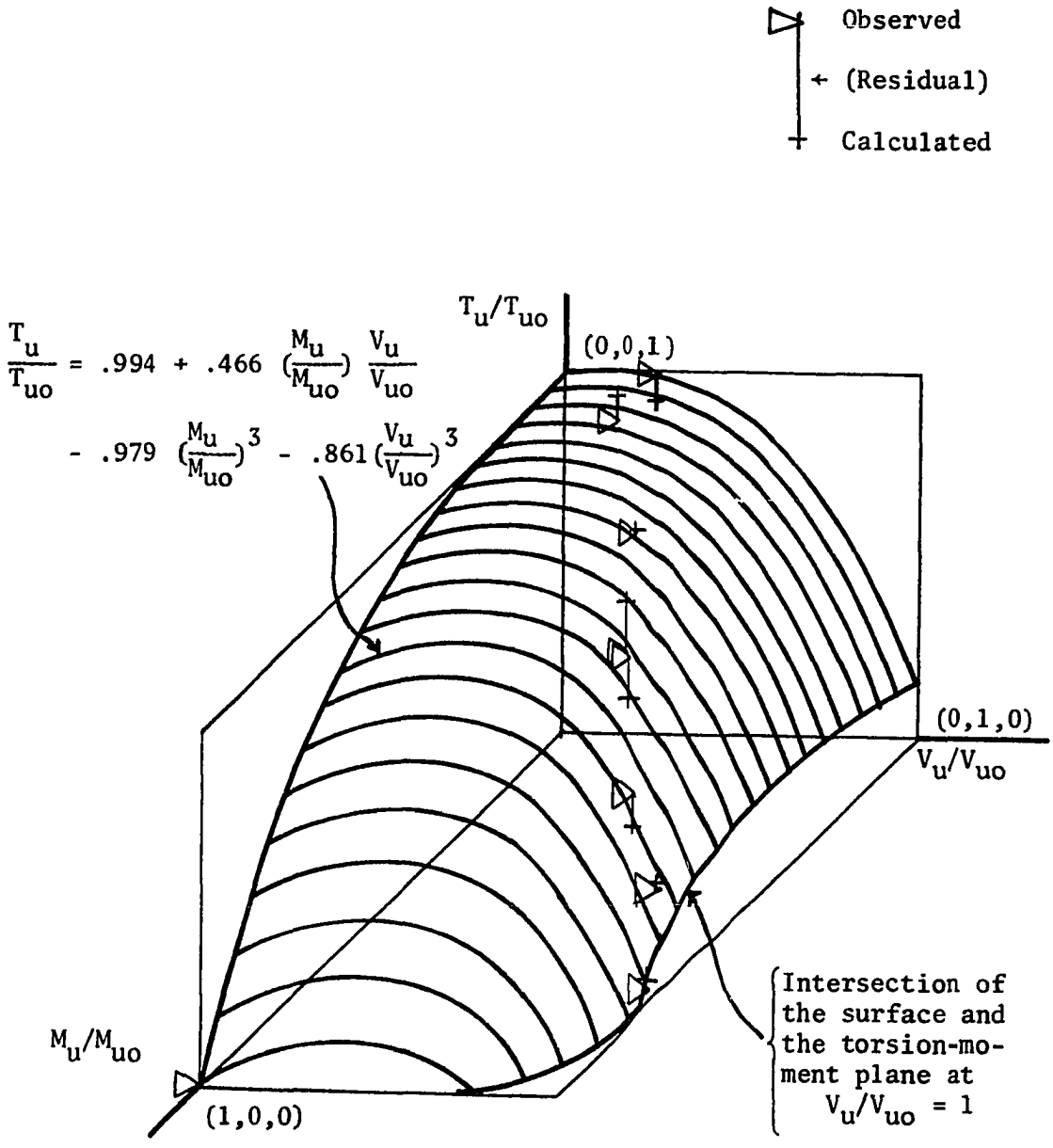


Figure 4.3 Unitless Interaction Surface for Series C by Regression Analysis

linear interaction in the torsion-shear plane at $M_u/M_{uo} = 0$ showed a curve in that plane, the circular interaction was implied.

These regression surfaces appear to have reasonable intersections with the torsion-moment plane at $V_u/V_{uo} = 0$ and the torsion-shear plane at $M_u/M_{uo} = 0$ and sufficient curvature to fit the data. The intersections of the surfaces and the torsion-shear plane at $V_u/V_{uo} = 1$ and the torsion-moment plane at $M_u/M_{uo} = 1$ appear to be questionable in view of the limited amount of past experimental data available.

Proposed Unitless Interaction Surface

The following proposed unitless interaction surface for torsion, shear and moment is based on the results of the previously described regression analysis of the writer's test data and the assumption that the developed equation of the surface must not only be manageable but give a conservative estimate of the actual capacity of the member being considered.

The following is a list of the basic assumptions used in the development of the proposed unitless interaction surface.

1. The interaction surface is governed by the non-dimensional parameters T_u/T_{uo}, V_u/V_{uo} and M_u/M_{uo} (see Figure 4.4) and passes through the points (0,0,1), (0,1,0) and (1,0,0).

2. The intersection of the interaction surface and the torsion-shear plane at $M_u/M_{uo} = 0$ (curve AB of Figure 4.4) is a quarter circle $T_u/T_{uo} = [1-(V_u/V_{uo})^2]^{\frac{1}{2}}$.

3. The intersection of the interaction surface and the torsion-moment plane at $V_u/V_{uo} = 0$ is given by a smooth decreasing curve, AD,

$T_u/T_{uo} = 1-[M_u/M_{uo})^3$.

4. The intersection of the interaction surface and the shear-moment plane at $T_u/T_{uo} = 0$ is a square, OBCDO.

5. The intersection of the interaction surface and a plane parallel to the torsion-shear plane at a distance of M_u/M_{uo} from the origin, ij, is a quarter of an ellipse with a major axis of $V_{uo}/V_{uo} = 1$ and a minor axis of $(T_u/T_{uo})_x$ (see Figure 4.4). The equation of a typical point, α, is given by $(T_u/T_{uo})_\alpha = (T_u/T_{uo})_x[1-(V_u/V_{uo})_\alpha^2]^{\frac{1}{2}}$.

Concerning the proceeding list of assumptions, the first appears to be a reasonable approach and has been suggested by past researchers [ACI SP-18, 1968].

The second assumption has been tentatively adopted by ACI Committee 318 in their proposed Building Code Requirements for Reinforced Concrete, 1971. The regression analysis predicts an equation of a smooth decreasing curve which approximates a quarter circle in the torsion-shear plane at $M_u/M_{uo} = 0$. Additional research is needed in this plane ($M_u/M_{uo} = 0$) to end the present controversy in the literature.

The third assumption is the result of the regression analysis of the writer's data. The smooth decreasing function has the disadvantage of not allowing the addition of a small moment to increase the torsional capacity. Although there is data in the torsion-moment plane [Reeves, 1962], [Rowe, 1968],[Mukherjee, 1971] to justify the increase in capacity in that plane, the writer has neglected it on the following grounds: first, there is no data available in the region of small moment and large shear and large torsion to allow the assumption that the increase capacity will effectively carry over into the interaction

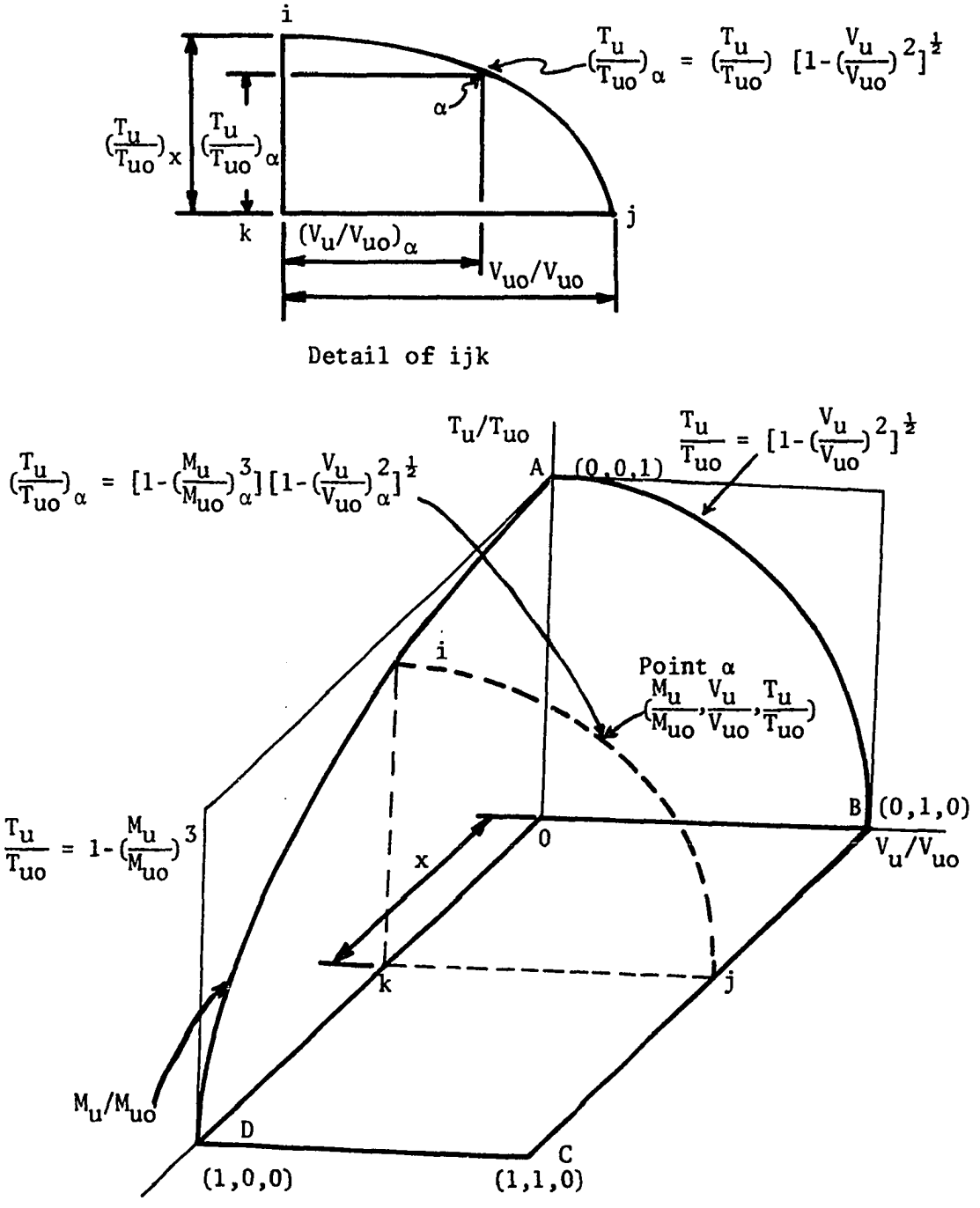


Figure 4.4 Basic Assumptions of the Proposed Unitless Interaction Surface for Torsion, Shear and Moment

surface; second, the test data available in the torsion-moment plane does not include the basic variable of load history and until this has been studied the writer questions the proposed increase in torsional capacity due to the application of moment. Third, the specimens studied in this investigation suggested that collapse due to large torsional loading was with but little warning indicating the need for a more conservative estimate at this time.

The fourth assumption is the product of the present method of designing for members resisting moment and shear, i.e., design for moment and check and design for shear if needed. This square interaction in the moment shear plane appears to be a reasonable approach for prestressed specimens, especially when the shear is controlled by that which occurs after flexural cracking as it was in this investigation. This interaction was also suggested by Mukherjee (1971).

The fifth assumption is based on the general shape of the previously discussed regression analysis interaction surface (Figures 4.1, 4.2 and 4.3) and the second assumption which requires the intersection of the interaction surface and the torsion-shear plane at $M_u/M_{uo} = 0$ to be a quarter circle. Although the assumption appears to be reasonable, it may need revision when additional test data are available, especially when additional variables are considered.

With these assumptions, the equation for the interaction surface in terms of the non-dimensional parameters is obtained by substituting the third assumption into the equation

$$(T_u/T_{uo})_\alpha = (T_u/T_{uo})_x[1-(V_u/V_{uo})_\alpha^2]^{\frac{1}{2}}.$$

The equation of the interaction surface is, dropping the subscripts, then:

$$T_u/T_{uo} = [1-(M_u/M_{uo})^3][1-(V_u/V_{uo})^2]^{\frac{1}{2}}$$

where the positive quadrant is the boundary condition.

Figure 4.5 shows a plot of the proposed unitless interaction surface.

A plot of the proposed interaction surface, the writer's test results and the predicted results using the interaction surface are shown in Figure 4.6. Due to the scatter in the data, the restriction of $T_u/T_{uo} = 0$ if either M_u/M_{uo} or $V_u/V_{uo}>1$ was adopted. This restriction will not be necessary in the application of the interaction surface to a design problem since the values of V_u/V_{uo} and M_u/M_{uo} will be less than or equal to 1.

Figure 4.6 indicates that the proposed interaction surface predicts the test data with the predicted values being slightly conservative for most of the points.

Figure 4.7 shows the test results of Mukherjee (1971) applied to the proposed interaction surface. The proposed surface gives a reasonable prediction of his data. Although the predictions are rather conservative in the range of large moment with small torsion and shear, it appears that the proposed surface can be used for his specimens which contained secondary web reinforcement.

Comparison of Proposed Interaction Surfaces

Mukherjee's proposed interaction surface and his basic assumptions were discussed in Chapter I. Figure 4.8 shows his proposed interaction surface applied to the writer's test data.

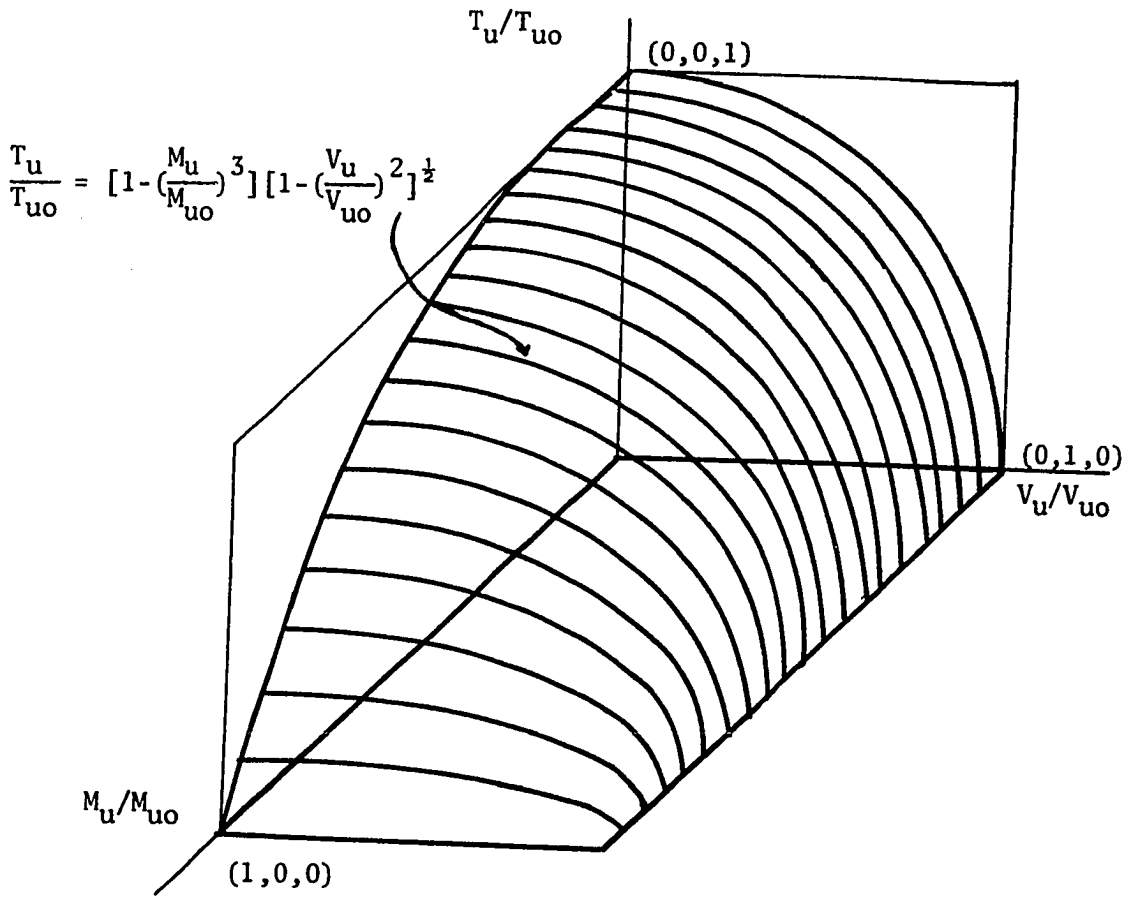


Figure 4.5 Proposed Unitless Interaction Surface for Torsion, Shear and Moment

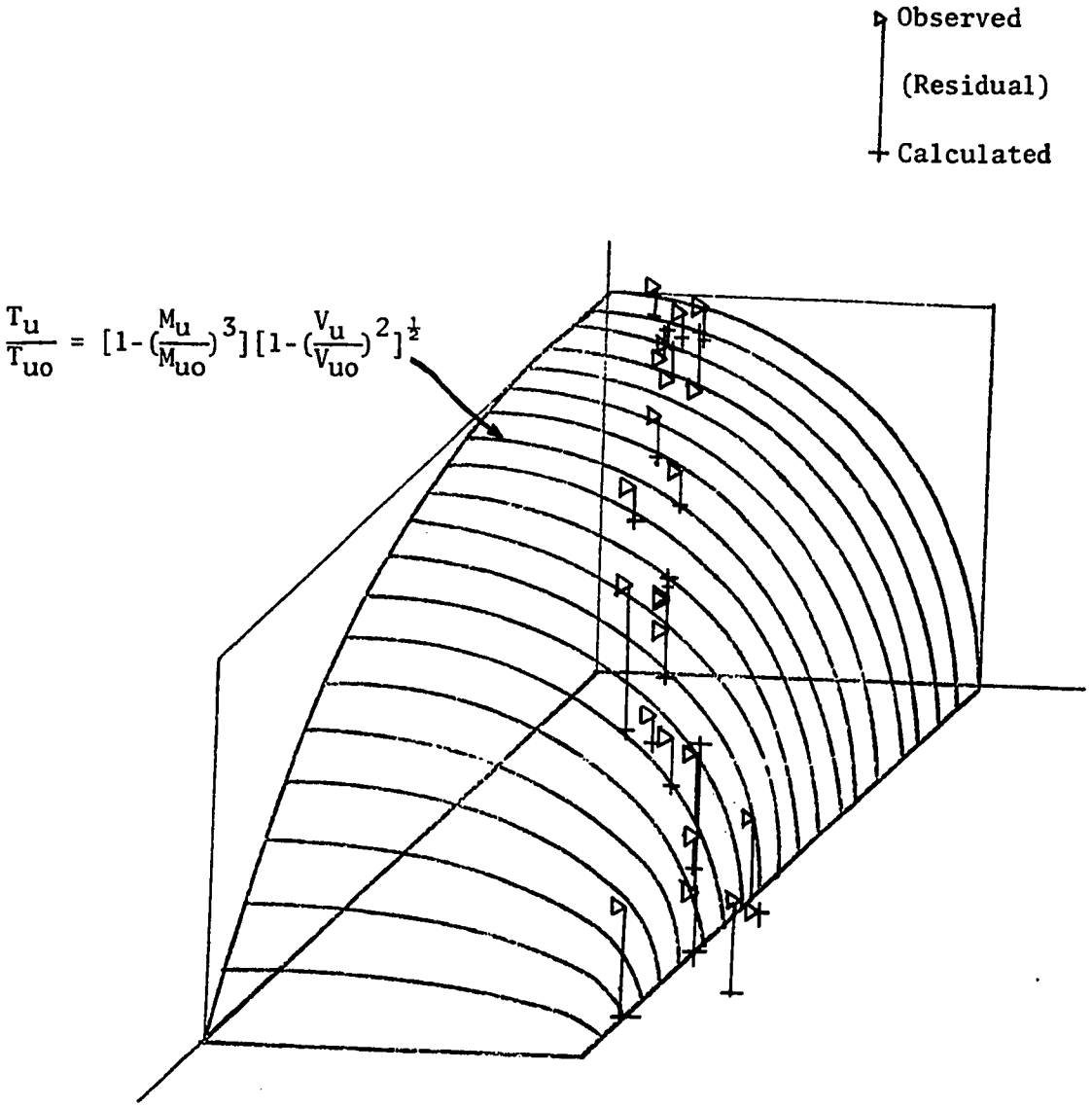


Figure 4.6 Proposed Unitless Interaction Surface with Series A, B, and C

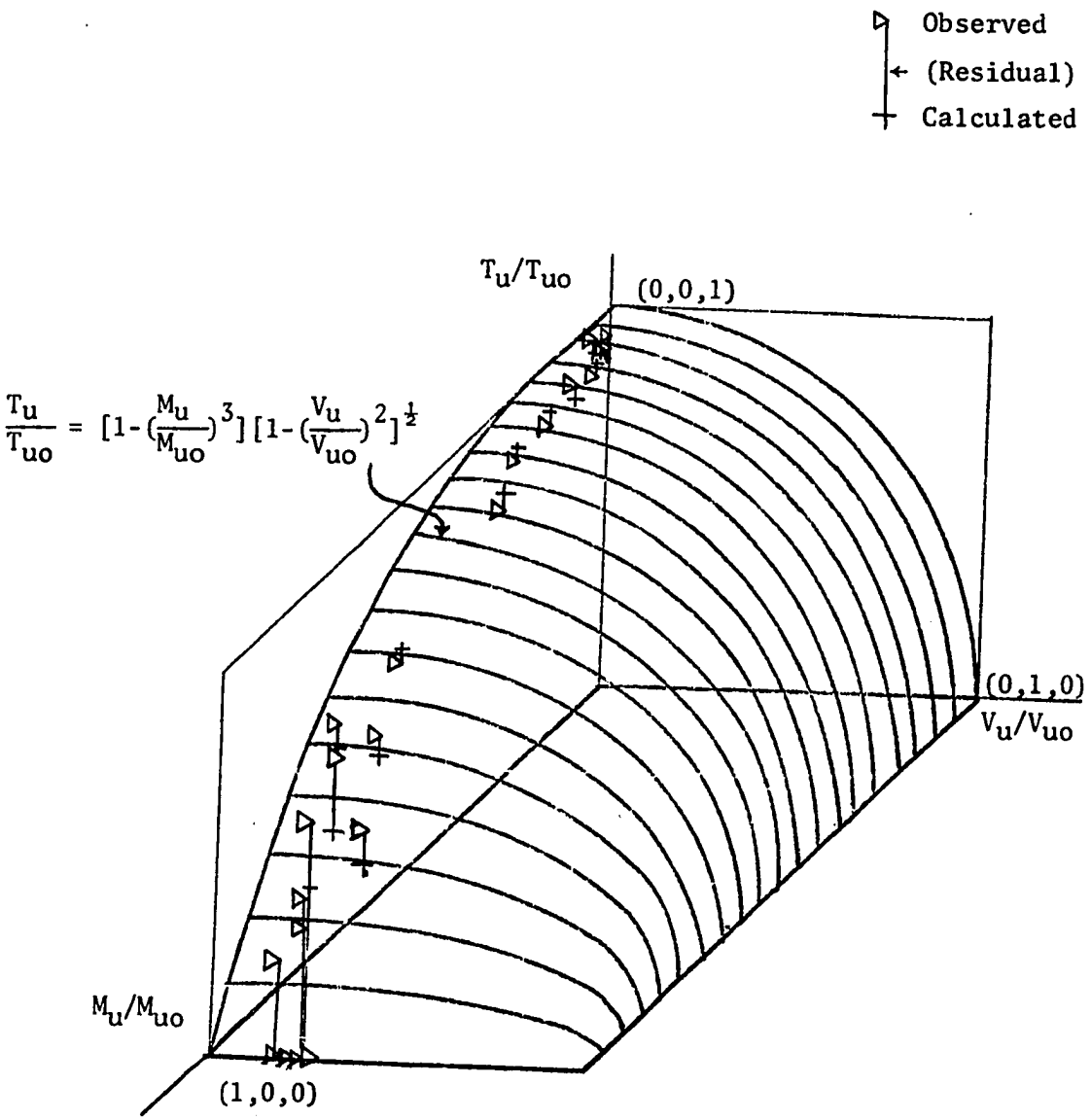


Figure 4.7 Proposed Interaction Surface with Mukherjee's (1971) Data

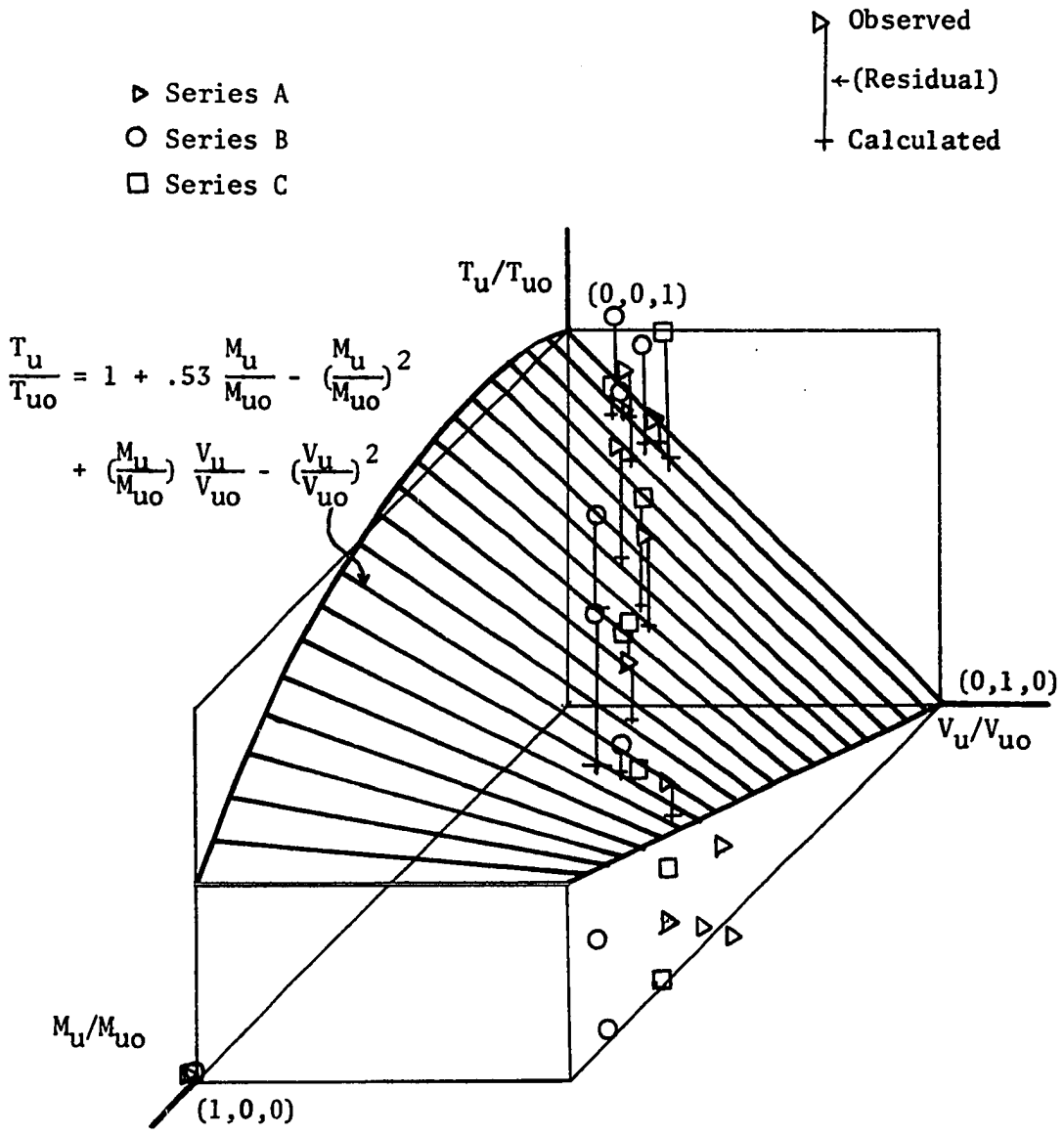


Figure 4.8 Mukherjee's Proposed Interaction Surface with Series A, B and C

The most significant differences between the interaction surface proposed by Mukherjee and the writer's propose interaction surface shown in Figure 4.6 are listed below. Each of the following are assumed to have the positive quadrant of the interaction surface as the boundary conditions.

1. Mukherjee's interaction surface interested the torsion-shear plane in a straight line versus a quarter circular intersection.

2. Mukherjee's interaction surface has two intersections in the torsion-moment plane at $V_u/V_{uo} = 0$ versus a smooth curve.

3. Mukherjee's interaction has a linear relation in the torsion-moment plane at $V_u/V_{uo} = 1$ versus an intersection of $T_u/T_{uo} = 0$.

4. Mukherjee's interaction surface shows a slight increase in the torsional capacity with the application of a small amount of moment versus a continuous decrease in the torsional capacity with the application of moment.

5. The intersection of Mukherjee's interaction surface and the torsion-shear plane at $M_u/M_{uo} = x$ is a straight line versus that of a quarter of an ellipse.

6. The intersection of Mukherjee's interaction surface and the torsion-shear plane at $M_u/M_{uo} = 1$ is a rectangle versus the line of $T_u/T_{uo} = 0$.

7. Mukherjee's interaction surface gives more conservative values for most of the data.

It should be remembered that Mukherjee's test specimens contained secondary web reinforcement while the writer's specimens contained only the prestressing steel. With this in mind, several of the differences

can be explained. For example, when a prestressed concrete beam without secondary reinforcement is tested with large torsional loading, the collapse is usually sudden with the formation of initial cracking while one with secondary web reinforcement will resist additional load after inidial cracking. This would partly explain items two and four. Item three can be partly explained by noting in Figure 4.7 that Mukherjee's test data was actually very close to the torsion-moment plane rather than farther out on the interaction surface. He assumed the rectangular portion of his surface on the torsion-shear plane at $M_u/M_{uo} = 1$ from the results of specimens that were not very different from those tested in the torsion-moment plane.

Since the torsion-moment plane is presented by the torsional axis in a two-dimensional plot of torsion and shear, Figure 4.9 further indicates that Mukherjee's three-dimensional test data was very close to the torsion-moment plane since it falls close to the torsional axis.

The proposed unitless interaction surface for torsion, shear and moment for eccentrically prestressed rectangular and L-beams proposed by the writer predicts with reasonable accuracy the writer's test data as well as the test data of Mukherjee (1971) which contained secondary web reinforcement.

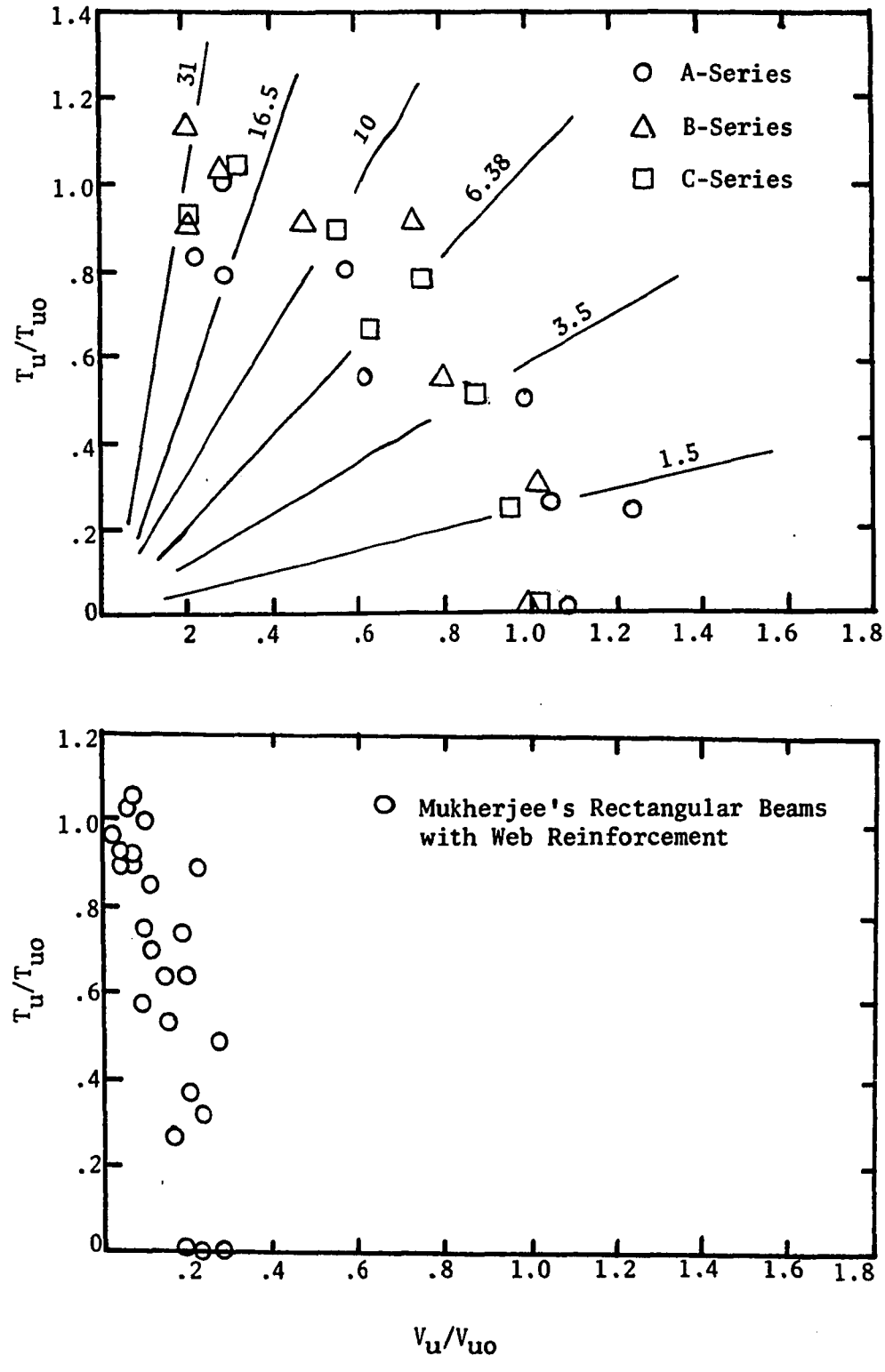


Figure 4.9 Unitless Interaction of Torsion and Shear.

CHAPTER V

CONCLUSIONS AND RECOMMENDATIONS

Twelve simply supported pretensioned prestressed concrete rectangular and eighteen L-beams without web reinforcement were tested with combined torsion, shear and moment. The main objectives of this experimental investigation were to study the load-deformation response, general crack patterns of the specimens and the effect of flange width, torque-to-shear ratio and effective prestress.

The following conclusions are submitted with consideration given to the size and type of specimens tested.

1. The effects of each variable on the crack pattern and ultimate capacity are summarized below.

a. The magnitude of the eccentricity was the most influential variable of this investigation. The initial as well as the ultimate crack pattern was directly related to the magnitude of the eccentricity as the load increased.

b. The flange showed its major influence by increasing the cracking and ultimate capacities.

c. The effective prestress had very little effect upon the crack pattern. The moment capacity was increased due to the effective prestress but the torsional capacity was decreased slightly.

2. The load-deformation response and effects of each variable are summarized below.

a. The eccentricity of the load played a prominent role on the shape in each of the load-deformation curves. They were initially linear up to first cracking where they immediately dropped due to loss in capacity with large eccentricities or became nonlinear with small eccentricities. Intermediate eccentricities resulted in a transition between the two extremes.

b. The flanges tended to increase the slopes of the initial portions of the load-deformation curves due to the increased rigidity of the flanged specimens. The increase cracking capacity and ultimate capacity tended to increase the length of the linear portion as well as the over-all height of the curves.

3. The following unitless interaction surface for torsion, shear and moment was developed with the aid of regression analysis and several simplifying assumptions.

$$T_u/T_{uo} = [1-(M_u/M_{uo})^3][1-(V_u/V_{uo})^2]^{\frac{1}{2}}$$

Although this proposed interaction surface predicts the test data of the writer's investigation and those of Mukherjee's it should be remembered that several assumptions were made that will need additional experimental justification.

4. More research is definitely needed in the area of torsion, shear and moment on prestressed concrete members.

a. The points that need immediate investigation appear to be loadings in the region of large shear and moderate to large moment

with varying amounts of torsion on rectangular prestressed beams to supplement Mukherjee's data.

b. Experimental data are urgently needed for T and L beams in all ranges of the loading for specimens with and without web reinforcement.

c. The torsion-shear plane's intersection with the interaction surface should be studied in detail to end the controversy of the quantification of this relation for prestressed concrete rectangular, T and L beams, especially eccentrically prestressed specimens.

d. The effect of the loading history upon the interaction surface is virtually untouched and should receive immediate attention.

e. A theoretical investigation, as well as, an experimental investigation of the pure torsional capacity of eccentrically prestressed T, L and rectangular specimens is urgently neeeded for specimens with and without web reinforcement.

BIBLIOGRAPHY

ACI Committee 318. "Proposed Revision of ACI 318-63, Building Code Requirements for Reinforced Concrete." *Journal of American Concrete Institute*, V. 67, No. 2, Feb. 1970, pp. 77-186.

ACI Committee 438. "Tentative Recommendations for the Design of Reinforced Concrete Members to Resist Torsion." *Journal of American Concrete Institute*, V. 66, No. 1, Jan. 1969, pp. 1-8. Discussion - V. 66, No. 7, July 1969, pp. 576-88.

Ables, P. W. and Hockley, C. H. "Small Scale Demonstration Tests on Prestressed Concrete Beams." *Structural Engineer* (London) V. 28, June 1950, pp. 146-53.

Behera, U. "Reinforced Concrete Beams, with Stirrups, under Combined Torsion." Ph.D. Thesis, University of Texas, 1969.

Bishara, Alfred. "Prestressed Concrete Beams under Combined Torsion, Bending and Shear." *Journal of the American Concrete Institute*, V. 66, No. 7, July 1969, pp. 525-28.

Bresler, B. and Pister, K. S. "Failure of Plain Concrete under Combined Stresses." *American Society of Civil Engineers*, Proc. V. 81, Separate No. 674, April 1955.

Brown, E. J. "Strength of Reinforced Concrete T-Beams under Combined Direct Shear and Torsion." *Journal of American Concrete Institute*, Proc. V. 51, No. 9, May 1955, pp. 889-902.

Collins, M. P., Walsh, P. F., Archer, F. E. and Hall, A. S. "Reinforced Concrete Beams Subjected to Combined Torsion, Bending and Shear. An Historical Review." *UNICIV Report*, No. 14, University of New South Wales, Oct. 1965.

Collins, M. P., Walsh, P. F., Archer, F. E. and Hall, A. S. "Experiments on the Strength of Concrete Beams in Combined Flexure and Torsion." *UNICIV Report* No. R-15. University of New South Wales, Feb. 1966.

Collins, M. P., Walsh, P. F., Archer, F. E. and Hall, A. S. "The Design of Rectangular Reinforced Concrete Beams Subjected to Combined Torsion, Bending and Shear." *UNICIV Report* No. R-16. University of New South Wales, Aug. 1966.

Colomb, C. A. "Histoire de l'Academie." Paris, 1784.

Cowan, H. J. "Design of Prestressed Concrete Beams Subject to Secondary Shear and Torsion." *Civil Engineering and Public Works Review* (London), V. 48, No. 570, 1953, pp. 1141-42; V. 49, No. 571, 1953, pp. 67-9.

Cowan, H. J. "The Strength of Plain, Reinforced and Prestressed Concrete under the Action of Combined Stresses with Particular Reference to Combined Bending and Torsion of Rectangular Section." *Magazine of Concrete Research*, V. 5, No. 14, Dec. 1953, pp. 75-86.

Cowan, H. J. "The Torsional Strength of Prestressed Concrete." *World Conference on Prestressed Concrete*, San Francisco, California, July 1957, Proc. pp. 18-1-12.

Cowan, H. J. "Design of Beams Subject to Torsion Related to the New Australian Code." *Journal of the American Concrete Institute*, V. 31, No. 7, Jan. 1960, pp. 591-618.

Cowan, H. J. and Armstrong, S. "Deformation of Concrete in Compression and Torsion." *Civil Engineering and Public Works Review* (London), V. 49, No. 580, Oct. 1964, pp. 1080-81.

Dixon, W. J. *University of California Publications in Automatic Computation No. 2.* Biomedical Computer Programs, University of California Press, Berkeley, Los Angeles, London 1970.

Draper, N. R. and Smith H. *Applied Regression Analysis.* John Wiley and Sons, Inc., New York, London, Sydney, 1st Edition, 1966.

Ersoy, U. "Combined Torsion in Semi-Continuous Concrete L-Beams without Stirrups." Ph.D. Thesis, University of Texas, 1965.

Farmer, L. E. and Ferguson, Phil M. "T-Beams under Combined Bending Shear, Torsion." *Journal of the American Concrete Institute*, V. 64, No. 11, Nov. 1967, pp. 757-66.

Gardner, R.P.M. "The Behavior of Prestressed Concrete I-Beams under Combined Bending and Torsion." *Cement and Concrete Association* (Great Britain), Technical Report TRA/31.

Gesund, H. and Boston, L. "Ultimate Strength in Combined Bending and Torsion of Concrete Beams Containing Only Longitudinal Reinforcement." *Journal of the American Concrete Institute*, V. 61, No. 11, Nov. 1964, pp. 1453-1469.

Hsu, Thomas. T. C. "Torsion of Structural Concrete-Interaction Surface for Combined Torsion, Shear and Bending in Beams without Stirrups." *Journal of the American Concrete Institute*, V. 65, No. 1, Jan. 1968, pp. 51-60.

Hsu, Thomas T. C. "Ultimate Torque of Reinforced Rectangular Beams." *Journal of the Structural Division, American Society of Civil Engineers*, V. 94, No. ST2, Proc. Paper 5814, Feb. 1968, pp. 485-510.

Hsu, Thomas T. C. and Kemp, E. L. "Background and Practical Application of Tentative Design Criteria for Torsion." V. 66, No. 1, Jan. 1969, pp. 12-24. *Journal of the American Concrete Institute.* Discussion V. 66, No. 7, July 1969, pp. 591-3.

Humphreys, R. "Torsional Properties of Prestressed Concrete." *The Structural Engineer.* (London), V. 35, No. 6, June 1957, pp. 213-24.

Kemp, E. L., Sozen, M. A. and Siess, C. P. "Torsion in Reinforced Concrete." *A Report on a Research Project Sponsored by the University Research Board*, The University of Illinois, Urbana, Illinois.

Klus, J. P. "Ultimate Strength of Reinforced Concrete Beams in Combined Torsion and Shear." *Journal of the American Concrete Institute*, V. 65, No. 3, March 1968, pp. 210-15.

Lessig, N. N. "Determination of the Load-Bearing Capacity of Reinforced Concrete Elements with Rectangular Cross-Section Subjected to Flexure with Torsion." Trudy, No. 5, Concrete and Reinforced Concrete Institute, Moscow, Russia, 1959, pp. 5-28.

Liao, Huey Ming and Ferguson, Phil. M. "Combined Torsion in Reinforced Concrete L-Beams with Stirrups." *Journal of the American Concrete Institute*, V. 66, No. 12, Dec. 1969, pp. 986-993. Discussion - V. 67, No. 6, June 1970.

Mirza, M. S. and Mc Cutcheon, J. O. Discussion of "Torsion of Structural Concrete-Interaction Surface for Combined Torsion, Shear, and Bending in Beams without Stirrups" by Thomas T. C. Hsu. *Journal of the American Concrete Institute*, Vol. 65, No. 7, July 1968, pp. 567-569.

Mukherjee, Priya and Warwaruk, Joseph. "Torsion, Bending, and Shear in Prestressed Concrete." *American Society of Civil Engineers*, Proc. V. 97, No. ST4, April 1971, pp. 1063-79.

Nadai, A. *Plasticity.* McGraw-Hill Book Co., New York, 2nd Edition, 1950, pp. 347-490.

Navaratnarajah, V. Discussion of "Torsion of Structural Concrete Interaction Surface for Combined Torsion, Shear Bending in Beams without Stirrups" by Thomas T. C. Hsu. *Journal of the American Concrete Institute*, Vol. 65, No. 7, July 1968, p. 570.

Nylander, H. "Torsion and Torsional Restraint of Concrete Structures." (in Swedish), Bulletin No. 3, Statens Kommittee for Byggnadsforskning, Stockholm, 1945.

Osburn, D. L., Mayloglou, B. and Mattock, Alan H. "Strength of Reinforced Concrete Beams with Web Reinforcement in Combined Torsion, Shear and Bending." *Journal of the American Concrete Institute*, V. 66, No. 1, Jan. 1969, pp. 31-41. Discussion - V. 66, No. 7, July 1969, pp. 593-595.

Reeves, J. S. "Prestressed Concrete Tee Beams under Combined Bending and Torsion." *Cement and Concrete Association* (Great Britain) Technical Report TRA/364, Dec. 1962, p. 17.

Rowe, R. E. Discussion, page 44. Third Congress of the Fédération Internationale de la Précontrainte, Berlin 1958.

Saether, Kolbjorn and Prachand, N. M. "Torsion in Spandrel Beams." *Journal of the American Concrete Institute*, V. 66, No. 1, Jan. 1969, pp. 24-30.

Saint-Venant, B. de. Mem. Acad. Sci. Inst. Imperial de France. Series II, 14, 233, Paris, 1856.

Swamy, N. "The Behavior of Ultimate Strength of Prestressed Concrete Hollow Beams under Combined Bending and Torsion." *Magazine of Concrete Research* (London) V. 14, No. 40, March 1962.

Torsion of Structural Concrete, Special Publication SP-18, American Concrete Institute, Detroit, 1968.

Victor, D. J. and Ferguson, Phil M. "Beams under Distributed Load Creating Moment, Shear and Torsion." *Journal of the American Concrete Institute*, V. 65, No. 4, April 1968, pp. 295-308.

Victor, D. J. and Ferguson, Phil M. "Beams under Distributed Load Creating Moment, Shear and Torsion." *Journal of the American Concrete Institute*, V. 65, No. 9, Sept. 1968, pp. 295-308.

Yudin, V. K. "Determination of the Load-Bearing Capacity of Reinforced Concrete Elements of Rectangular Cross-Section under Combined Torsion and Bending." Beton i Zhelezobeton, No. 6, June 1962, pp. 265-268.

Zia, Paul. "Torsional Strength of Prestressed Concrete Members." *Journal of the American Concrete Institute*, V. 31, No. 10, April 1961, pp. 1337-59. Ph.D. Thesis, University of Florida, 1960, p. 169.

Zia, Paul. "What Do We Know About Torsion in Concrete Members?" *Journal of the Structural Division, Proceedings of the American Society of Civil Engineers*, V. 96, No. ST6, June 1970, pp. 1185-99.

APPENDIX A

DETAIL DISCUSSION OF EACH SPECIMEN

APPENDIX A

Series A

All of the beams of series A were of the same size (3"x6") and had the same effective prestress. The primary variable of this series was the eccentricity of the load, i.e., the shear-torque ratio.

Beam A-1

Beam A-1 was tested at zero eccentricity with a point load at mid-span to obtain the capacity of the A series loaded with shear and flexure.

The first crack occurred as a vertical flexural crack at a live load of 2.63 kips at mid-span. The crack pattern was very symmetrical with a new crack on either side of the centerline and extensions of existing cracks until a load of 3.13 kips. With application of this load, the previous cracks extended and a new one formed approximately at the east quarter point and propagated approximately one-half the depth of the web and at an inclination of 60 degrees toward the load. After the cracks were marked, extension of the loading ram was required to compensate for creep. When the load was increased to 3.09 kips, the top of the quarter point crack propagated 4 inches at an angle of about 20 degrees toward the load. Upon application of the next load of 3.18 kips, the east quarter point crack on the south face propagated horizontally toward mid-span and a new crack formed on the north face at the intersection of the initial quarter point crack and the location

of the cable and made an angle of 45 degrees toward the load. The specimen behaved linearly up to the first cracking load as can be seen in the shear-centerline deflection curve given in Appendix B.

Beam A-2

Beam A-2 was tested at an eccentricity of 6.38 inches in two cycles. The specimen was loaded with increments up to a live load of 1.86 kips and then the load was removed in increments with data taken on the complete load-unload cycle. No cracks were observed in this load cycle.

The second load cycle was continued until collapse of the specimen occurred. The first crack occurred in the top of the loading arm at its intersection with the web at a load of 1.37 kips. The first crack in the primary specimen occurred at a load of 1.86 kips as a vertical flexure crack in the bottom of the north web at mid-span.

The failure crack pattern will now be described to give an indication of the resultant cracks but not the manner of their formation. The failure pattern on the north face was unsymmetrical with respect to mid-span. The west side had a crack that started at the bottom of the web and propagated at an angle of 45 degrees for approximately 2 inches where it turned horizontally to 6 inches west of the loading diaphragm. It turned at this point toward the top of the web at an angle of approximately 30 degrees.

The east side of the north face had a similar crack but it started approximately 10 inches from mid-span rather than the quarter-point.

The south face was a little more symmetrical. The west side had a crack from the bottom at 10 inches from mid-span to 2 inches below the top at mid-span. The east side had a similar crack except it started approximately 6 inches from mid-span.

Although no cracks were observed in cycle one, the shear-centerline deflection curve indicates that the beam had started into its non-linear region. The second cycle shear-centerline curve has an initially linear portion up to the first cracking shear similar to cycle one indicating that no significant cracks had formed in the first cycle. The torque-twist curve for cycle one does not show any deviation from linearity and that of cycle two is similar up to the first cracking at which point it deviates from linearity.

Beam A-3

Due to unintensional mislocation of the southeast box-section of the forms, beam A-3 was cast with an east web thickness of 3¼ inches rather than the desired 3 inches. This specimen was tested with an eccentricity of 10.0 inches.

The crack pattern was unsymmetrical with collapse being in the east side where the effective prestress was less due to the increased web thickness.

When the load reached 2.02 kips, a crack formed in the south east face of the web at 16 inches from mid-span and propagated over the top at an angle of approximately 30 degrees toward mid-span. When the crack reached the north face, secondary shear failure caused it to propagate back toward the east support rather than continue on its spiral path. The collapse occurred as one continuous crack with a minimum amount

of warning, but it was not an explosive failure primarily because of the low load level at which it failed.

The shear-centerline deflection curve shows a linear response up to the first observed cracking at which point the load capacity dropped considerably and the measured deflection decreased. This decrease in the measured deflection can be explained by noting that the specimen failed unsymmetrically on the east side which reduced the capacity of the section but allowed the mid-span to come back up.

The torque-twist curve shows the linear response up to first cracking but shows loss of capacity and an increase in the measured twist.

Beam A-4

Beam A-4 was tested at an eccentricity of 31.0 inches which required the use of the loading arm attachment and the collars at the support diaphragms. The crack pattern was symmetrical with respect to the mid-span of the beam.

With the application of 0.71 kips, a crack formed at the bottom of the south web at each support and propagated in a spiral path up the web at an angle of 45 degrees and over the top at an angle of 40 degrees due to the torsional effect. When the cracks reached the north web, the secondary shear failure caused them to propagate back toward the supports rather than continue on their spiral path. With further extension of the loading ram, but a decrease in load, the cracks in the north face extended toward the bottom of the north face at the supports. The shear-centerline deflection and the torque-twist curves

indicate a linear response up to the first cracking at which point loss of capacity occurred and an excessive amount of deflection and twist occurred.

Beam A-5

Beam A-5 was tested at an eccentricity of 1.5 inches. The crack pattern of this specimen was very symmetrical with respect to mid-span of the beam up to the ultimate load which caused a typical flexure-to-shear type failure crack to form on the east side.

The first crack formed as a vertical flexural tension crack in the bottom of the web at a load of 2.42 kips. As the load was increased, vertical flexural tension cracks formed in the web and propagated vertically for a short distance and then turned toward the load. At the load of 3.34 kips three of these typical cracks had formed on each side of the centerline of the specimen at a spacing of approximately 4 inches. With the application of a load of 4.65 kips, the top of the center crack on the east side extended to the load and the bottom extended toward the support until it reached the bottom of the specimen resulting in complete collapse of the specimen.

The shear-centerline deflection and the torque-twist curves indicate a linear response up to first crack. This beam was primarily a flexure-to-shear type failure as can be seen by the long nonlinear tail on the shear-centerline deflection curve.

Beam A-6

Beam A-6 was tested at an eccentricity of 21.5 inches which required the use of the loading arm attachment and the collars at the support diaphragms.

The first observed cracks in the primary specimen were the collapse cracks which formed at a live load of 1.01 kips symmetrically at each end of the beam. The location of the failure surface is described as follows with the point of initiation not observed since the failure occurred without warning and all eyes were on the gages in an effort to obtain the readings at the instant of failure. The failure crack ran from the bottom of the south web at the support up the web at an angle of 45 degrees and over the top at an angle of 45 degrees in a spiral path similar to A-4. When the crack reached the top of the north face, secondary shear caused it to turn back toward the support rather than continue on its spiral path. With further extension of the loading ram, but a decrease in load, the cracks on the north face extended down the face toward the supports resulting in reduced capacity.

The shear-centerline deflection and the torque-twist curves indicate a linear response up to the cracking load and that the capacity of the specimen dropped considerably at the formation of the first crack.

Beam A-7

Beam A-7 was tested with a two-point load system symmetrical with the mid-span to give a pure moment region over the center third of the span. Vertical stirrups were placed outside of the pure moment region to force failure to occur in the pure moment region.

The specimen was loaded in two cycles with the first cycle being stopped at a maximum value of 2.02 kips and then reduced to zero. Readings were taken to allow the load deformation response of the first cycle to be observed. No cracks were observed in the first cycle of

loading and the shear-centerline deflection curve verifies this by its linear variation.

Cycle two took the specimen up to collapse. The first crack occurred at a live load of 3.53 kips as a vertical flexural tension crack in the bottom of the web. The failure load of 6.77 kips caused crushing of the concrete in the top fibers in the pure moment region with vertical cracks equally spaced over the center half of the span.

The shear-centerline deflection curve indicates a linear response up to the first cracking load. The flexural type failure can be seen by noting the long nonlinear tail of the curve.

Beam A-8

Beam A-8 was tested at an eccentricity of 3.5 inches. The crack pattern was very symmetrical with respect to the mid-span of the specimen.

The crack pattern on the south face gave the general appearance of a flexure-to-shear type failure with the initial cracking in the bottom of the web at a load of 2.52 kips and with increased load they propagated toward the concentrated load. The final collapse at 3.79 kips was a shear type extension of both ends of previous cracks located approximately 12 inches on either side of the mid-span.

The crack pattern of the north face was very similar to that of the south face at low load levels except the cracks in general had propagated farther in the south face. However, the final failure pattern of the two faces was significantly different. The cracks in the north face did not reach the top of the web. The failure surface sloped from

the top of the south face at mid-span to a point approximately 2 inches below the top of the north face, but at the quarter points the surface connected the bottom of the south face to a point approximately 2 inches from the bottom on the north face.

The shear-centerline deflection, the shear-slope at the ends and the torque-twist curves indicate that the response was linear up to the first cracking load.

The shear-slope at the ends curves show no variation of the slope at the west end as compared to the east end which implies that the load deformation response was symmetrical.

Beam A-9

Beam A-9 was tested at zero eccentricity at mid-span with one concentrated load to obtain the flexure-shear capacity of the series This was a companion to specimen A-1. Although the capacity of this specimen was considerably larger than A-1, the crack pattern and collapse mode was similar.

The cracks were vertical flexural tension cracks in the bottom of the web at a load of 2.92 kips. The crack pattern was symmetrical with respect to mid-span until the crack causing collapse developed. This was a typical flexure-to-shear type pattern up to a load of 4.21 kips. When the loading ram was extended, the top of the west quarter point crack propagated to the load while the bottom extension split the specimen from the quarter point to the west support along the cable. The specimen collapsed completely and suddenly.

The shear-centerline deflection curve indicates a linear response up to a load of 2.34 kips which was the next load previous to that which cracks were observed indicating that actually the first cracks occurred between the two load levels.

The shear-slope at the ends indicate that the response was not symmetrical with respect to the mid-span.

Beam A-10

Beam A-10 was tested at an eccentricity of 26.5 inches which required the use of the loading arm attachment and the collars at the support diaphragms. The crack pattern was symmetrical with respect to the mid-span.

Collapse of the specimen occurred without warning in one continuous crack at a live load of 1.04 kips. The crack pattern was similar to A-4 except the crack were displaced 6 inches from the supports. The failure mode was primarily torsional on the south face and the top of the web with secondary shear developing in the north face.

The shear-centerline deflection, the shear-slope at the ends and the torque-twist curves indicate a linear response up to first cracking and loss of capacity at first cracking.

The shear-slope at the ends curves indicate that the specimen responded fairly symmetrical with respect to mid-span but there is a deviation in the shape of the two curves. The west end appeared slightly more linear than the east.

Beam A-11

Beam A-11 was tested at an eccentricity of 16.5 inches. Due to illness of the pump operator during the test, this specimen had a

particular variation in the testing procedure. The load was applied in increments up to a load of 1.41 kips which was allowed to remain on the specimen for 45 minutes. The load was re-established and a second set of readings were taken. Then the load was incremented until failure in the same procedure as the other specimens. No cracks were observed in the specimen either before or after the time interval and the readings indicated only a minor amount of creep took place.

The west end failed with a spiral crack which had its bottom at approximately the quarter point on the south face and intersected the top at the point of application of the load and appeared as a secondary shear crack on the north face. The east side of the specimen failed in a spiral type curve similar to the west side but it had its initial point at the bottom of the web at the east support and intersected the top at an angle of 30 degrees with the horizontal. The spiral crack crossed the top of the beam at which point secondary shear caused it to turn back toward the support.

The shear-centerline deflection and the torque-twist curves show a linear response up to 1.11 kips which is approximately two-thirds of the cracking load.

The shear-slope at the ends curves indicate a linear response up to cracking load and symmetry up to the cracking load also.

Beam A-12

Beam A-12 was a companion to A-5 with an eccentricity of 1.5 inches. The crack pattern was very symmetrical with respect to mid-span up to the load causing collapse.

The first cracks appeared as vertical flexural tension cracks in the bottom of the web at a load of 2.92 kips. At a load of 3.88 kips, six initially vertical cracks which propagated toward the load had formed at an equal spacing of 4 inches. With the application of a load of 4.27 kips, the top of the crack at the east quarter point extended to the point of loading and with the same angle of approximately 25 degrees to the bottom of the web resulting in complete collapse of the beam.

The shear-centerline deflection and the torque-twist curves indicate a linear response up to the load previous to the one that cracks were observed indicating that the cracks actually occurred between the two load levels and probably closer to the previous load of 2.34 kips. The shear-slope at the ends curves indicate that the response was symmetrical with respect to mid-span.

Series B

Series B had two basic modifications from series A. The first was that a 1"x6" flange was added to the top of the south side of the web which resulted in an L-beam.

The second modification was in the effective prestress of the section. The prestress of this series caused tension cracks in the top north corner of the web equally spaced (4") over most of the span. They extended vertically down the north face approximately 1 inch horizontally across the top about 2 inches.

Beam B-1

Beam B-1 was tested at zero inches eccentricity to obtain the flexure-shear interaction capacity.

The first cracks were observed at a live load of 4.04 kips as vertical flexural tension cracks in the bottom of the web. With additional load, new vertical cracks and extension of the existing cracks occurred. The crack pattern was unsymmetrical with more cracks on the east side, but the ones on the west side propagated further. At a load of 4.55 kips 2 had formed on the west side and 3 on the east side and 1 at mid-span in the north face equally spaced at approximately 4 inches.

With the application of 5.30 kips, a diagonal tension crack caused collapse on the west side at approximately the quarter point on the bottom and the point of application of the load at mid-span. The collapse was sudden as expected for a diagonal tension to compression mode with a large segment of the west web below the calbe falling off and crushing of the concrete in the compression zone.

The shear-centerline deflection and the shear-slope at the ends curves indicate a linear response up to a load of 3.03 kips which is considerably below the observed cracking load level of 4.04 kips.

The shear-slope at the ends curves indicate a symmetrical response up to the last three load levels which show that the west end had less slope than the east end.

Beam B-2

Beam B-2 was tested at an eccentricity of 6.38 inches. The initial cracking appeared as vertical flexural tension cracks in the

center of the span at 3.03 kips. With application of additional load, the cracks on the south face resembled those of flexure-to-shear. The effect of torsion was observed by noting the cracks on the bottom were not perpendicular to the longitudinal axis, but propagated slightly toward the supports.

At the ultimate load of 3.69 kips, 2 quarter circular segments were formed in the flange on either side of the loading arm with the loading arm forming one side and the south edge of the flange forming the other straight edge.

The north face also showed the effect of torsion when the height of the flexural cracks were compared with their longer companion cracks on the south face. The cracks causing collapse on the north face did not follow any of the existing flexural cracks and did not reach the top of the web but joined the east and west spans at 2 inches below the top. The bottoms of the cracks on the north face intersected the bottom of the north web at the quarter points.

The shear-centerline deflection, the shear-slope at the ends and the torque-twist curves indicate a linear response up to the cracking load. The shear-slope at the ends curves indicate that the specimen responded symmetrically by the close agreement between the slope at the east end compared to that of the west end.

Beam B-3

Beam B-3 was tested at an eccentricity of 31.0 inches which required the use of the loading arm attachment and the collars at the support diaphragms. Except for some tension cracks in the top of the loading arm, the specimen collapsed without warning in the test portion.

The crack pattern was symmetrical with the exception that the west crack occurred at the support while the east crack was displaced approximately 4 inches toward mid-span.

The cracks were spiral in nature with the general location as follows although the actual formation could not be recorded since the crack formed without warning and as one failure mode. The west crack was located with an initial point at the bottom of the south edge of the web and propagated up the web at an angle of 30 degrees to the intersection of the web and flange. A crack was visible on the top of the flange and web and propagated down the north edge of the web to the bottom at an angle of 40 degrees.

The east crack was very similar except that it was displayed approximately 4 inches toward mid-span and that the crack on the north face propagated only approximately 5 inches rather than completely to the bottom. With further extension of the loading ram, the failure mode became that caused by secondary shear.

The shear-centerline deflection and the torque-twist curves indicate a linear response up to the first cracking load which was the collapsing load also.

Beam B-4

Beam B-4 was tested at an eccentricity of 26.5 inches which required the use of the loading arm attachment and the collars at the supports. This specimen failed in torsion with secondary shear being evident on the north east face. Similar cracks formed on each end except the ones on the west end were displaced approximately 6 inches toward the loading arm.

With the application of a live load of 0.74 kips, a crack was formed on the south web which connected the intersection of the flange and the bottom of the web with an angle of approximately 45 degrees. The north west face of the beam showed this spiral type crack to be from the top of the specimen to the bottom while the north east face did not travel completely to the bottom and it also showed signs of shear with a small crack formed at the top third of the face and turned toward the support.

The top of the specimen showed one crack on the west end at this load level that had propagated about 2 inches but the top of the east end did not show any cracks.

With the application of 0.66 kips, extension of the existing cracks caused collapse. The crack on top of the west end propagated through the flange in a spiral nature joining the crack in the south web. The crack in the top of the east end also crossed the top and connected the crack in the south face.

The crack in the north west face extended in a shear type crack toward the support. With additional extension of the loading ram, a failure plane joined the crack at the junction of the flange and the web to the lower part of the loading arm.

The shear-centerline deflection and the torque-twist curves indicate a linear response up to the first cracking load with the first cracking load being the same as the maximum recorded load. It should be noted that it was not possible to take the readings of the gages at the maximum load since the collapse was instantaneous and without warning.

The maximum load was observed and recorded and was used in the plots and calculations in the previous portions of this paper.

Beam B-5

Beam B-5 was tested with an eccentricity of 3.5 inches. The collapse was very symmetrical with respect to the loading arm in the east and west sides and very destructive with portions of the flanges on either side of the loading arm, as well as, portions of the web falling off of the specimen.

The first crack occurred at a load of 3.51 kips and up until the final load of 4.52 kips the crack pattern appeared to be a flexure-to-shear type failure. Torsional effects were noticed, however, by the height of the cracks on the south face being slightly higher than their companions on the north face and the cracks on the bottom were not perpendicular to the longitudinal axis.

The final failure resembled that of B-2 with the cracks in the north face not reaching the top of the specimen but connecting about two inches below the top. The cracks on the south face did reach the top with quarter-circular segments falling out of the flange.

The shear-centerline deflection, shear-slope at the ends and the torque-twist curves indicate a linear response up to a load of 2.92 kips. This is the load previous to that at which cracks were actually observed indicating that cracking occurred between the two load levels.

The shear-slope at the ends was linear and indicated that the specimen responded symmetrically with respect to mid-span by the agreement between the slopes at the ends.

Beam B-6

Beam B-6 was tested with an eccentricity of 1.5 inches. The first crack appeared as a vertical flexural tension crack at a load of 3.51 kips. The crack pattern was symmetrical with respect to the loading arm until the final crack occurred. The general crack pattern resembled that of a flexure-to-shear type failure.

With application of 4.09 kips, cracks formed at the south junction of the flange and each side of the loading arm. With an increase in the load, the cracks in the web progressed up and toward the point of the application of the load while those in the flange progressed slightly toward the web. A new crack formed at a load of 4.97 kips in the flange approximately 6 inches to the east of the loading arm propagating from the south edge about 4 inches toward the web. When the load was increased to 5.01 kips, complete collapse took place. The descriptions of these cracks are intended to locate them rather than explain how they were formed. On the south face a crack formed from the intersection of the top of the web and the loading arm to the steel location at the west support. A similar crack was formed on the north face except it was approximately 3 inches below the top of the web at mid-span. The north-east face of the web had a flexural crack approximately at the quarter-point at the bottom which developed into a shear crack at the top and propagated almost horizontally until it reached mid-span where it propagated through the compression zone.

The shear-centerline deflection and the torque-twist curves indicate a fairly linear response up to a load of 2.34 kips. With additional loading, the torque-twist curve indicates considerably more twist

indicating a reduction in the torsional rigidity of the specimen. The shear-slope at the ends indicates an almost linear response up to collapse. The good agreement between the slopes of the ends indicates a symmetrical response of the specimen.

Beam B-7

Beam B-7 was tested with an eccentricity of 10 inches. The first crack occurred in the bottom of the south edge of the flange at its intersection with the west side of the loading arm at a live load of 1.46 kips. At a load of 2.34 kips, the original crack had propagated to the web on the bottom of the flange and approximately 2 inches on the top of the flange.

With the application of the ultimate load of 2.55 kips several new cracks were observed. The intersection of the west side of the loading arm and the south edge of the flange showed a crack approximately 2 inches in length on the top. The south face had two diagonal tension cracks on either side of the loading arm. The north face had one short crack in the bottom of the web on either side of the loading arm.

With additional extension of the loading ram, a diagonal tension crack formed in the north face and the south face and ran from the bottom at the west quarter point to the top of the web at the loading arm.

The shear-centerline deflection and the torque-twist curves indicate a linear response up to a load of 2.05 kips which indicates a loss of structural rigidity that can be explained by the formation of the first crack between the flange and the loading arm.

The shear slope at the ends curves indicate a symmetrical response up to the last two load levels.

Beam B-8

Beam B-8 was tested with a two-point load system symmetrical with the mid-span to give a pure moment region over the center third of the span. Vertical stirrups were placed outside of the center third of the span to force failure to occur in the pure moment region.

The first cracks were observed with the application of 4.68 kips at 3 inches on either side of the mid-span as vertical flexural tension cracks.

When the load was incremented, new cracks formed in the bottom of the web as vertical tension cracks equally spaced at approximately 4 inches and the existing cracks propagated vertically toward the compression zone. When the live load had reached 6.43 kips, horizontal bending was noted by the observation of cracks in the south edge of the flange. With an increase in load, the crack in the web and the flange propagated toward the top of the web. Final collapse occurred with crushing of the concrete on the top north edge of the specimen in the pure moment region. The cracks in the flange had progressed approximately 4 inches and were spaced approximately 8 inches apart.

The shear-centerline deflection curve indicates a linear response up to a live load of 3.51 kips which was the load previous to the cracking load indicating that the cracking took place between the two load levels.

Beam B-9

Beam B-9 was tested with an eccentricity of 21.5 inches which required the use of the loading arm attachment and the collars at the support diaphragms. The failure mode was primarily torsional with the secondary shear causing failure after the capacity had been reduced due to torsion.

The first crack was observed in the south face at the west support at a live load of 1.05 kips. With the application of the next load increment, a new crack formed in the south web at the east end. With the application of 1.21 kips which was the ultimate capacity of the specimen, a crack formed in the south face at the east support.

The shear-centerline deflection and the torque-twist curves indicate a linear response up to the first cracking load. The shear-slope at the ends curves indicate a linear symmetrical response up to the initial cracking load at which point the slopes are no longer equal. The slope of the west end was less than that of the east end.

Series C

Series C consisted of the same basic cross-section as series B but the effective prestress was comparable to that of series A. The primary variable considered in this series was the eccentricity of the load.

Beam C-1

Beam C-1 was tested with an eccentricity of 3.5 inches. Vertical tension cracks were observed in the bottom of the web at mid-span with the application of 2.92 kips. The vertical cracks became inclined toward the load when it was increased to 3.51 kips.

The effect of torsion was observed by comparing the length of the cracks on the south face with the shorter ones on the north face. Tension cracks were observed in the south edge of the flange at a load of 4.09 kips. When the load reached 4.43 kips, complete collapse occurred with quarter-circular segments being formed in the flanges on either side of the loading diaphragm, as well as, complete collapse of the web symmetrically on either side of the loading diaphragm.

The torsional effect on the ultimate failure mode was observed by noting on the north face the failure surface on either side of the loading diaphragm joined each other 2 inches below the top of the web while the crack at collapse on the south face extended to the top of the web at the junction of the loading diaphragm and the web.

The shear-centerline deflection, shear-slope at the ends and torque-twist curves indicate an initial straight line portion up to the load preceeding the one at which initial cracking was observed. The shear-slope at the ends curves indicate a symmetrical response up to collapse.

Beam C-2

Beam C-2 was tested at an eccentricity of 6.38 inches and failed very symmetrically relative to mid-span. The collapse was not very sudden but did occur with a minimum of warning.

The first crack was observed at a load of 2.92 kips and appeared as a vertical flexural tension crack at mid-span but extended approximately halfway up the web. When the loading ram was extended but the load was decreased to 2.74 kips, a crack on either side of the loading diaphragm formed an elliptical shaped crack in the flange. A new

failure crack was also formed in the bottom at the web. The north face started at the quarter points and propagated in an elliptical path to 2 inches below the top at mid-span.

The south face had a similar crack but was displaced approximately 3 inches toward mid-span and reached the intersection of the flange and the web at mid-span.

The shear-centerline deflection, shear-slope at the ends and the torque-twist curves indicate a linear response up to the first cracking load which was the ultimate capacity of the specimen. The shear-slope at the ends curves indicate a symmetrical response with the slope of the east end being the same as that of the west end.

Beam C-3

Beam C-3 was tested with an eccentricity of zero inches. It was tested in two cycles with the first cycle reaching a maximum of 4.39 kips and then being unloaded in four increments. The second cycle took the specimen to complete collapse.

The crack pattern was symmetrical relative to mid-span with the first cracks occurring as vertical flexural tension cracks at a load of 2.92 kips. With an increase in load the flexural cracks extended toward the load and new ones formed approximately equally spaced on either side of mid-span. At a load of 4.89 kips, the flexural crack on the west side at approximately 12 inches from mid-span developed into a diagonal tension failure crack at approximately 30 degrees.

Cracks perpendicular to the longitudinal axis in the south edge of the flange formed at 3.74 kips and 4.68 kips on the east and west span respectively which indicated the beam had horizontal bending.

The shear-centerline deflection curves for the two cycles have the same basic shape with the second cycle having a shorter linear region. The first cycle was linear up to 2.34 kips which was the load previous to the one at which cracking was observed.

The shear-slope at the ends shows unsymmetrical response with the east end slope being significantly different from that of the west end throughout the load history of the two cycles.

Beam C-4

Beam C-4 was loaded with an eccentricity of 31.0 inches which required the use of the loading arm attachment and the collars at the support diaphragms. The failure mode was primarily torsional with shear causing a secondary shear failure after the capacity had been reduced due to the torsion. The failure modes of each end was the same except the critical section on the west end was displayed approximately to the quarter point of the span while that of the east end was at the support.

The east end had a critical crack that formed in the south web at the support and propagated at an angle of 30 degrees to the junction of the web and the flange. An additional crack formed from the junction of the south edge of the flange and the support arm at an angle of 30 degrees measured from the south edge of the flange across the top of the specimen. At the north edge of the top, the crack continued on its spiral path approximately halfway down the north face. With additional extension of the loading ram but a reduction of actual load, the crack propagated to within 2 inches of the bottom of the north face.

With the next application of load, the crack propagated to approximately 1 inch of the bottom of the north face in its spiral path but a secondary shear crack developed about 2 inches from the top of the north face at the existing crack and extended toward the support.

The west end had a similar failure mode except the critical section was displaced 12 inches from the west support. The spiral crack on the west end did reach the bottom of the north face at a load of .91 kips and with additional loading a secondary shear crack developed at 2 1/2 inches from the top of the north face at the existing spiral and extended toward the west support.

The shear-centerline deflection, shear-slope at the ends and the torque-twist curves indicate a linear response up to the first observed cracking. The shear-slope at the ends curves indicate a symmetrical response up to cracking load.

Beam C-5

Beam C-5 was loaded with two cycles. The first cycle had an eccentricity of 31.0 inches which required the use of the loading arm attachment and the collars at the support diaphragms. When the load was increased to 0.82 kips, the south end of the concrete loading arm collapsed along the arm's reinforcement allowing the loading arm attachment to rotate and reduce the loading on the specimen. No cracks were observed in the primary test section of the specimen. The reason for the collapse appeared to be that the load from the attachment was being transferred to the concrete loading diaphragm by bearing of the bolt rather than by friction.

The loading attachment was removed and the beam was tested with a new eccentricity of 10.0 inches with the collars on the support diaphragms.

The shear-centerline deflection and the torque-twist curves for the first cycle indicate a linear response up to the live load of .82 kips which seems to be of questionable value as stated above. The shear-slope at the ends curves indicate a linear and symmetrical response.

The crack pattern of the second cycle was symmetrical with respect to mid-span. The first crack in the primary test specimen occurred at midspan in the north face as a vertical flexural tension crack at a load of 2.92 kips. When the load was increased to 2.99 kips, a new crack formed on either side of mid-span and the capacity of the specimen dropped. The new cracks resembled diagonal tension type cracks on the south face with the resultant cracks being from the bottom of the south face at approximately 12 inches from mid-span to the intersection of the web and the flange approximately 4 inches on either side of mid-span.

The north face had a similar crack pattern except the presence of the torsion displaced the bottom of the cracks toward the supports and the tops of the cracks joined approximately 1 inch below the top of the web. With the additional extension of the loading ram, a large elliptical section of the flange was formed by the crack at collapse with mid-span being the center of symmetry and the crack being from the quarter points across the top of the web.

The shear-centerline deflection and the torque-twist curves indicate a linear response up to 2.63 kips which was the one previous to that at which cracking was first observed.

The shear-slope at the ends curves indicate a symmetrical response up to actual collapse of the specimen.

Beam C-6

Beam C-6 was tested with an eccentricity of 1.5 inches. The crack pattern was very symmetrical up to the load causing collapse. Vertical flexural tension cracks were observed in the bottom of the web at mid-span with the application of 2.92 kips. When the load was increased, the existing flexural cracks extended vertically until they were approximately mid-height at which points they extended toward the load and new cracks formed at a spacing of approximately 6 inches.

Bending in the horizontal plane was observed by noting that at a load of 4.38 kips tension cracks in the south edge of the flange at 6 inches on either side of the loading diaphragm had formed.

When the load reached 4.68 kips, secondary shear caused the inclined portion of the existing cracks at 10 inches on either side of mid-span to propagate not only upward but downward. The symmetry of the cracks was destroyed with the formation of a new crack on the west wide at approximately mid-height extending from the secondary shear crack just described to the west support.

The shear-centerline deflection, the shear-slope at the ends and the torque-twist curves indicate a linear response up to initial cracking. The shear-slope at the ends curves indicate a symmetrical response up to the collapse of the specimen.

Beam C-7

Beam C-7 was tested with a two-point load system symmetrical with the mid-span to give a pure moment region over the center third of the span. Vertical stirrups were placed outside of the center third of the span to force collapse to occur in the pure moment region.

The first crack was observed as a vertical flexural tension crack in the bottom of the web at mid-span. With additional loading, new cracks formed in the bottom of the web approximately equally spaced at 3 inches and the existing ones propagated vertically.

Horizontal bending was noted by observing flexural tension cracks in the south edge of the flange on either side of mid-span at a live load of 5.55 kips. At a load of 7.02 kips two cracks had formed on either side of mid-span at a spacing of 6 inches and had propagated approximately 3 inches toward the web. At a load of 7.41 kips, the first crack on the west side had propagated to the intersection of the flange and the web.

Crushing of the concrete in the compression zone caused collapse at a load of 7.41 kips. Seven vertical cracks had formed in the web symmetrically on either side of mid-span.

The shear-centerline deflection and the shear-slope at the ends curves indicate a linear response up to the initial cracking live load of 3.51 kips. The shear-slope at the ends curves indicate a symmetrical response up to the load of 6.44 kips at which point the east end slope was less for each of the remaining load levels.

Beam C-8

Beam C-8 was tested with an eccentricity of 21.5 inches which

required the use of the loading arm attachment and the collars at the supports. The failure mode was primarily torsional with secondary shear.

The crack pattern was similar on each side except the east failure crack was located approximately at the quarter point rather than at the support as the west one was. The type of crack on either side was of a spiral nature which extended up the south face over the top and down the north face with the direction of travel from the support toward mid-span at an angle of 35 degrees. The crack on the west end reached the bottom of the north face while the one on the east side only propagated 3 inches from the top before secondary shear failure developed. Horizontal bending was observed by noting the tension cracks on the south edge of the flange at a load of 1.39 kips.

The shear-centerline deflection and the torque-twist curves indicate a linear response up to the load preceeding the observed cracking load indicating that the cracking occurred between the two load levels.

The shear-slope at the ends curves indicate that the specimen responded symmetrically up to the load causing collapse after which the slopes were no longer equal.

Beam C-9

Beam C-9 was tested with an eccentricity of 6.38 inches. Although the crack pattern was not as symmetrical as most of the other specimens, the actual collapse was the same type on either side of mid-span.

The first cracks occurred as vertical flexural cracks at a load of 2.92 kips in the north face. The one on the west side was located

approximately 3 inches from mid-span while the one on the east side occurred at approximately 6 inches from mid-span. At a load of 3.5 kips, two more cracks had formed on the west side on the north face while on the east side the first crack had extended but no new cracks had occurred.

The crack pattern of the south face of the web appeared more symmetrical than that of the north face with collapse occuring in only one zone on either side of mid-span with the west side being displayed slightly toward the west support.

The shear-centerline deflection, the torque-twist and shear-slope at the ends curves indicate a linear response up to the initial cracking load.

APPENDIX B

LOAD-DEFORMATION CURVES

Shear-Centerline Deflection Curves 132

Torque-Twist Curves. 139

Shear-Slope at the Ends Curves 142

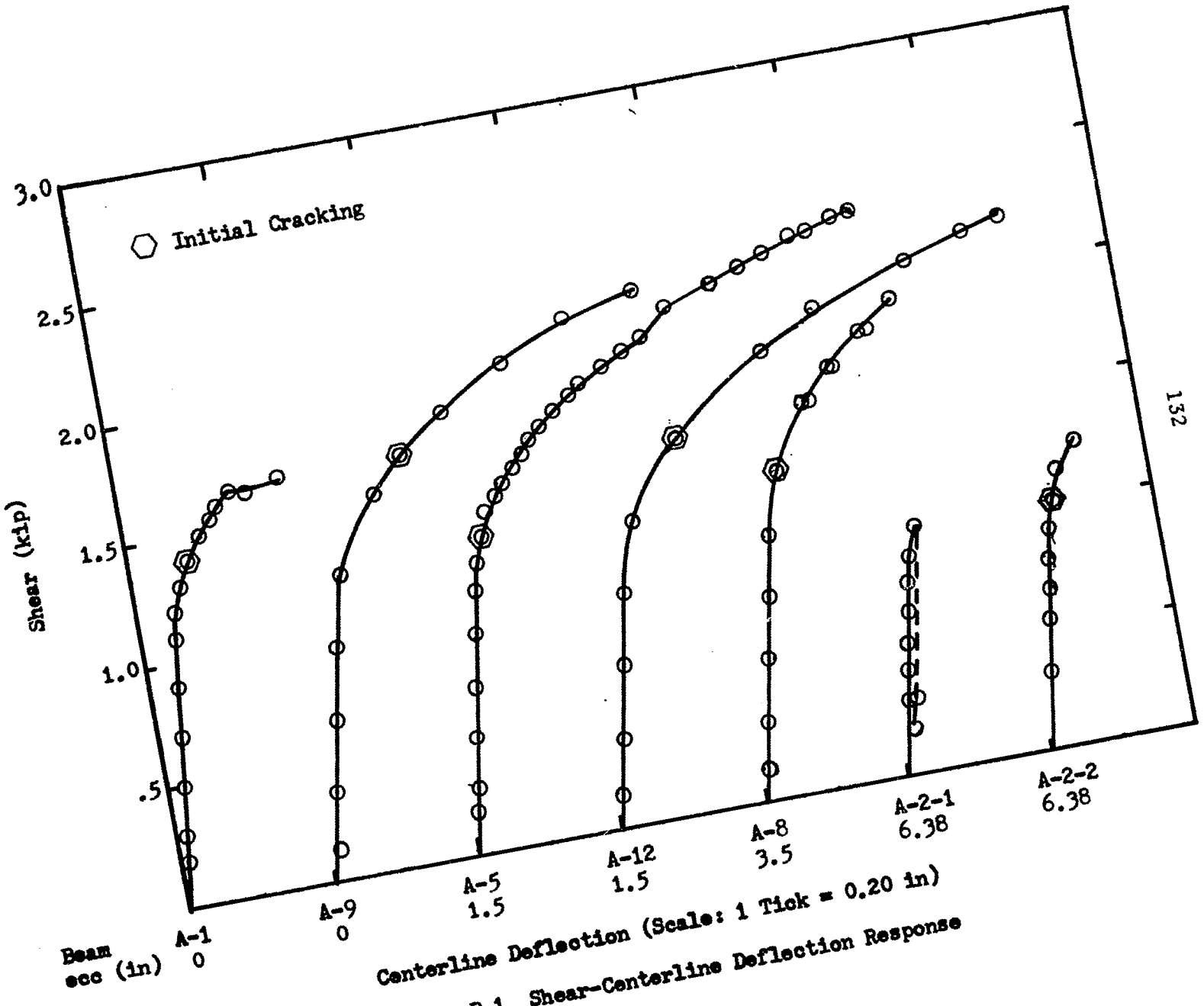


Figure B.1 Shear-Centerline Deflection Response

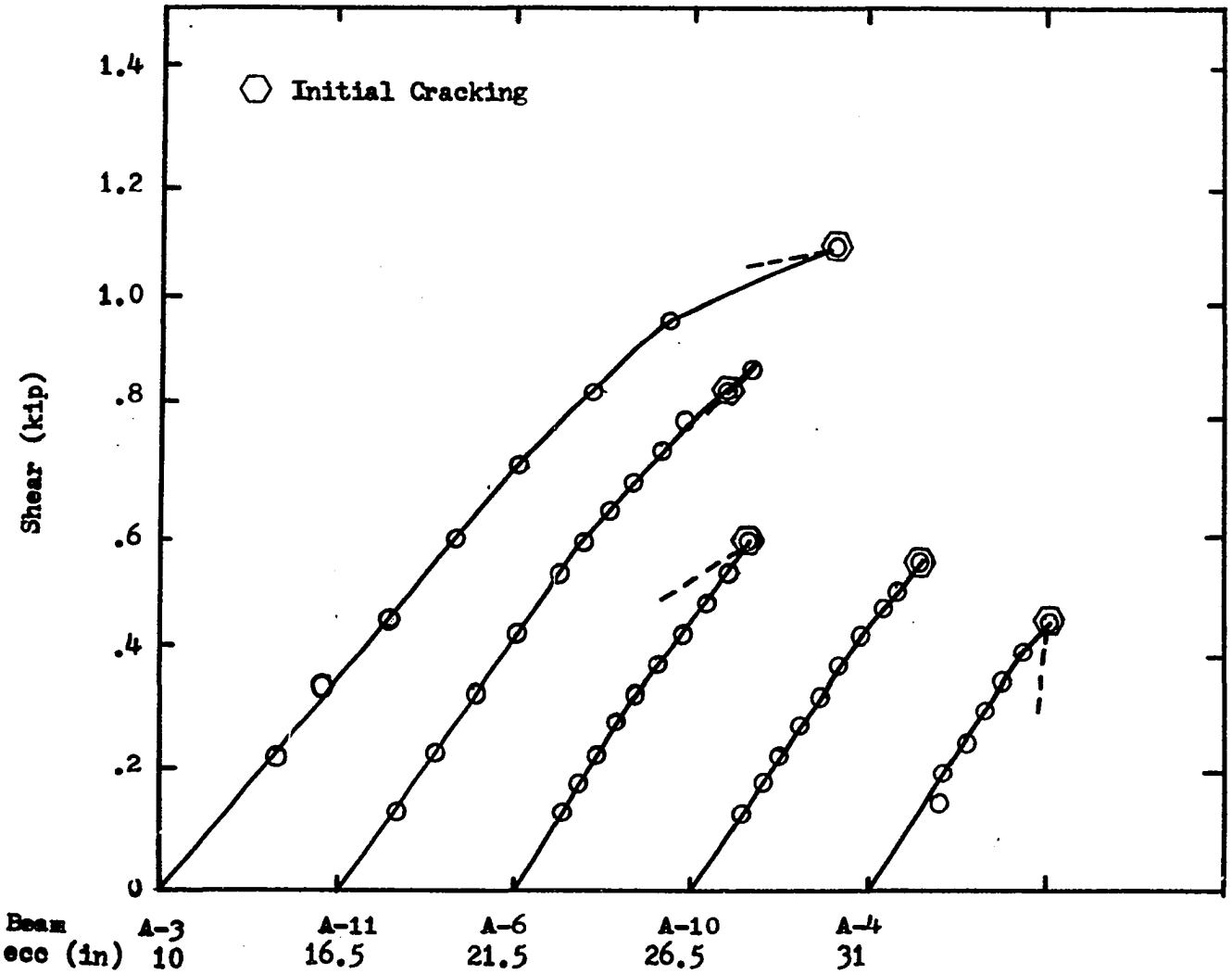


Figure B.2 Shear-Centerline Defletion Response

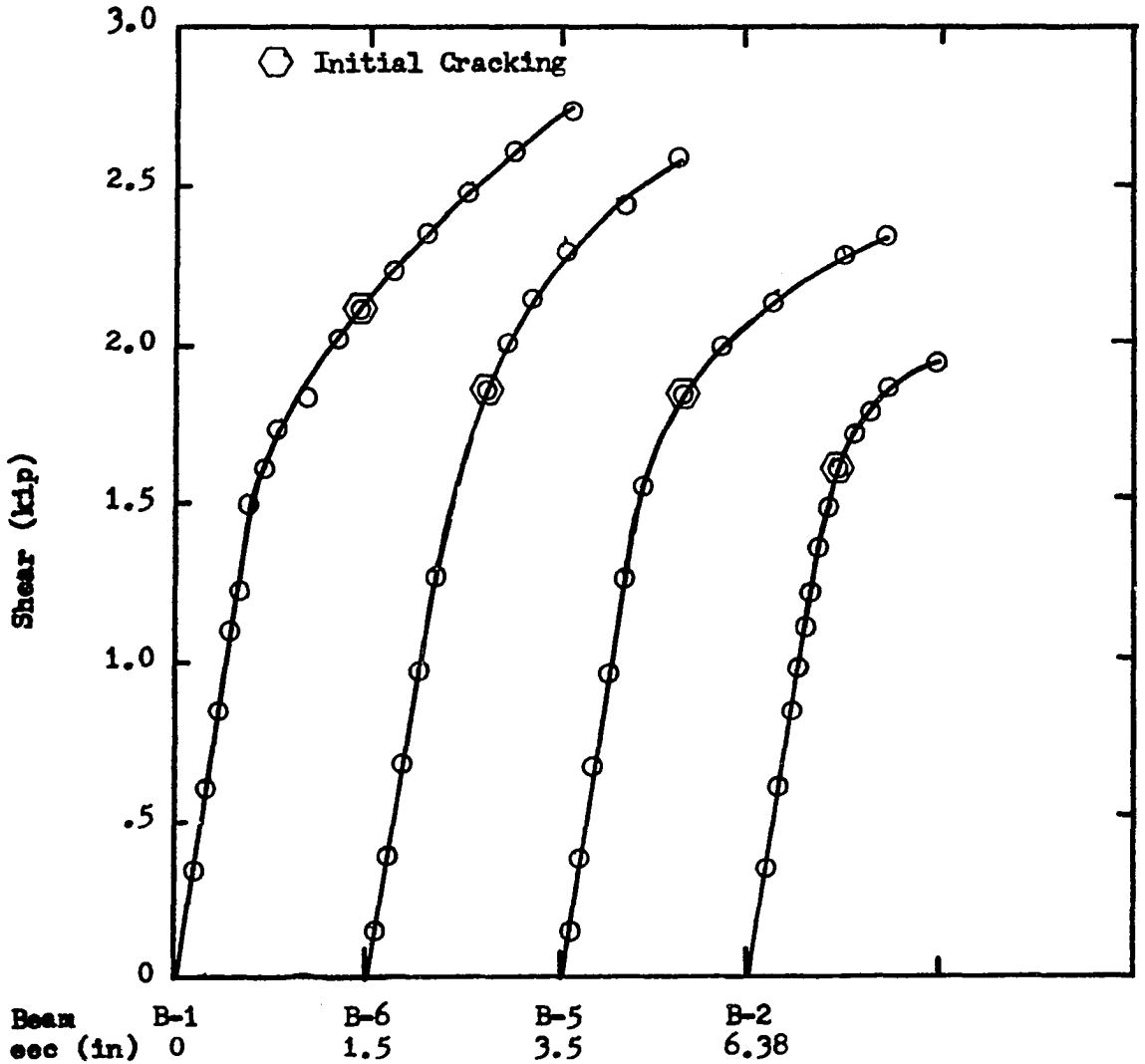


Figure B.3 Shear-Centerline Deflection Response

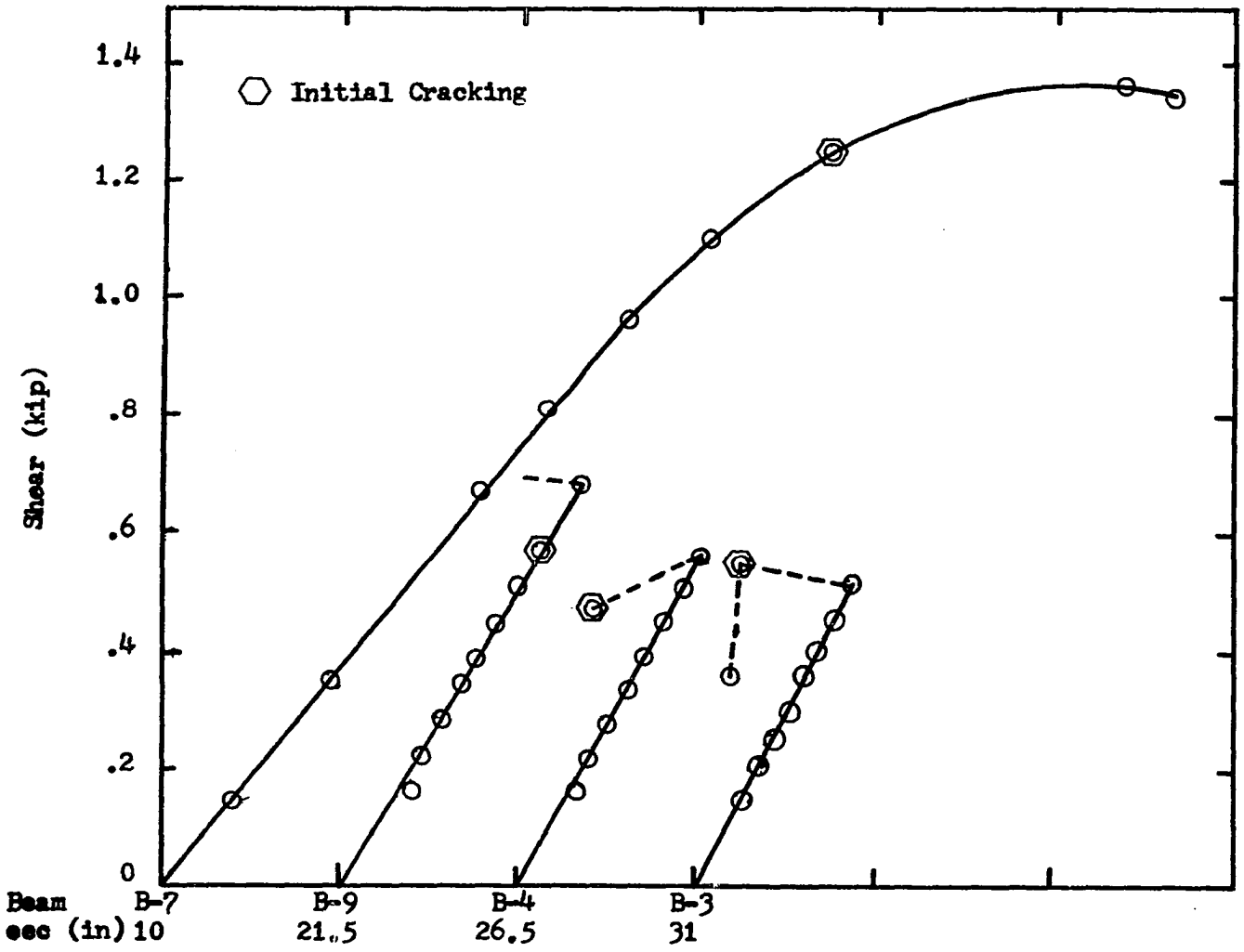


Figure B.4 Shear-Centerline Deflection Response

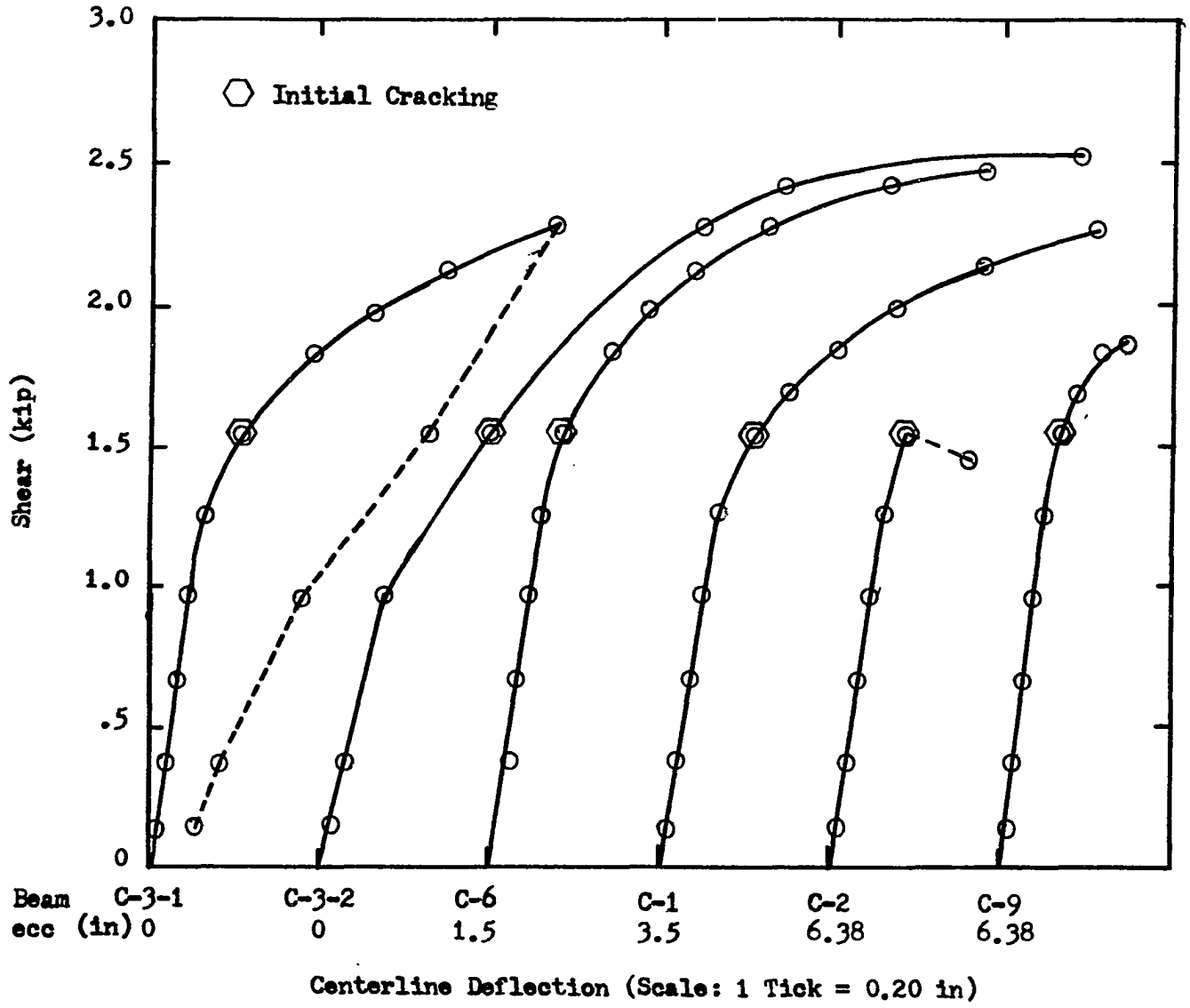


Figure B.5 Shear-Centerline Deflection Response

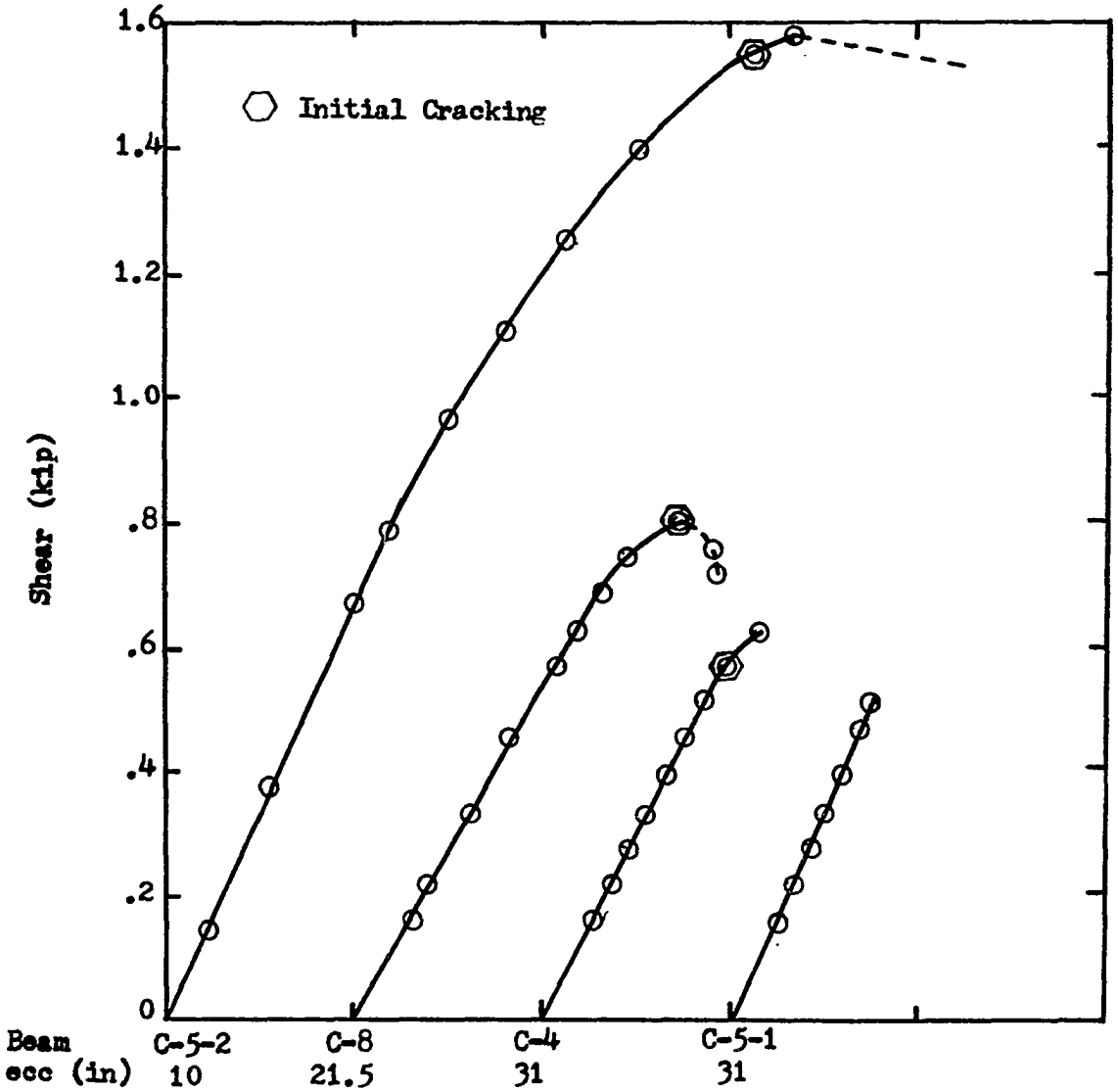


Figure B.6 Shear-Centerline Deflection Response

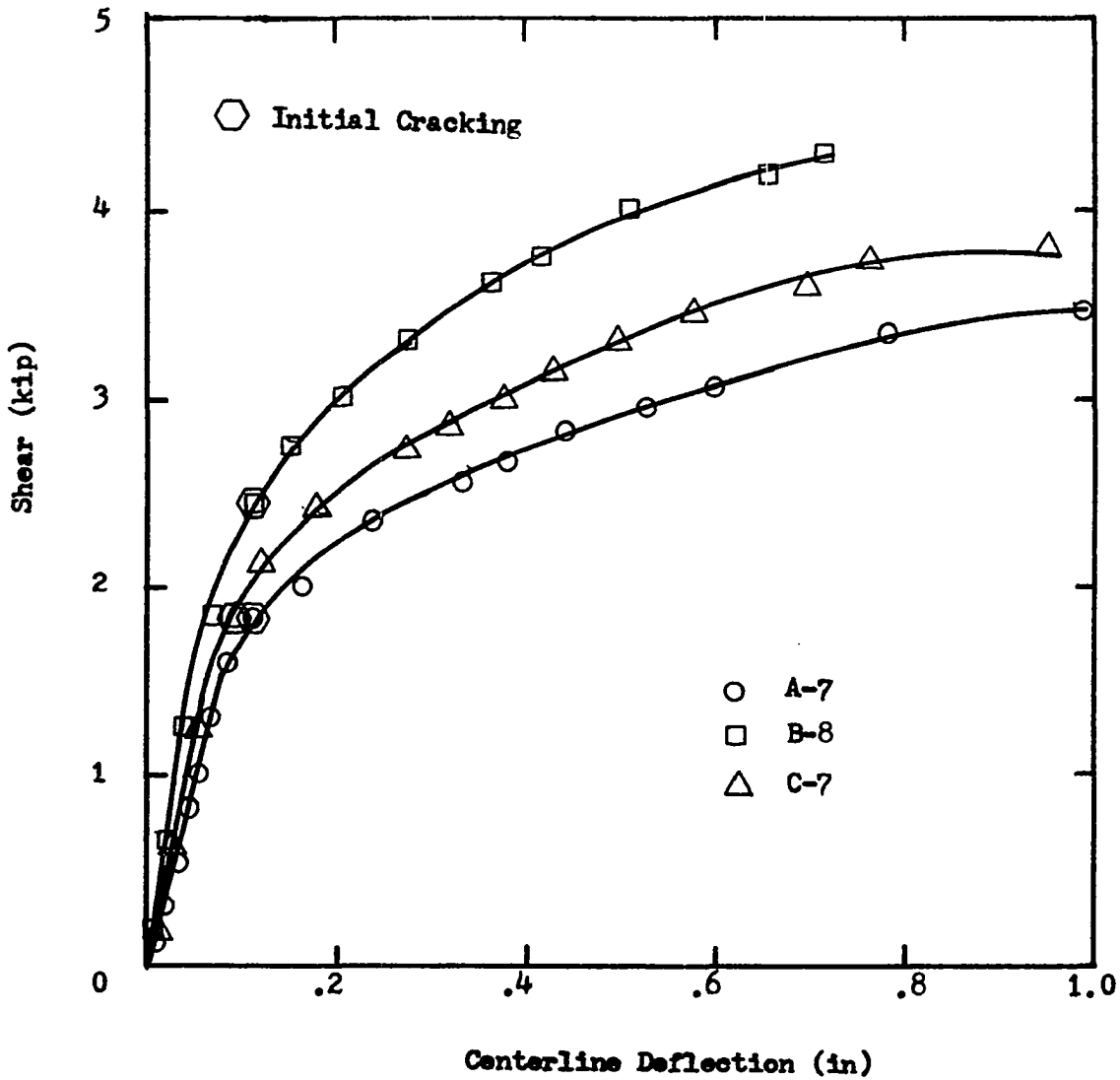


Figure B.7 Shear-Centerline Deflection Response

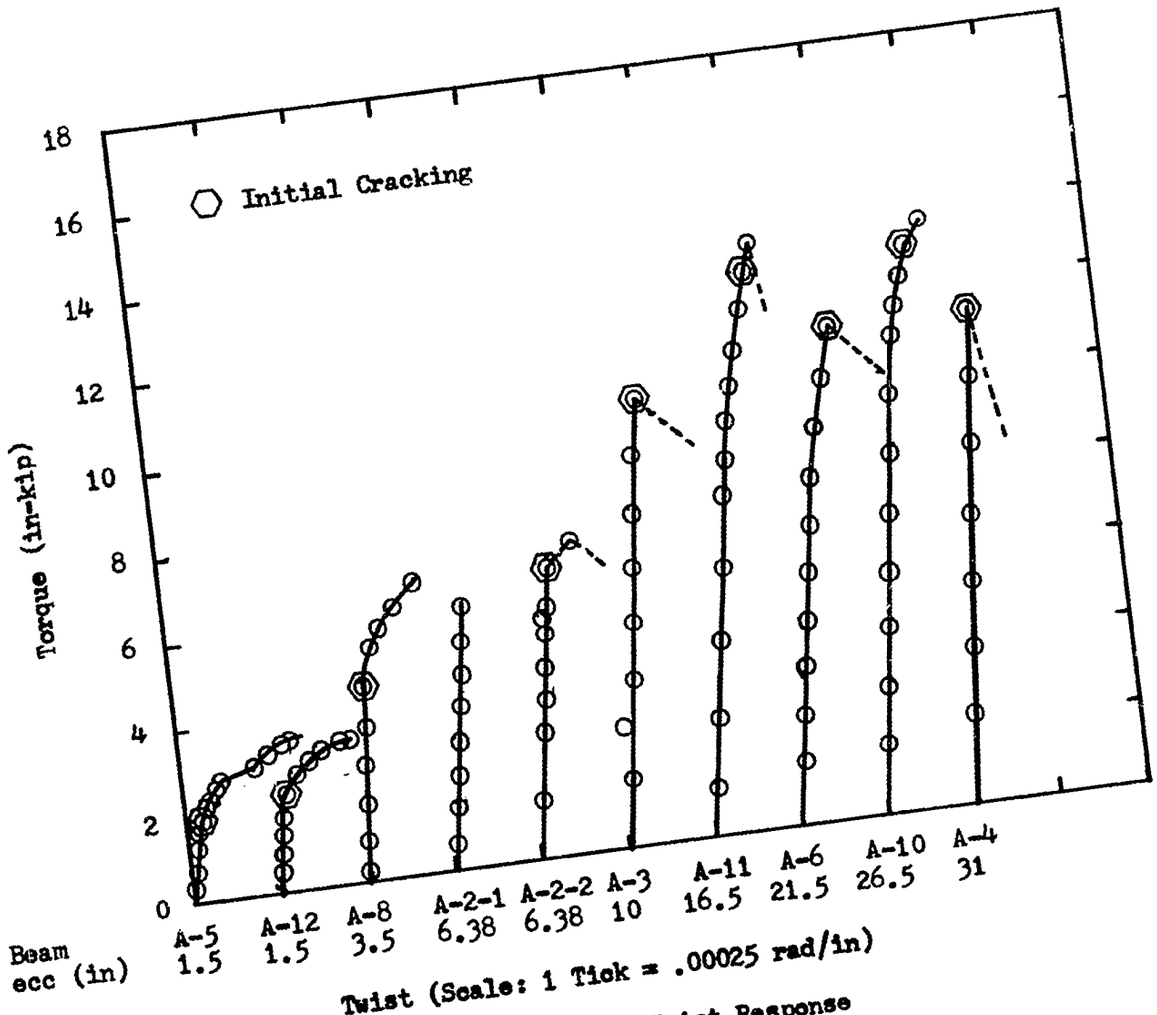


Figure B.8 Torque-Twist Response

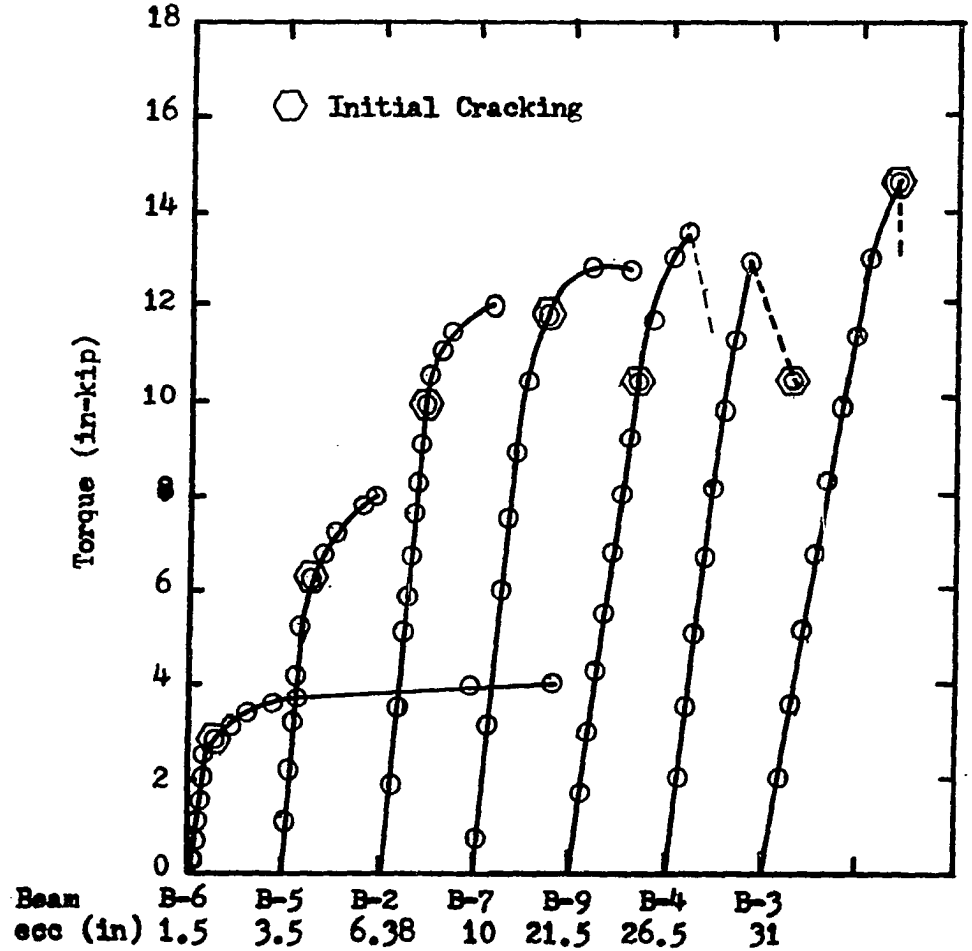


Figure B.9 Torque-Twist Response-Series B

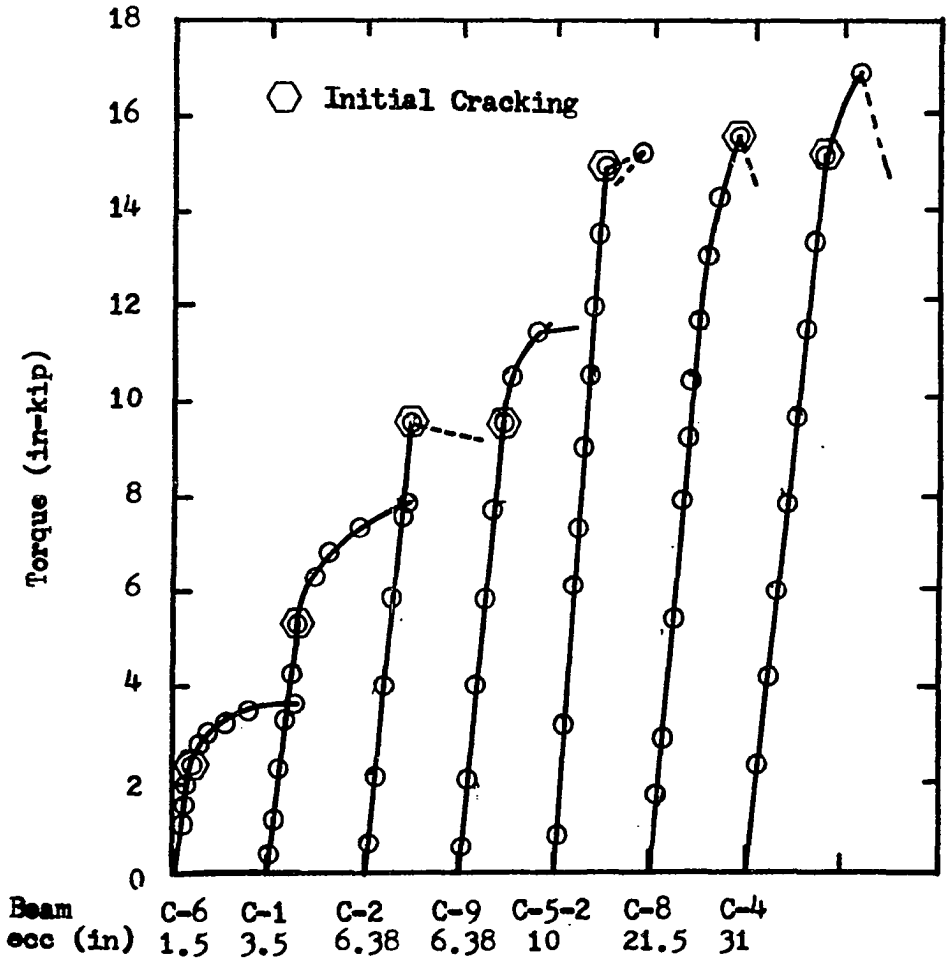


Figure B.10 Torque-Twist Response-Series C

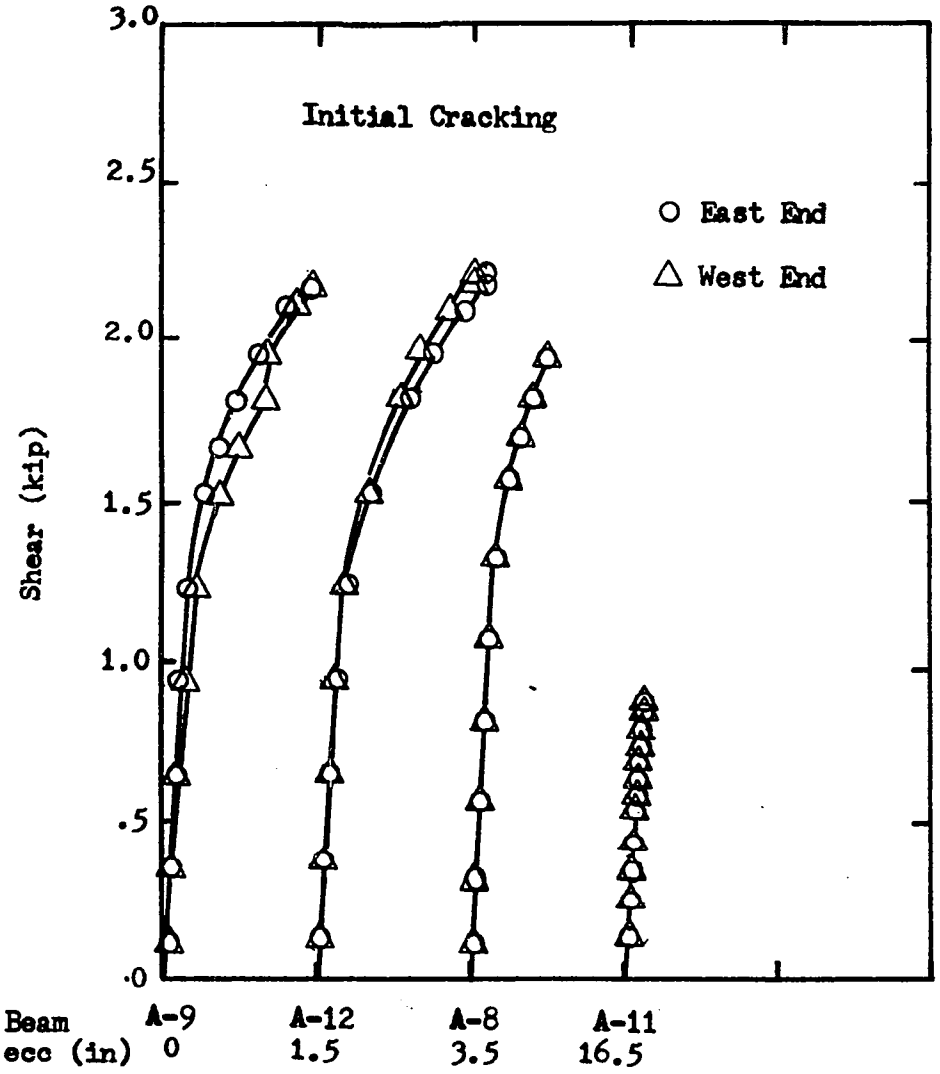


Figure B.11 Shear-Slope at Ends

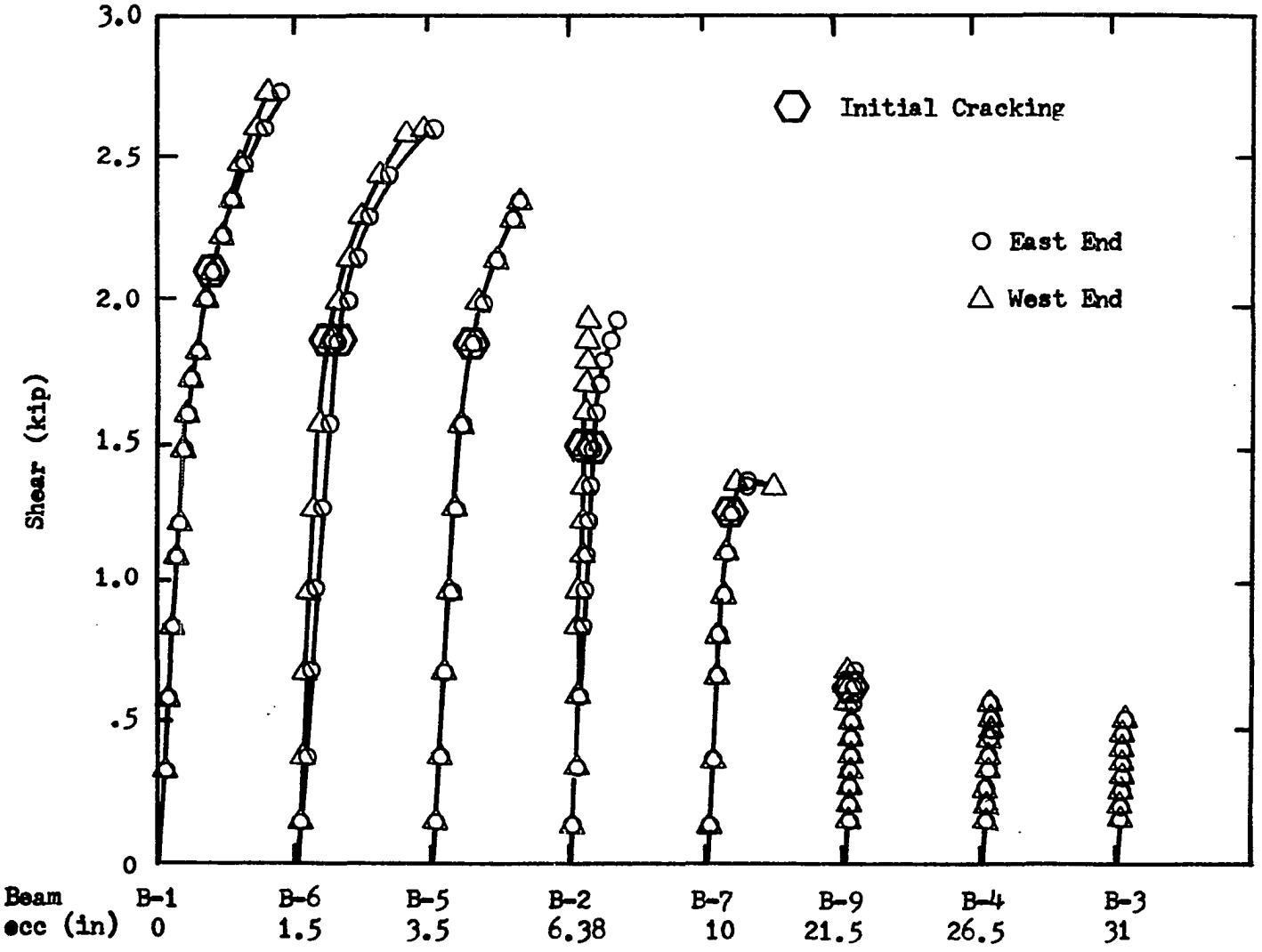


Figure B.12 Shear-Slope at Ends

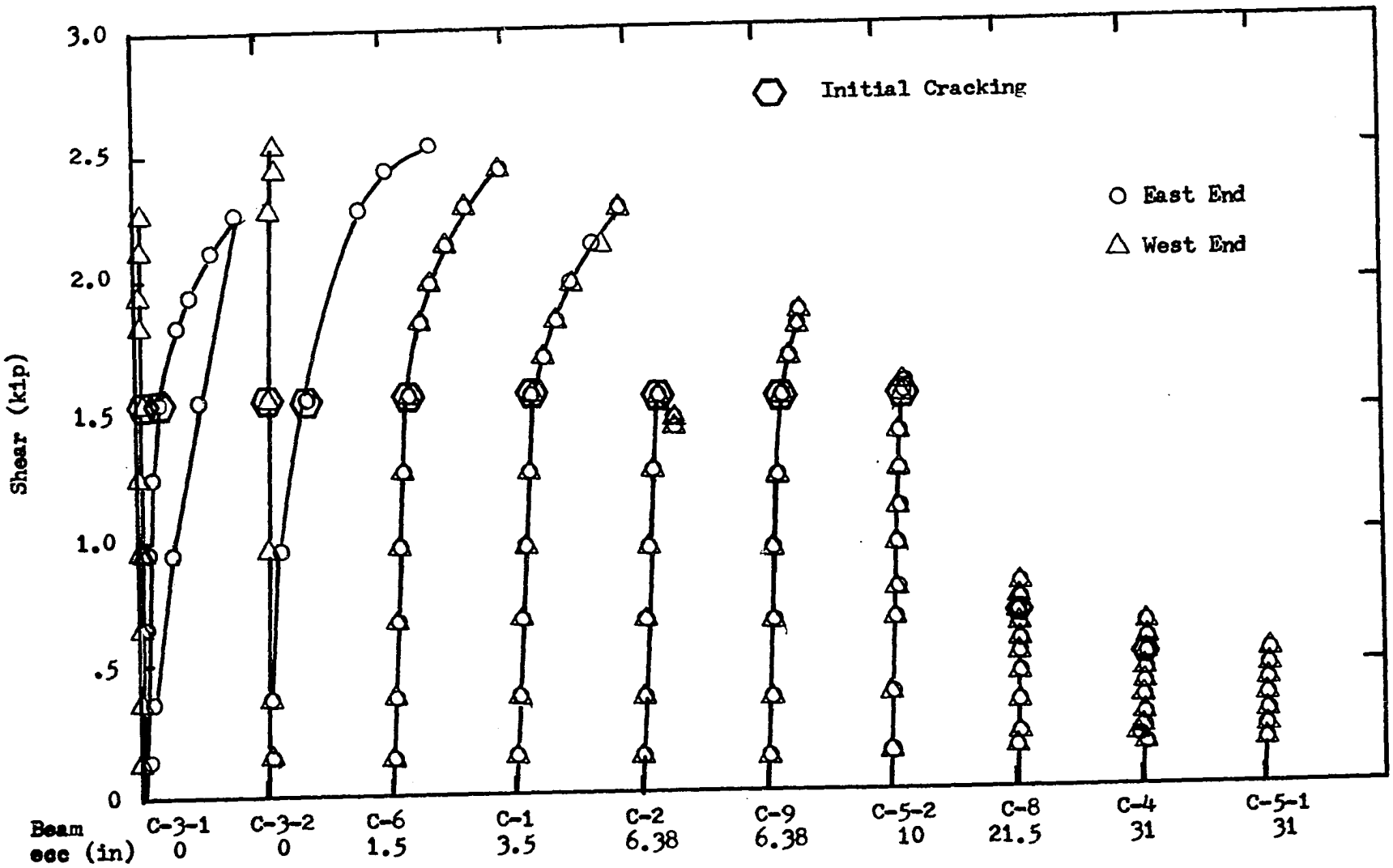
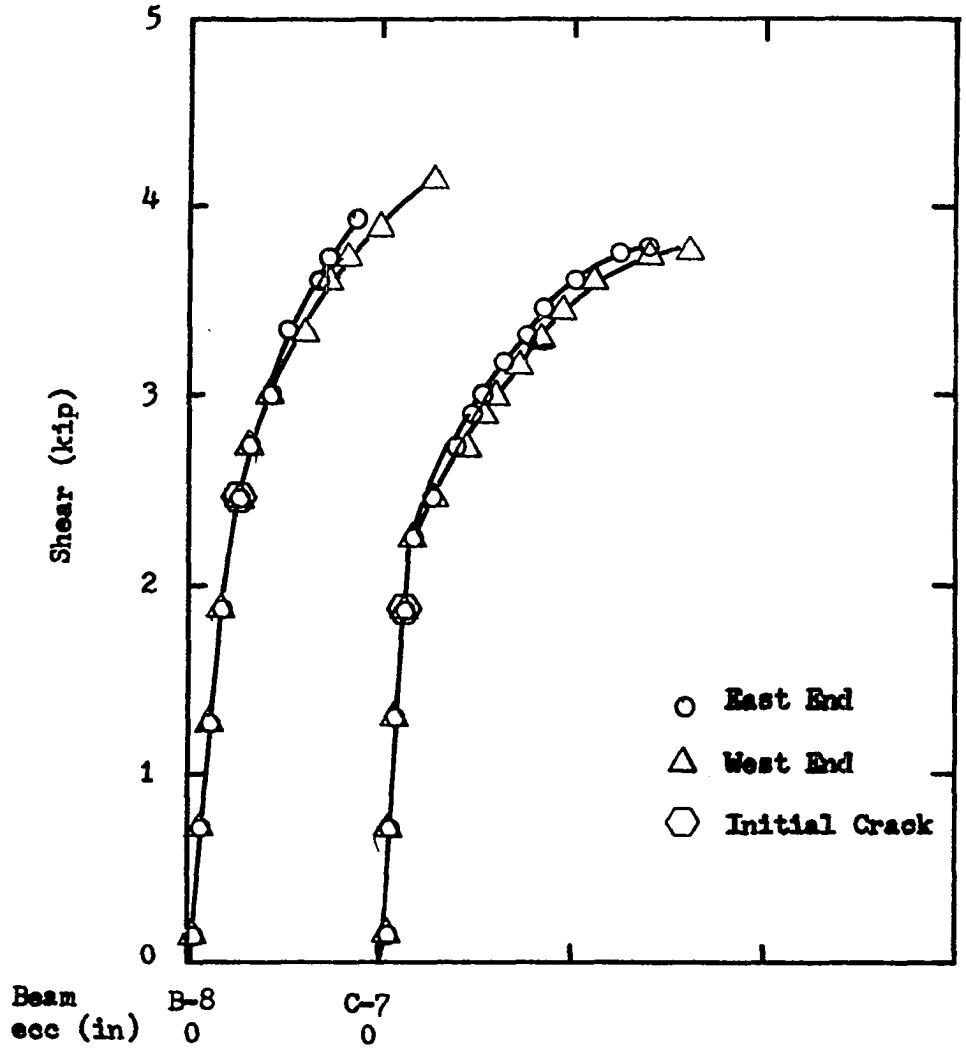


Figure B.13 Shear-Slope at Ends



Slope (Scale: 1 Tick = .025 rad)

Figure B.14 Shear-Slope at Ends

APPENDIX C

MATERIAL PROPERTIES

Sieve Analysis 147

Load-Strain Curve for Prestressing Cable 148

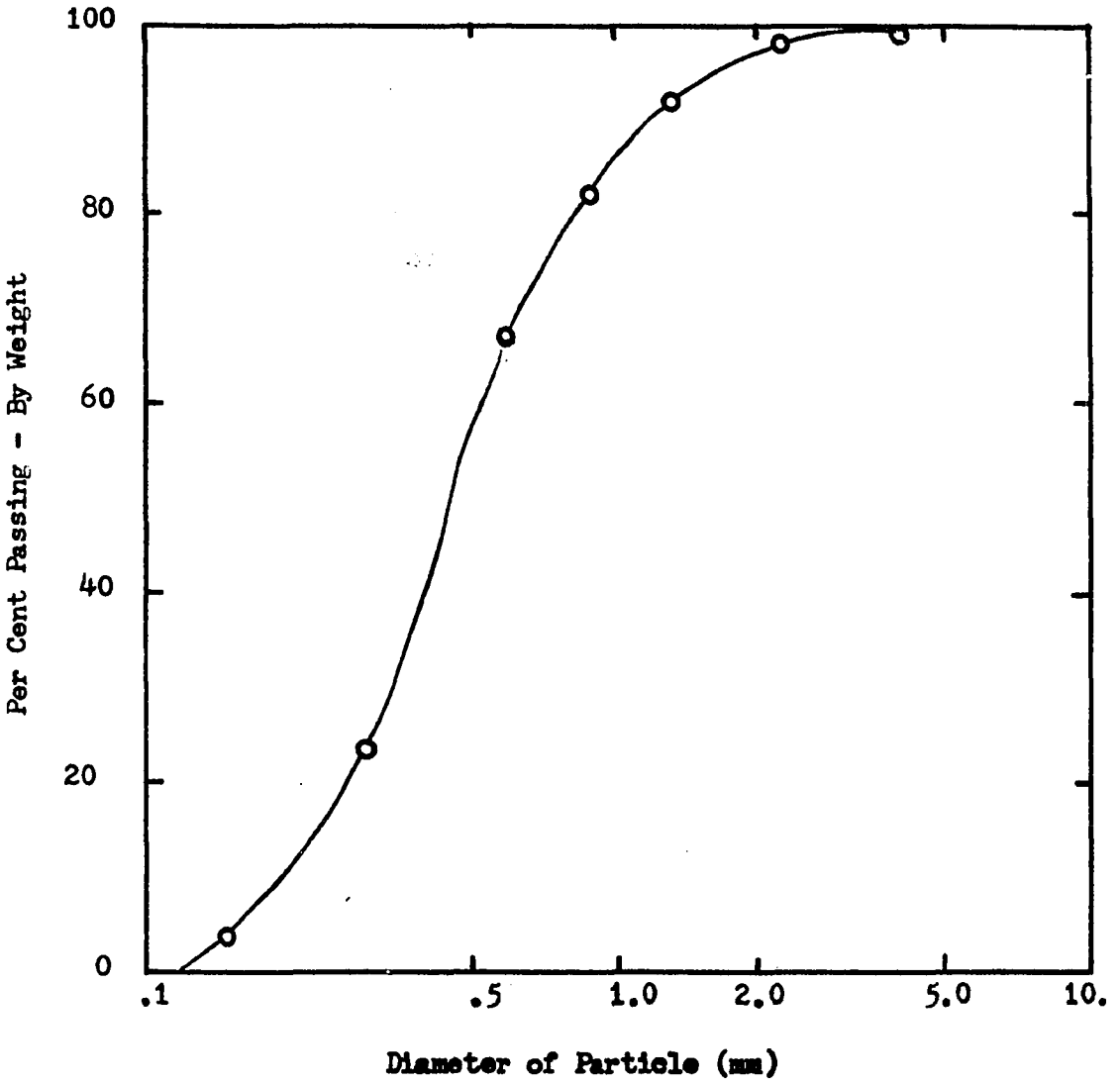


Figure C.1 Sieve Analysis for Sand

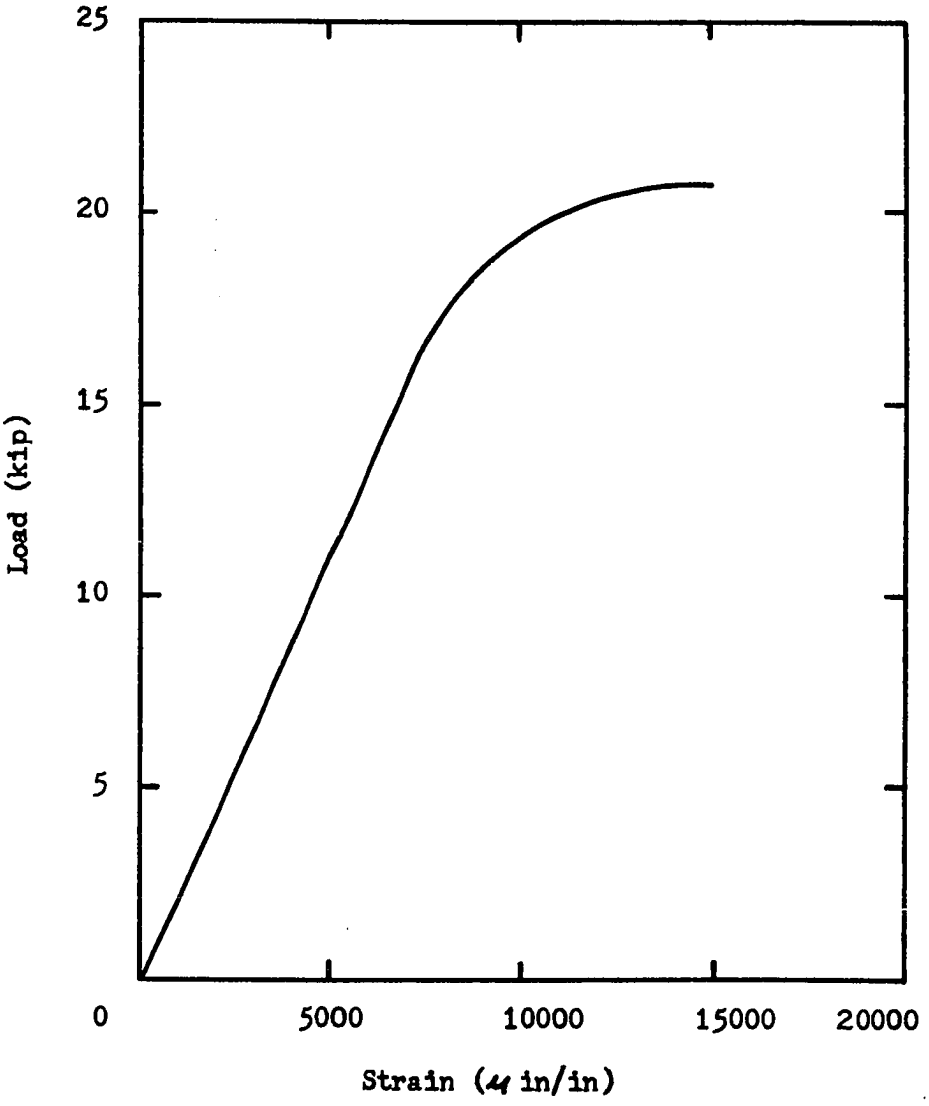


Figure C.2 Load-Strain Diagram for Prestressing Cable

APPENDIX D

LOAD CELL CALIBRATION CURVES

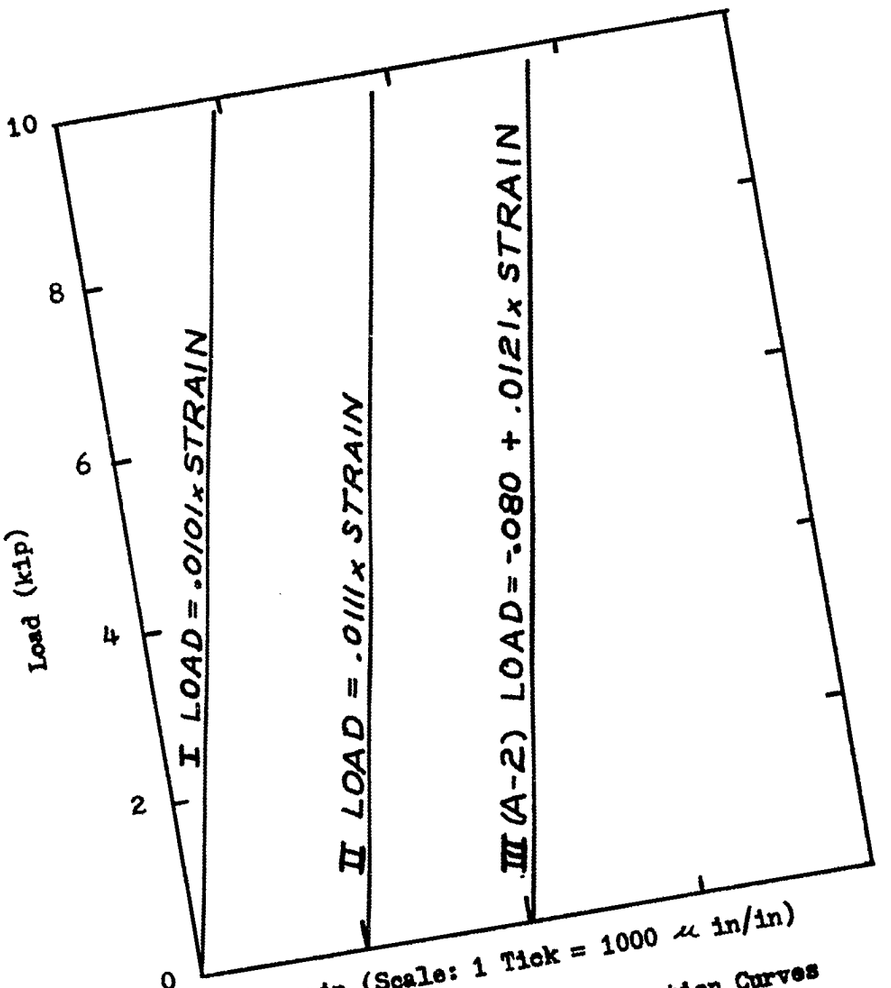


Figure D.1 Load Cell Calibration Curves

VITA

Jimmy Dean Hahs was born in Sedgewickville, Missouri on March 13, 1940, the son of Raymond and Tillere Hahs. After attending Farmington, Missouri elementary and high schools, he entered the University of Missouri School of Mines and Metallurgy, Rolla, Missouri and was awarded the degree of Bachelor of Science in May, 1961. He received the degree of Master of Science in October of 1965 from the University of Missouri at Rolla, Rolla, Missouri.

In 1965 he entered the graduate school of the University of Oklahoma, Norman, Oklahoma where he received a Ford Foundation Forgivable Loan. In 1966 he was the recipient of a traineeship from the National Science Foundation.

In 1968 he returned to the University of Missouri-Rolla as an Instructor in Civil Engineering. He is a registered Professional Engineer in the state of Missouri and is a member of ASCE, ACI, NSPE, MSPE and the Engineers' Club of St. Louis.

He is also a member of Sigma Xi, Tau Beta Pi, Chi Epsilon and Phi Kappa Phi.

In 1961 he was married to Ruth Ann Pope and they have three children, Daniel, Janet and Dennis.